RELATIONSHIP BETWEEN EXTREME PRECIPITATI ON AND CLIMATIC CYCLES UNDER CLIMATE CHANGE IN TEXAS

A Dissertation

by

KYUNGTAE LEE

Submitted to the Office of Graduate and Professional Studies of
Texas A&M University
in partial fulfillment of the requirements for the degree of

DOCTOR OF PHILOSOPHY

Chair of Committee,	Vijay P. Singh
Committee Members,	Srinivasulu Ale
	Anthony T. Cahill
	Mohsen Pourahmadi
Head of Department,	Stephen W. Searcy

August 2020

Major Subject: Biological and Agricultural Engineering

ABSTRACT

Texas has a spatial rainfall pattern with a decreasing gradient from east to west that greatly influences land use, vegetation, and river flow. From a hydrometeorological perspective, this variation leads to unfavorable conditions for agricultural production and water management. To minimize the risk due to extreme precipitation, Probable Maximum Precipitation (PMP) is used for designing major hydraulic structures, such as dams and reservoirs, nuclear power plants, and flood protection works. It is also used for rehabilitating old existing dams. However, the estimation of PMP is associated with uncertainties that have received significant attention in recent years, because meteorological extremes are projected to become more frequent, severe, and uncertain owing to climate change. The global-scale climatic cycles and atmospheric circulation reveal the controlling mechanisms of precipitation regimes. The main objective is to investigate into precipitation extremes and characteristics under the effect of climatic cycles and atmospheric phenomenon. The dissertation is organized into five chapters. The first chapter addresses the objectives and organization of the dissertation. The second chapter quantifies the uncertainty associated with PMP estimation and emphasizes the necessity of including the effect of climate change on PMP. The third chapter examines the impact of major Atlantic and Pacific Ocean based climatic cycles, including Atlantic Multidecadal Oscillation (AMO), North Atlantic Oscillation (NAO), Pacific Decadal Oscillation (PDO), Pacific North American Pattern (PNA), and Southern Oscillation Index (SOI), on extreme precipitation in various climate zones in Texas. The fourth

chapter investigates into the effect of climatic cycles and Rossby Wave on extreme precipitation. The relationship between Rossby Wave frequency and precipitation characteristics is investigated. The fifth chapter evaluates future precipitation extremes and PMP using Coupled Model Intercomparison Project Phase 5 (CMIP5) using both historical observations and future CMIP5 projections. It is concluded that extreme precipitation showed non-stationarity which affected the PMP shift during the historical period, and the global scale climatic indicators (AMO, NAO, PDO, PNA, SOI, and ESPI) can provide regional response to meteorological extreme events. These findings can help raise the community's attention to research needs for broader insights into understanding extreme meteorological events.

ACKNOWLEDGEMENTS

First of all, I would like to thank my academic advisor, Professor Vijay P. Singh for guidance and contribution throughout the course of this research in Texas A&M University. Without his encouragement and support, I cannot imagine I can finish this dissertation successfully. I am so grateful for being a member of his research group and learning through his tremendous experiences and knowledge.

I would like to thank my committee members, Dr. Ale, Dr. Cahill, and Dr. Pourahmadi for their insightful guidance and support to finalize my dissertation. Thanks also go to my friends and colleagues and the department faculty and staff for making my time in Biological and Agricultural Engineering at Texas A&M University a great experience.

Finally, thanks to my parents, my brother, sister-in-law, and my adorable nephew for continuous support, patience, and love.

CONTRIBUTORS AND FUNDING SOURCES

Contributors

This work was supervised by a dissertation committee consisting of Professor Vijay P. Singh and Professor Srinivasulu Ale of the Department of Biological and Agricultural Engineering, Professor Anthony T. Cahill of the Department of Civil Engineering, and Professor Mohsen Pourahmadi of the Department of Statistics.

Funding Sources

Graduate study was supported by a Dissertation Fellowship from Office of Graduate and Professional Studies and a Graduate Student Competitive Scholarship from the Department of Biological and Agricultural Engineering in Texas A&M University.

NOMENCLATURE

A-D	Anderson-Darling
AMO	Atlantic Multidecadal Oscillation
AMP	Annual Maximum Precipitation
ATP	Annual Total Precipitation
AVG	Average
BCSD	Bias Correction and Spatial Disaggregation
BRB	Brazos River Basin
CICS	Cooperative Institute for Climate and Satellites
CMIP5	Coupled Model Intercomparison Project Phase 5
CONUS	Contiguous United States
COOP	Cooperative Observer Network
C-S	Chi-Square
DAD	Depth Area Duration
ECMWF	European Centre for Medium-Range Weather Forecast
ENSO	El Nino-Southern Oscillation
ERA	European Centre for Medium-Range Weather Forecast Reanalysis
ESPI	El-Niño–Southern Oscillation Precipitation Index
ESSIC	Earth System Science Interdisciplinary Center
FEMA	Federal Emergency Management Agency
FFC	Frequency Factor Curve

GCM	Global Climate Model
GEV	Generalized Extreme Value
GIS	Geographic Information System
GPCP	Global Precipitation Climatology Project
H	Hershfield
HMR	Hydrometeorological Report
K-S	Kolmogorov-Smirnov
MAMP	Mean Annual Maximum Precipitation
MEL	Mild El-Niño
MLN	Mild La-Niña
MPP	Maximum Possible Precipitation
MTH	Method
NAO	North Atlantic oscillation
NCDC	National Climatic Data Center
NEXRAD	Next Generation Weather Radar
NOAA	National Oceanic and Atmospheric Administration
NRW	no Rossby Wave
NST	Non-stationarity
NWS	National Weather Service
PDO	Pacific Decadal Oscillation
PMP	Probable Maximum Precipitation
PNA	Pacific North American Index

PV	Potential Vorticity
PVU	Potential Vorticity Unit
RCM	Regional Climate Model
RCP	Representative Concentration Pathway
RW	Rossby Wave
S	Site-specific
SEL	Strong El-Niño
SLN	Strong La-Niña
SOI	Southern Oscillation Index
SPAS	Storm Precipitation Analysis System
STDEV	Standard Deviation
TCEQ	Texas Commission on Environmental Quality
TPO	Topography
TWDB	Texas Water Development Board
WMO	World Meteorological Organization

TABLE OF CONTENTS

Page

LIST OF FIGURES

Page

LIST OF TABLES

Page

CHAPTER I

INTRODUCTION

1.1 Introduction

Due to the physical complexity of formation of Probable Maximum Precipitation (PMP) and limited availability of data, only approximations are available for the upper limits of storms (WMO, 2009). There is no true value of PMP, and the estimation of PMP is theoretical with its own scientific reasoning. PMP was formerly defined as Maximum Possible Precipitation (MPP) which could not be exceeded theoretically. Since MPP has been surpassed by actual precipitation events, its name has been changed to PMP due to the complexity of estimation of extreme precipitation (Benson, 1973). The World Meteorological Organization (WMO, 2009) stated "It should be noted that due to the physical complexity of the phenomena and limitations in data and the meteorological and hydrological scenarios, the approximation is only available currently for the upper limits of storms and their associated floods." Thus, there is no upper boundary of PMP estimation (Papalexiou and Koutsoyiannis, 2006).

There are uncertainties involved in the PMP estimation regardless of the method used to calculate it (Salas et al., 2014; Singh, 2016; Zhang et al., 2019). The uncertainty of PMP estimation depends on how to define a storm center from a local storm event and there are variables that influence the PMP values, including the overall weather condition, variation of atmospheric moisture, and storm path (Micovic et al., 2015). The situation under extreme events may worsen in the future, because an increase in heavy precipitation has been reported in many regions, including the U.S., through the first part of the 21st

century (Field et al., 2012; Seneviratne et al., 2012). Further, extreme precipitation shows a statistically significant increasing trend in North America (Guilbert et al., 2015; Kunkel et al., 2013; Roque-Malo and Kumar, 2017). This study emphasizes that the PMP values previously reported need updating, considering climate change and non-stationarity during the historical period, because maximum precipitation shows non-stationarity during the historical period in Texas.

In Texas, tropical cyclones occur along the Texas Gulf coast (NWS, 2017). About 40 tropical cyclones happened during the past 70 years (1950-Current), mostly during June through September. However, extreme precipitation may occur in different months or seasons. The extratropical cyclones are rare events in Texas, such as winter storms or blizzards (Schmaltz, 2003) which happen only in the Texas Panhandle area. The global scale climatic cycles are the key mechanisms of precipitation regimes, such as the intensity of precipitation and 24-hour extreme events (Gerlitz et al., 2016; Jones and Carvalho, 2014; Marani and Zanetti, 2015). Several studies have investigated the relationship between climatic cycles and precipitation which helps understand the changing regional hydro-climatic regimes (Chan and Zhou, 2005; Renard and Lall, 2014). Thus, the effect of major Atlantic and Pacific Ocean based climatic cycles on extreme precipitation was investigated for Texas, considering El-Niño and La-Niña in different climate zones. In addition, the frequency of Rossby Wave and its joint effect with climatic cycles on extreme precipitation were investigated. Because Rossby Wave has recently been highlighted in the field of climate and atmospheric interaction. Rossby Wave is a type of inertial wave

naturally occurring in rotating fluids (NOAA, 2020) and is defined by the high potential vorticity that can serve as a carrier of air mass exchange.

The statistically downscaled climate projections from the Coupled Model Intercomparison Project Phase 5 (CMIP5) (Maurer, 2007; Reclamation et al., 2013) was adopted for future climate scenarios. Using statistical (Hershfield and site-specific) method, future PMP was estimated and compared to historical PMPs. The results showed that 16 CMIP5 models had a chance to exceed historical PMPs under two greenhouse gas concentration scenarios (RCP 2.6 and RCP 8.5).

1.2 Objectives

This dissertation investigates the relationship between extreme precipitation and climatic cycles under climate change in Texas. Extreme precipitation, including probable maximum precipitation, has long been discussed. However, there was no universal definition of probable maximum precipitation, thus we intend to address different sources of uncertainty in the estimation of probable maximum precipitation. The primary objective is to improve the understanding of precipitation extremes and characteristics under the effect of climatic cycles and atmospheric phenomenon. Here, we formulate the specific research objectives as:

- Quantify the uncertainty associated with PMP estimation and emphasize the necessity of including the effect of climate change induced non-stationarity on PMP;

- Estimate the contribution of each of the uncertainty sources (methodology, topography, and non-stationarity) to PMP estimation;
- Examine the relationships between global scale climatic indicators and regional precipitation extremes;
- Assess the El-Niño and La-Niña effect on the annual cycle of monthly precipitation under different climate zones and explain what causes the difference between the two phases;
- Investigate into the impact of major Atlantic and Pacific Ocean based climatic cycles on extreme precipitation with Rossby Wave breaking;
- Calculate the number of events and how extreme precipitation are affected under the joint events of climatic cycles and Rossby Wave;
- Examine precipitation characteristics (number of rain days, duration, depth, and intensity of precipitation events) under different zones of RW frequency; and
- Estimate extreme precipitation and PMP under future climate conditions in Texas

1.3 Organization of the dissertation

This dissertation presents the study in five chapters following the above-stated objectives. The first chapter assesses the uncertainty and non-stationarity in probable maximum precipitation. The second chapter examines the relationship between extreme precipitation and climatic cycles including El-Niño and La-Niña. The third chapter explores the effect of climatic cycles and Rossby Wave on extreme precipitation. The fourth chapter estimates future precipitation extremes and PMP using climate model

projections. Finally, the fifth chapter recaps and discusses the future direction of the study which contributes to water resources management and understanding the meteorological extreme events in Texas.

CHAPTER II

ANALYSIS OF UNCERTAINTY AND NON-STATIONARITY IN PROBABLE MAXIMUM PRECIPITATION IN BRAZOS RIVER BASIN

2.1 Synopsis

Probable Maximum Precipitation (PMP) is used for designing major hydraulic structures, such as dams and reservoirs, nuclear power plants, and flood protection works. However, the estimated PMP values are associated with uncertainties that have received significant attention in recent years, partly because hydrologic extremes are projected to become more frequent, severe, and uncertain with non-stationarity and natural climate variability. This study compared four methods of estimating PMP, ranging from hydrometeorological to statistical, including up-to-date grid based and site-specific in the Brazos River basin (BRB). BRB is the largest river basin in Texas and it contains a range of climates from subtropical arid to subtropical humid. The objective of this study was to quantify the uncertainty associated with PMP estimation in terms of the change in the PMP value and emphasize the necessity of including the effect of non-stationarity on PMP. The uncertainty analysis incorporates the effect of three sources of error: (1) PMP estimation method, (2) topography, and (3) non-stationarity. The contribution of each of the uncertainty sources to the 24-hour PMP estimation was quantified and found to be as 53.5% (selection of method), 31.4% (effect of non-stationarity), and 15.1% (effect of topography). The uncertainty of PMP estimation was more sensitive to the existing observation statistics and the selection of method than to the differences between climate

zones. Results showed an overall significant increase in 24-hour record precipitation (+19.5 mm) and PMP (+22.3 mm) in BRB between two historical periods 1940-1976 and 1977-2013. Thus, it is concluded that extreme precipitation in BRB showed non-stationarity which affected PMP shift during the historical period.

2.2 Introduction

Probable Maximum Precipitation (PMP) is theoretically the maximum possible precipitation for a given duration under likely meteorological conditions. In other words, there must be a physical upper limit in the storm that atmospheric circulation could produce at a given place for a given time interval. The referred definition of PMP from WMO highlights the PMP as a physical upper limit, and it is generally regarded as a quantity that cannot be surpassed (WMO, 2009). There are two fundamental approaches to PMP estimation: hydrometeorological and statistical. Under the hydrometeorological approach, one of the earliest methods of PMP estimation defines the physical state of the atmosphere considering moisture maximization and transposition (Paulhus and Gilman, 1953). It is, however, difficult to find a physical justification for the upper boundaries of any meteorological factor used in storm maximization, because maximum precipitation is often unexpectedly exceeded and very high (Yevjevich, 1968). If there is a physical boundary to the possible maximum precipitation amount, this boundary is likely to be much greater than the maximum precipitation computed by any maximization method (Sicular, 1969). Schreiner and Riedel (1978) estimated the PMP values in the east Rocky Mountain area of the United States by analyzing 55 historical (1878-1972) extreme storm

events. The National Weather Service (NWS) has prepared Hydrometeorological Reports (HMR) that describe the procedures for estimating the PMP values for the United States since the 1940s. The main assumption of HRM is that there is the optimum combination of available moisture in the atmosphere and the efficiency of causative mechanisms in the storm that will produce maximum precipitation. In practice, PMP estimates are location-dependent and sensitive to the available dataset (Papalexiou and Koutsoyiannis, 2006).

Under the statistical approach, the Hershfield method is perhaps the most popular method which gives a single value of PMP (Hershfield, 1961a; Hershfield, 1965). The benefit of using the Hershfield method is its application with limited hydrometeorological data. This method takes into account the uncertainty in the PMP estimation arising from the uncertainty of sample mean and sample standard deviation. The uncertainty can be quantified in the determination of frequency factor, mean, standard deviation of extreme precipitation values, and the selection of frequency distribution (Salas et al., 2014).

PMP values are generally presented as deterministic values, however, there is uncertainty in these values due to several factors (Micovic et al., 2015), such as the amount of available data, data quality, and the depth of analysis. The U.S. National Research Council also considers two types of uncertainties that are summarized as follows (Council, 2000): (1) Natural uncertainty represents the inherent variability of the physical system; it cannot be reduced. (2) Knowledge uncertainty is due to the lack of understanding of the system and insufficient data. It is difficult to specify an upper bound with zero risk, because there have been instances where storms in the U.S. have exceeded the PMP estimates (Dooge, 1986). Schreiner and Riedel (1978) concluded that the PMP estimates

were too low east of 105th meridian where 18 storms out of 75 exceeded 70% of the PMPs. The estimated PMP was much higher than the longest return period (e.g. 100-year) precipitation amounts for the same duration (Kunkel et al., 2013; Schreiner and Riedel, 1978). Klemes (1993) argued that it is possible that in any given year, the maximum one-day rainfall may arise from any combination of the convergence and orographic components (Klemes et al., 1992).

Even though climate change has been receiving much attention since the early 1960s (Yevjevich, 1968), there does not seem to be as much attention to the assessment of PMP under changing climate (Beauchamp et al., 2013). The World Meteorological Organization (WMO) report of 2009 mentioned "PMP and climate change" which indicates that climate change could lead to an increase of PMP (WMO, 2009). Globally, increases in heavy precipitation have been reported in many regions, including U.S. through the first part of the 21st century (Field et al., 2012; Seneviratne et al., 2012). Further, extreme precipitation events show statistically significant trends in North America (Guilbert et al., 2015; Kunkel et al., 2013; Rajah et al., 2014; Roque-Malo and Kumar, 2017). It is generally agreed that climate change does have an impact on severe precipitation extremes and its effect should therefore be considered (Simonović, 2012). Kunkel et al. (2013) examined potential climate change effects on PMP along with a significant future increase in mean and maximum precipitation. With climate change, hydrologic extremes are projected to become more frequent, more severe, and more uncertain (Goodess, 2013; Trenberth et al., 2015). Globally PMP values would increase in the future due to large atmospheric moisture content and moisture transport into storms.

Due to the increase in the intensity of heavy to extreme precipitation events, the increase in total precipitation has been observed (Karl et al., 1995).

National Centers for Environmental Information in National Oceanic and Atmospheric Administration (NOAA) reported that there was an increasing trend in precipitation and temperature in most of the basins in Texas (NOAA, 2018). Jakob et al. (2008) showed a strong influence of climate change on moisture maximization and its role in the estimation of PMPs. Kunkel et al. (2013) suggested that projected changes in maximum precipitable water over North America would contribute to an increase in PMPs. Using regional climate models (RCMs) and global climate models (GCMs), Lee et al. (2016), Rousseau et al. (2014), Stratz and Hossain (2014), and Wehner (2013) assessed the impact of climate change. Mailhot et al. (2012) and Monette et al. (2012) reported for Quebec, Canada, that climate change would likely modify the amount, seasonality, and distribution of precipitation events. A study of extreme rainfall in Houston, Texas, by van Oldenborgh et al. (2017) concluded that global warming caused nearly 15% more intense precipitation, or equivalently made extreme events about three times more likely due to the increasing moisture content and stronger winds or updrafts driven by the heat of moisture condensation.

As the available data and our understanding increase, it may be appropriate to refine and adjust PMP estimates with regional or site-specific studies (FEMA, 2004; Zhang et al., 2019). Unlike PMP reports (HMR) which cover multiple states, site-specific PMP estimation considers regional climate conditions within the basin or state. As a continuing effort, Texas Commission on Environmental Quality (TCEQ) prepared a grid-

based PMP report for Texas (TCEQ, 2016). This report provided spatial patterns of PMP and compared the results with HMR-51 PMPs. It was found that the overall PMP percentage change from HMR-51 was an 11% reduction in Texas and the maximum reduction (40%) was captured in the northwestern part of Texas, upstream of Brazos and Colorado River basins with relatively drier conditions. Therefore, the PMP values reported in HMR-51 need updating, considering climate change and non-stationarity during the historical period.

This study also notes that maximum precipitation exhibits non-stationarity during the historical period and compares PMP values using four different methods: (1) Hydrometeorological Reports (HMR), (2) TCEQ Grid PMP report that adopted hydrometeorological method, (3) Hershfield, and (4) Site-specific methods that followed the statistical method. In this study, methods (3) and (4) were implemented, because they are relatively simple and computationally inexpensive for developing a site-specific enveloping curve (Zhang et al., 2019). When the site-specific PMP method was used in this study, the PMP estimates were lower than those in HMR-51 Report, which is likely to be economically beneficial in the design of hydraulic structures. This finding is consistent with the recent grid PMP report from Texas Commission on Environmental Quality (TCEQ, 2016). Then, PMP values were compared to show their uncertainties across BRB due to the selection of the method, the effect of topography, and the effect of non-stationarity (historically-based). The contribution of each of the sources of uncertainty to the PMP estimation is quantified. Since the PMP estimates involve many

sources of uncertainties, it is suggested to use the ensembles of PMP values rather than using a single method.

2.3 Study area

The Brazos River basin (BRB) is the second largest river basin (119,174 km^2) by area within Texas (U.S. Geological Survey, 2008). It is the state's third longest river (1,352 km) and has the largest average annual flow volume (237.5 m^3/s) in Texas (Hendrickson Jr, 2002). BRB consists of five Hydrologic Unit Codes (HUCs) and is covered by seven climate zones. The annual mean precipitation varies greatly for different climatological zones from subtropical arid to subtropical humid (Larkin and Bomar, 1983; Narasimhan et al., 2008). The annual mean precipitation ranges from 254 to 381 millimeters in the northern part and from 1143 to 1194 millimeters in the southern part of BRB (PRISM Climate Group, 2011). There are two precipitation peaks in May and September (Lee et al., 2017). The average annual temperature ranges from 15.0 ^oC in the upper basin to 21.1 ^oC in the lower basin (TBRA, 2018). This diverse climate range manifests itself in large spatial and temporal variations in precipitation and temperature. In 1899, the Brazos River basin had a flood that caused over 9 million dollars of property damage and 284 casualties (Life on the Brazos River, 2013; Roth, 2010). Recently, the area near Houston (Brays Bayou in Harris County) received about 278.4 mm of precipitation during a 12-hour period on May 26, 2015, causing damages to 1,185 residential properties (Bass et al., 2016). During August 25–30, 2017, Hurricane Harvey struck Texas (particularly Houston) and generated extreme precipitation causing extensive flooding. The return period of the

highest observed three-day precipitation amount (1043.4 mm at Baytown) was more than 9000 years (van Oldenborgh et al., 2017). National Centers for Environmental information of National Oceanic and Atmospheric Administration (NOAA) reported that there was an increasing trend in precipitation and temperature in most of the basins in Texas (NOAA, 2018).

2.4 Data

A total of 46 gauge stations which have more than 30 years of data were selected (Figure II-1). Hourly precipitation data (https://www.ncdc.noaa.gov/cdo-web/) were obtained from NOAA National Climatic Data Center (NCDC) to estimate PMP. The maximum precipitation during certain durations was obtained from each year using sliding maxima (van Montfort, 1990). Because rainfall is a continuous variable and fixed time interval approach may have potential source of underestimation (Papalexiou et al., 2016). The fixed series are not appropriate for the estimation of rainfall maxima (Hershfield, 1961b). From 1-hour duration precipitation, the maximum precipitation depth on sliding intervals (6- and 24-hour) within a year in a continuous time domain was determined (van Montfort, 1997). Each station had the maximum precipitation values from each duration in every year.

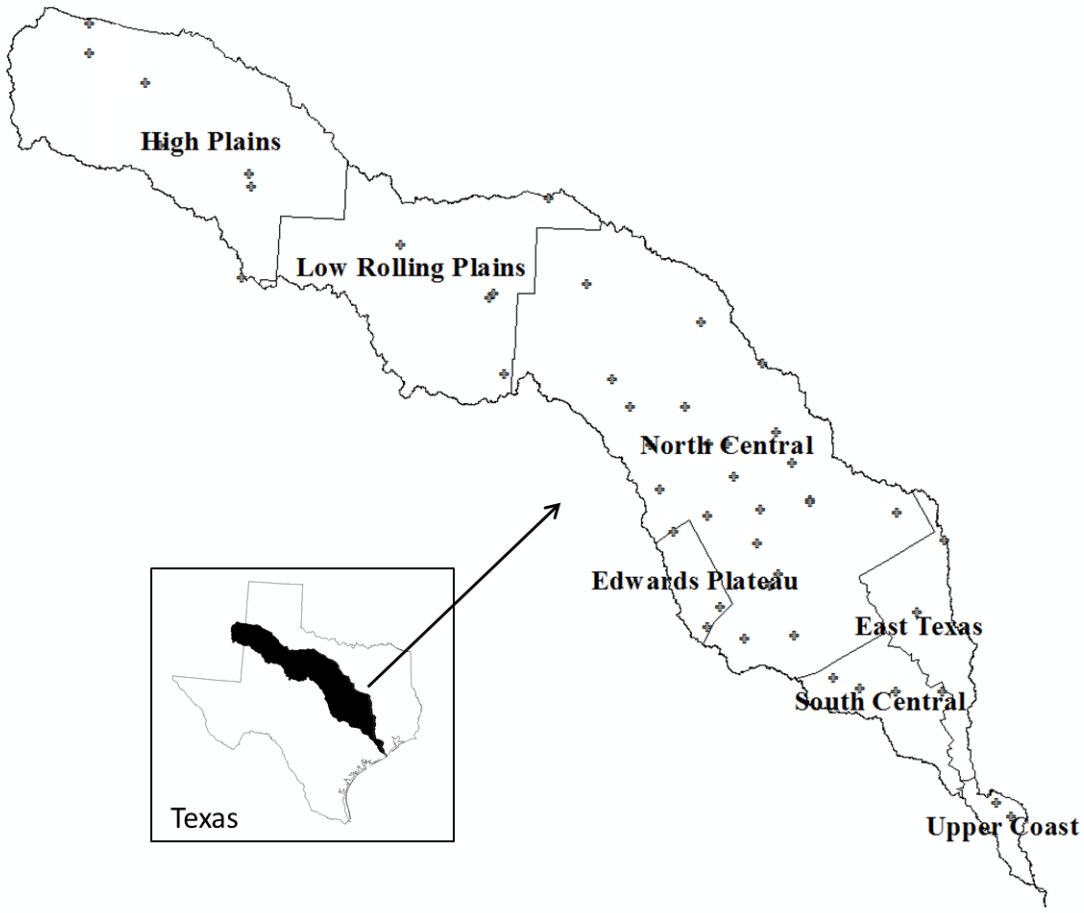

Figure II-1 46 rainfall gauge stations and 7 climate zones in BRB

2.5 Methods of PMP estimation

The most common methods to estimate PMP are hydrometeorological and statistical (Beauchamp et al., 2013; Casas et al., 2011). In this study, the PMP products from two hydrometeorological (e.g. storm maximization) methods, HMR-51 (Schreiner and Riedel, 1978) and Texas Commission on Environmental Quality (TCEQ, 2016) were adopted for comparison. Then, we calculated PMP from two statistical methods (Hershfield and site-specific methods). A short discussion of these methods is given below.

2.5.1 Hydrometeorological method (HMR-51)

HMR-51 adopted the hydrometeorological PMP estimation which refers to the process of increasing storm rainfall depth for the storm location and season for higher atmospheric moisture than the actual storm (Schreiner and Riedel, 1978). The precipitable water at the target site is maximized and the PMP estimation is based on following equation:

$$PMP = \frac{W_{max}}{W_p} \times P_a \quad (1)$$

where P_a = the observed precipitation depth, W_p = the precipitable water in the air column, and W_{max} = the maximized precipitable water. Moisture maximization involves maximizing the meteorological conditions (e.g. precipitable water and moisture content) that control the occurrence of convective precipitation (Chavan and Srinivas, 2015). The transposition adjustment is applied to relocate the precipitation values with the ratio of the precipitable water for maximum 12-hr persisting dew point for the transposed location

where the actual storm takes place (Schreiner and Riedel, 1978). This method assumes that a region has homogeneous meteorology and topography (Salas et al., 2014). The main assumption in the estimation of PMP was that the optimum combination of available moisture in the atmosphere and the efficiency of the convective mechanism in the storm that would lead to maximum precipitation events (Singh, 2016). The elements of PMP estimation comprised depth-area-duration analysis of massive storms, storm transposition, storm maximization, and envelopment (Salas et al., 2014). The methods using storm models relied on dew points, storm depth, and inflow and outflow fluxes of storm types (Collier and Hardaker, 1996). A study by Douglas and Barros (2003) argued that the PMP estimation was constrained by the length of record and the spatial resolution of rainfall gauge stations in the eastern United States.

2.5.2 Grid-based hydrometeorological method (TCEQ PMPs)

The recent grid-based PMP also adopted the hydrometeorological PMP estimation method. In the grid-based method, the National Weather Service (NWS) Next Generation Weather Radar (NEXRAD) data were used for storm analysis (TCEQ, 2016). Unlike HMR-51 PMPs, the geographic transposition factor was considered to define the geographical effect (elevation, terrain, and moisture source) on rainfall. TCEQ provides a tool to calculate the gridded PMP values for an area of interest using Geographical Information System (GIS) within Texas. This product provided the gridded PMP values for the project domain at a spatial resolution of 0.025 decimal degrees by 0.025 decimal degrees (approximately 6.5-square kilometers, on average).

The approach based on identifying major storms that occurred within the region considered transpositionable to any location within the domain. Each of the main storm types (local storms, tropical storms, and general storms) with extreme rainfall was investigated. The moisture content of each storm was maximized to produce extreme-case rainfall estimation at the location where storm occurred. Storms were then transposed to each grid cell with regions of similar meteorological conditions and topography. The adjustment factors were applied to each storm to represent the amount of rainfall that storm would have generated at the new location versus the original location. These adjustments consisted of the in-place maximization factor, the moisture transposition factor, and the geographical factor (TCEQ, 2016).

2.5.3 Hershfield method

The Hershfield statistical method (Hershfield, 1961a; Hershfield, 1965) is widely used in practice as an alternative to the physical method, especially when hydrometeorological data (such as humidity and dew point temperature) are not sufficiently available. The Hershfield equation can be expressed as

$$PMP = \overline{X_n} + K \cdot S_n \quad (2)$$

where $\overline{X_n}$ = the mean of annual maximum precipitation series, S_n = the standard deviation of annual maximum precipitation series, K = the frequency factor, and n = the sample size. The mean and standard deviation of annual maximum precipitation were calculated from the annual maximum time series for different durations (1-, 6-, and 24-hour) from each station. The frequency factor is selected from the Hershfield enveloping curve for

each station. The frequency factor was established from a large number of historical annual maximum precipitation data (2645 stations), about 90% of which were from the United States and the remaining 10% were from other parts of the world. A total of about 95,000 station-year data were used for the estimation of PMP. Further adjustment is made, based on the length of record, observation time intervals, and depth-area-duration relationship (Salas et al., 2014; WMO, 2009; Zhang et al., 2019). The adjustment is simply multiplying the fraction with respect to the given adjustment graph from Hershfield (1961a) based on the length of record. The Hershfield method is based on an equation similar to that of Chow (1951) where a quantile of the underlying distribution is expressed as a function of sample mean, sample standard deviation, and a frequency factor K (Chow et al., 1988) which is related to the skewness of data. In the Hershfield method, K was calculated using a large number of historical data of annual maxima which were not publicly provided. Then, the upper bound of K was determined from the frequency factor curve, which was always bigger than the actual K values from historical data (Salas et al., 2014).

2.5.4 Site-specific method

The site-specific method is restrictive to a certain watershed and generally provides smaller values than the PMP values generalized for a large area (e.g. HMR). This is because of a smaller number of rainfall events, which produce smaller PMP values. For example, the site-specific 24-hour PMP for the Cherry Creek Dam watershed (999.74 km^2) in Colorado, estimated by the U.S. National Weather Service, was approximately 25%

less than the HMR-52 value (Tomlinson et al., 2003). HMR-52 (Hansen et al., 1982) is the follow-up report of HMR-51 with the application of derived PMP estimates to serve as a guidance in the use of PMP. It is noted that HMR-52 relies on extreme rainfall events that cover two-third of the country in the east. The disagreement between HMR and site-specific method depends on the location. Formerly, the Hershfield method enclosed a broad range of frequency factors by a frequency factor curve (FFC) under different mean annual maximum precipitation (MAMP) values from extensive regions. However, this method did not consider variations in topography and climate of the region, which could lead to unreliable frequency factor obtained from the Hershfield FFC. The construction of a site-specific FFC is therefore necessary to obtain reliable PMP values.

Site-specific analysis is normally more accurate for PMP estimation based on the available data (Micovic et al., 2015). Since Hershfield method only provides a graphical solution from Hershfield curve (frequency factor curve), the actual values of annual maximum precipitation and the standard deviation of annual maximum precipitation (e.g. about 95,000 station-year data) were not given. Only the final frequency factor curve was provided. Therefore, this study developed the frequency factors from precipitation observations within the basin (site-specific) using the Hershfield frequency factor given by equation (3)

The site-specific frequency factor (K_s) was calculated for each station for different durations as:

$$K_s = \frac{X_m - \overline{X_{n-1}}}{S_{n-1}} \quad (3)$$

where X_m = the largest annual maximum precipitation value of a given duration, $\overline{X_{n-1}}$ = the mean excluding the highest value from the series, and S_{n-1} = the standard deviation excluding the highest value from the series. Once site-specific frequency factors are obtained corresponding to different durations, a site-specific enveloping curve is plotted using the Jennings relation (Jennings, 1950). The new K_s value is then selected from the enveloping curve for each station. In other words, each station with a corresponding MAMP is assumed to have the extreme possibility of K_s followed by the Hershfield method (Hershfield, 1965). The site-specific method follows the frequency factor (K) in the Hershfield method, but the site-specific frequency factor (K_s) is derived from observations in Brazos River basin.

The FFC was plotted by connecting a few upper points in the two-dimensional plot through a free hand sketch (Rakhecha et al., 1992) or a function. We used a function to build the enveloping curve in this study. For example, Rakhecha and Soman (1994) developed FFC for 417 stations in North Indian Region and Indian Peninsula using an empirical equation. The same method was adopted for 145 stations in Catalonia region in Spain (Casas et al., 2008; Casas et al., 2011). A typical form of equation for the fitted curve was

$$FFC = A \times exp(B \times MAMP) \quad (4)$$

where A and B denote the parameters of the enveloping curve which were estimated by regression fitting. A equals 20 which followed the beginning point of the Hershfield enveloping curve (Hershfield, 1961a; Zhang et al., 2019). FFC is the fitted curve from the scatters of K_s values (Figure II-2). This study assumed that this maximum threshold can

be applied to the FFC estimation for the consistency of application, because Hershfield found the frequency factor to be the upper limit of 20 in his analysis considering 95,000 station-years of annual maximum rainfall data from 2645 stations. It was also assumed that the enveloping curve decayed exponentially (Chavan and Srinivas, 2017). The constructed curve was shifted upward to enclose all the points on the upper boundary (Casas et al., 2008). To enclose all the points, +0.001 is added to the *B* value obtained from the regression fitting. In this study, the observation based enveloping curve was calculated for 1-, 6-, and 24-hour durations based on the available durations of Hershfield enveloping curve for comparison purposes. The value of parameter *B* from site specific enveloping curve equation is -0.01707 (1-hour), -0.01441 (6-hour), and -0.00891 (24-hour).

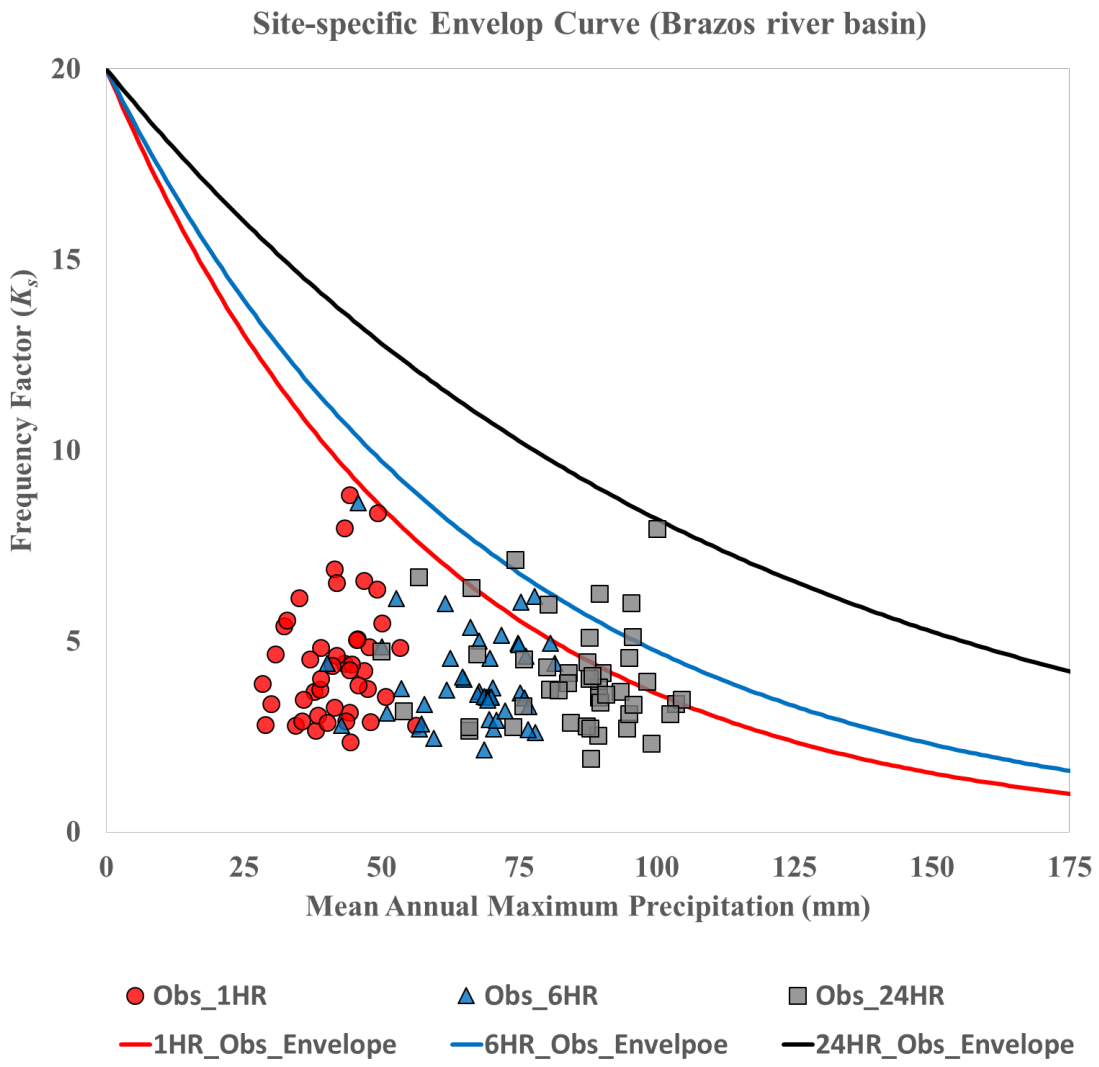

Figure II-2 Site-specific envelop curve for BRB

2.6 Historical precipitation extremes in BRB

It is necessary to investigate how often and how much extreme precipitation events occurred during the historical period for understanding the area of BRB. The recent TCEQ report provides a list of extreme storm events over Texas, which potentially affect the PMP values. The list contains all the storms analyzed by Storm Precipitation Analysis System (SPAS) from Applied Weather Associates (Iizumi et al., 2013).

There were six extreme storm events captured in BRB during the historical period: (1) On June 27th to 30th 1899, torrential rain fell at city of Hearne in Robertson County within BRB. The maximum rainfall was 876.3 mm during the storm event which resulted in ten million dollars of damage and 24 deaths (Life on the Brazos River, 2013; Roth, 2010). (2) On September 9th to 10th 1921, 812 mm of rainfall fell in 12 hours in the north of Thrall, Texas. The river overflowed its bank at least 2.1 m higher than ever before. The combination of unstable moist air mass and rapidly increasing wind velocity brought about 19 million dollars' worth of property damage (Lott, 1953). (3) The maximum recorded rainfall of 519 mm occurred during 48 hours on November 24th to 25th 1940 at Hempstead, Texas (Breeding, 1948). (4) On August 4th 1978, a total of 737 mm of rainfall was recorded during 24 hours at Albany in Shackelford County (Schroeder et al., 1979). About 1.8 m of water inundated the town of Albany and flood waters overtopped the spillway. The property damage was estimated at 110 million dollars and 33 people perished (Schroeder, 1987). (5) During October 11th to 13th in 1981 at Clyde, Texas, a storm produced rainfall of more than 508 mm. The rainfall caused the water level to rise by 4 m and the storage in Hubbard Creek Reservoir increased nearly twice (Wells et al., 1984). (6) The combination

of thunderstorm and heavy rain over already saturated lands in Tahoka caused 231 mm of rainfall during a 24-hour period on May 5th 2015 (Service, 2015).

Figure II-3 shows the historical annual maximum precipitation (AMP) over 46 stations in BRB for 1-, 6-, and 24-hour durations (1940-2013). Each box plot represents the maximum, mean, median, and minimum values of annual maximum precipitation from 46 stations. Since BRB has a large spatial variation of both precipitation and temperature, there are large differences among AMPs in a certain year. For example, the mean 1-hour AMP in 1992 from all stations was only 25 mm, however, the maximum 1-hour precipitation was 274.3 mm at Granger Dam in the same year which was nearly 10 times higher than the mean value. In 1994, the maximum 24-hour precipitation was captured as 388.6 mm at the Washington state park. Historically this was the first maximum 24-hour value above 300 mm from 1940 to 2013 amongst 46 stations. If we used the maximum precipitation values before 1993 to estimate the probable maximum precipitation without considering maximum record in 1994, the PMP values would likely be underestimated for the later period (after 1994). Therefore, including all observations within the catchment is essential to estimate the PMP accurately and reliably.

The standard deviation of AMP over 46 stations for each year was calculated for 1-, 6-, and 24-hour durations (Figure II-4). The average value of standard deviation for 24-hour (34.89 mm) was larger than the average value of standard deviation for 1-hour (20.37 mm). The linear trend of standard deviation of 6-hour and 24-hour AMP increased, while the 1-hour standard deviation of AMP decreased. Both trends were statistically significant at alpha of 0.05 level (1-hour, decreasing) and alpha of 0.1 level (6-hour and

24-hour, increasing) from Mann-Kendall test (Hamed and Rao, 1998). In recent years, the difference between 24-hour and 1-hour standard deviations has been increasing. The maximum standard deviation was captured in the same year as the maximum precipitation occurred (1-hour in 1992, 6-hour in 1992, and 24-hour in 1994) in. This is because the mean and standard deviation of AMP had a linear relationship during this period in BRB (Figure II-5). The average of AMP over 46 stations for each year was calculated for 1-, 6-, and 24-hour durations. 24-hour statistics had a stronger correlation than 1-hour and 6-hour statistics between the mean and the standard deviation of AMP. The slope of the linearly fitted line was the largest for 1-hour duration but it decreased as duration increased.

The role of maximum value in the annual maximum precipitation series was estimated using the coefficient of variation (Table II-1). The mean and standard deviation of AMP with and without the maximum value were calculated separately. The coefficient of variation (CV) after removing the maximum decreased (0.48 to 0.42 for 1-hour, 0.42 to 0.37 for 6-hour, and 0.42 to 0.8 for 24-hour) on average of 46 stations. Each station had a variation of CV values. Among durations, the maximum difference between CV with and without maximum values was 0.51 for 1-hour at Granger Dam. This station received an exceptional 1-hour maximum precipitation of 274.3 mm in 1992. The relationship between the mean annual maximum precipitation (MAMP) and PMP using the site-specific method was investigated (Figure II-6). The range of correlation was 0.40 to 0.57 between MAMP and PMP. Even though the values of PMP were correlated to MAMP,

PMP was not entirely dependent on MAMP, because PMP estimation also accounts for the standard deviation of AMP and frequency factors.

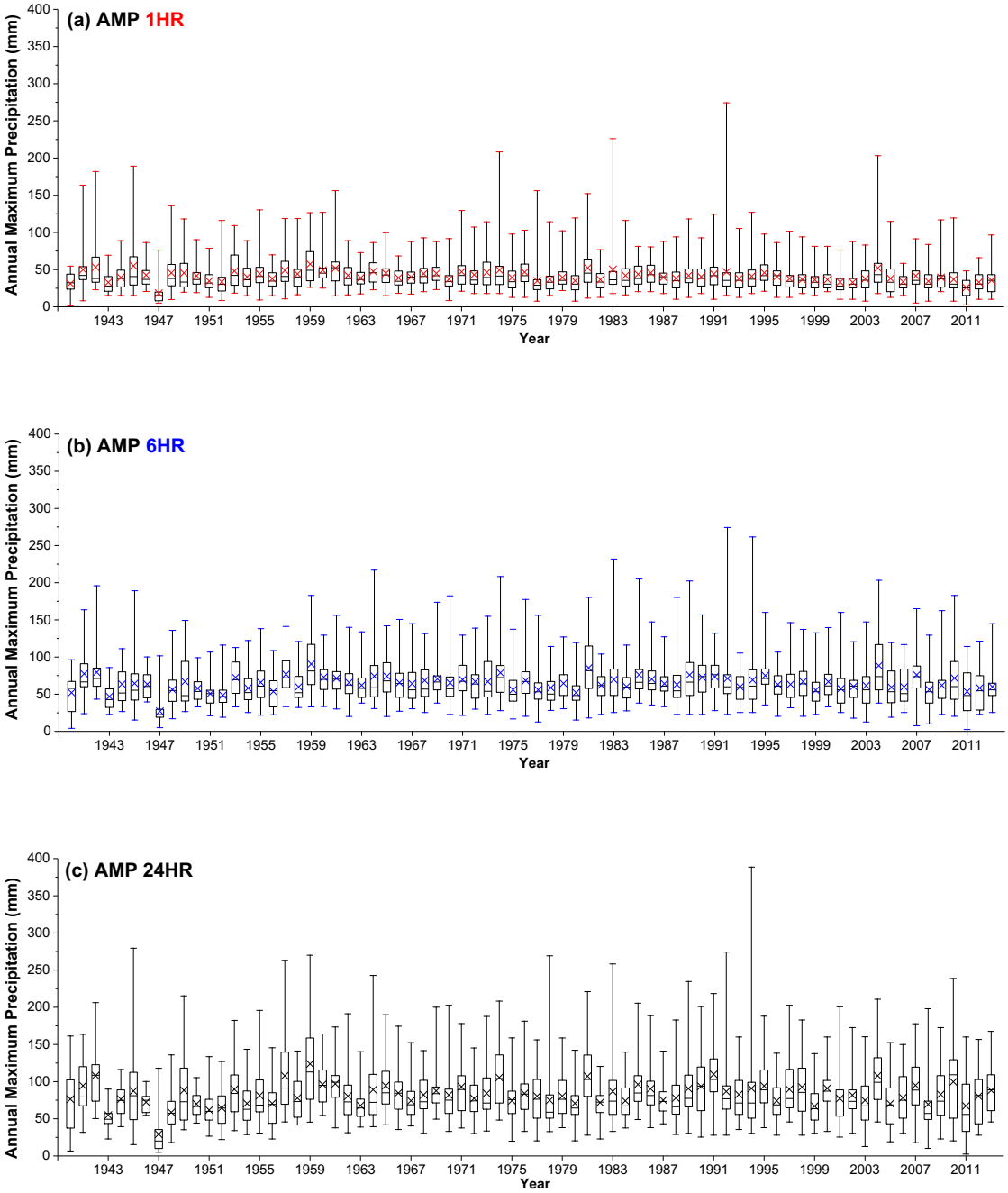

Figure II-3 Box plot of AMP 46 stations range for each year

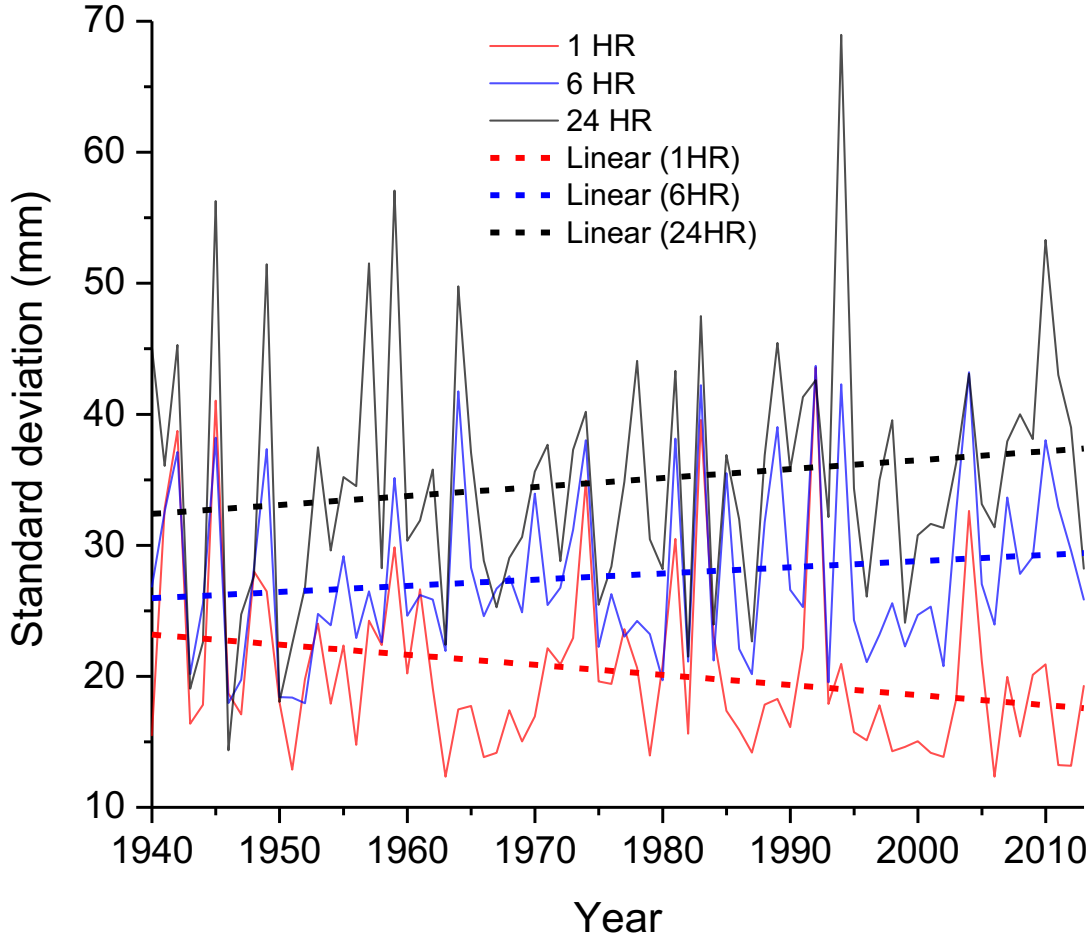

Figure II-4 Standard deviation of AMP in BRB

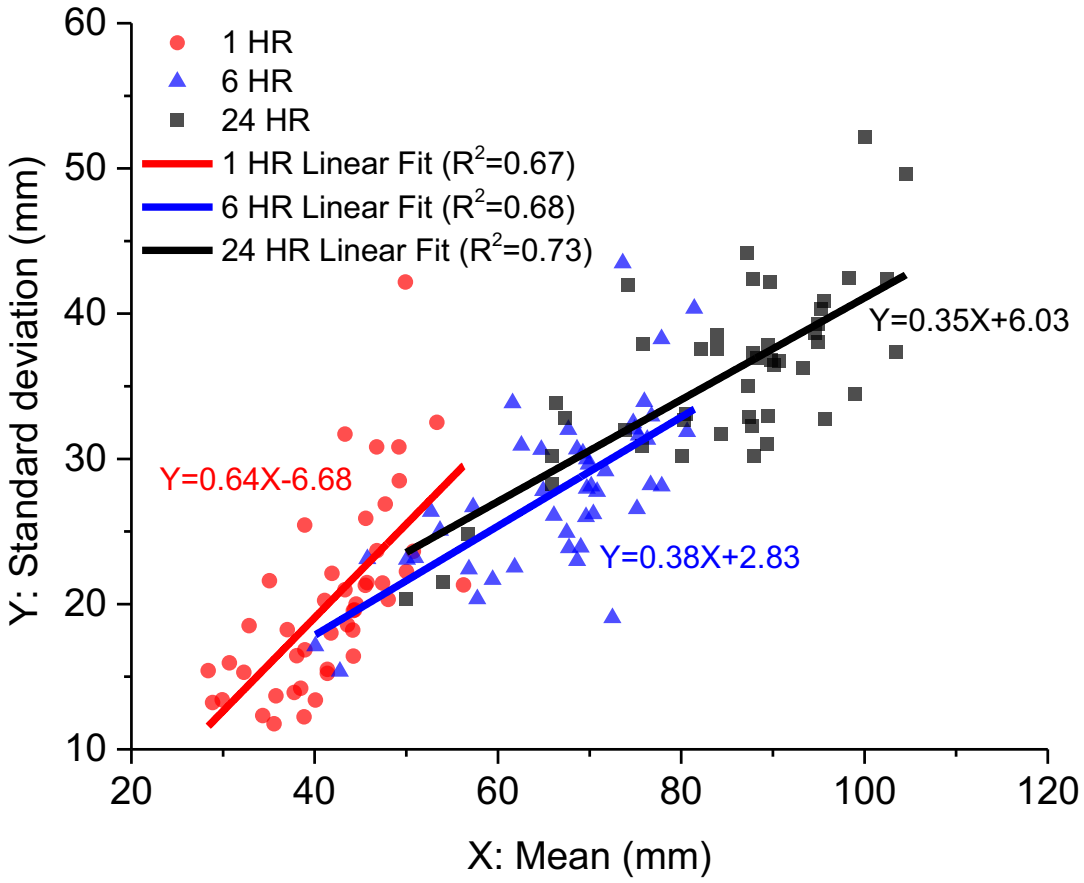

Figure II-5 Relationship between statistics in AMP

Table II-1 Mean, standard deviation, and coefficient of variation of AMP

	1-hour	**6-hour**	**24-hour**
Mean of AMP	41.81 mm	66.52 mm	84.85 mm
Standard deviation of AMP	20.23 mm	27.82 mm	35.78 mm
Coefficient of variation (CV)	0.48	0.42	0.42
	1-hour (without maximum value)	**6-hour (without maximum value)**	**24-hour (without maximum value)**
Mean of AMP	40.27 mm	64.60 mm	82.42 mm
Standard deviation of AMP	16.72 mm	24.13 mm	31.17 mm
Coefficient of variation (CV)	0.42	0.37	0.38

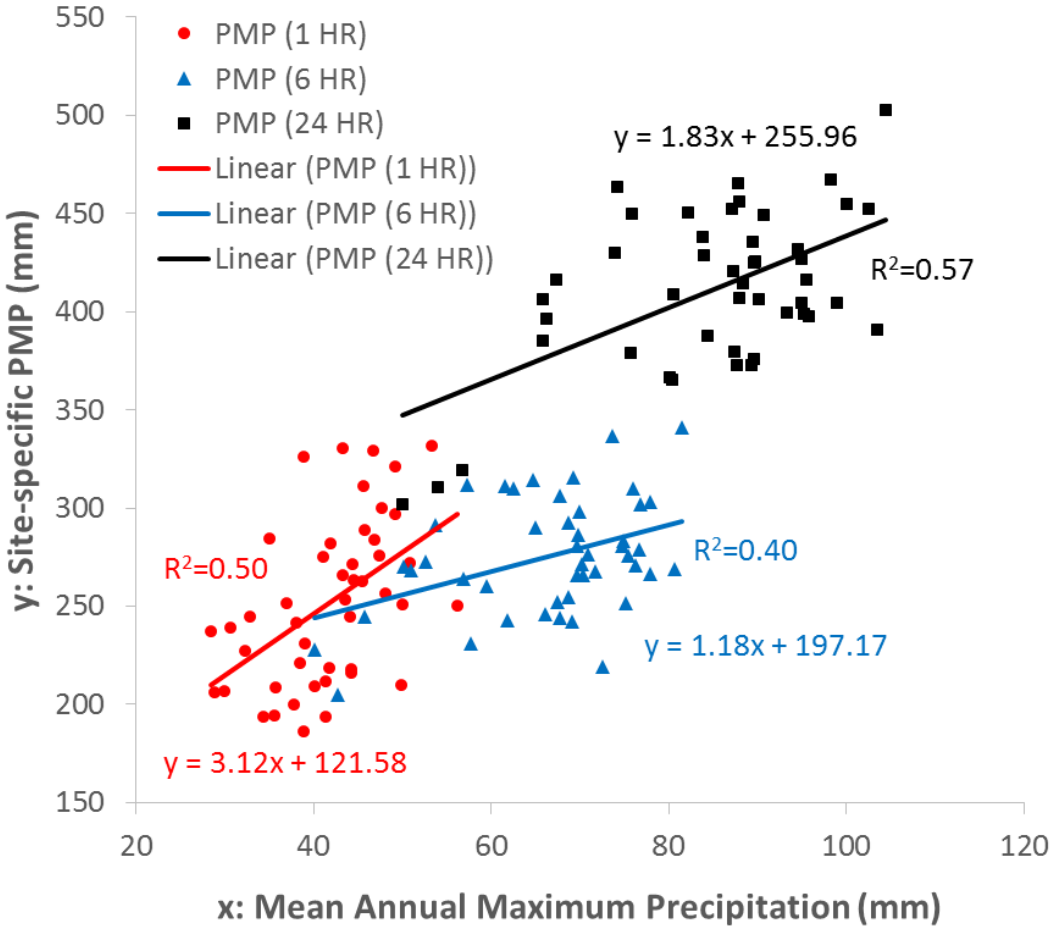

Figure II-6 Relationship between MAMP and PMP

2.7 Uncertainty analysis

2.7.1 Selection of methods

To compare different PMP values from different methods, the values should be for the same area, because PMP values are dependent on the given storm area by definition (Hansen et al., 1982; WMO, 1986). Since HMR-51 provided PMP values under certain areas, the four methods for PMPs were compared for the same area of 5,000 mi^2 as an example for 1-, 6-, and 24-hour durations; (1) HMR-51 and (2) TCEQ Grid PMP report as the hydrometeorological method, and (3) Hershfield method and (4) Site-specific statistical method. Beforehand, the Depth-Area-Duration curve for BRB was plotted, based on the records of HMR-51 storms on an area to compare PMPs accordingly (Figure II-7). This DAD curve was generated from HMR-51 report that provided the precipitation depths based on each duration (1-hour, 6-hour, 24-hour, etc.) and area (10 mi^2, 200 mi^2, 1000 mi^2, 5000 mi^2, etc.) of precipitation events. There were four points of reading for each duration and a fitted function was developed to find a relationship between area and depths of precipitation events. The purpose of this plot was to show how to manage PMP values under different areas. For example, we used this Depth-Area-Duration curve to handle Hershfield and Site-specific PMP estimations by multiplying the ratio of DAD curve, because Hershfield and site-specific PMP are point measurement values which need to be adjusted with respect to the area (WMO, 2009). Other than different methods, another possible source of uncertainty is the type of output. For example, HMR-51 is an isoheytal (a line drawn on a map connecting points having equal values) and TCEQ PMP is the grid type of values at the resolution of 0.025 degree (approximately 2.78 km), while

Hershfield and site specific methods have point outputs. For the consistency of comparison, 46 station (point) values and nearest values from the isoheytal map and grids were selected. Specifically, the PMP from gauge observations (Hershfield and site-specific) were point measurements, HMR-51 PMP values were given in a line drawn on a map, and the grid PMP was calculated at a resolution of 0.025 decimal degree. There were no conflicting rainfall gauge stations which fell into same grid of PMP.

Each marker for a duration denotes the mean value of 46 stations and each bar denotes the ensemble mean of 4 different PMP values accordingly for an area of 5000 mi^2 (Figure II-8). In overall PMP ensembles, HMR-51 values were nearly capped as the upper limit of PMP for all durations. Also, the HMR values were found to be overestimated in other regions, for example, by studies in Michigan-Wisconsin (Tomlinson, 1993) and Nebraska (Tomlinson et al., 2008). This was because the HMR values did not represent a specific location well and provided generalized rainfall values that were not basin-specific and tended to represent the largest PMP values for broad regions. The possible reasons for disagreement between HMR-51 and TCEQ Grid PMPs were the inclusion of new storm observations, improved analysis procedures (radar precipitation with higher temporal and spatial resolutions), and the use of GIS software (Tomlinson and Kappel, 2009) in the TCEQ Grid method.

After HMR-51, the Hershfield values were overall the second largest group among PMP values. The difference between the two statistical methods (Hershfield and site-specific) values increased as the duration increased. Due to the significant disagreement between PMP estimations, there was considerable uncertainty in the selection of a PMP

estimation method. It may therefore be more informative to provide the ensembles of four different PMP methods with their uncertainty range than using a single method of PMP. Using the ensembles of PMP for each duration, the design criterion was calculated for each level of hazard. As FEMA (2012) suggested, different levels of hazards (low, significant, high, and severe; 25%, 50%, 75%, and 100% of PMP) were computed for guiding decision making in dam design (Table II-2). Each hazard level denotes the percentile value (e.g. 100% refers to the maximum value from the ensemble) from four different PMPs at each duration, because many regulatory agencies do not just use the maximum PMP for design in the U.S., for example, 50 to 75% of PMP is used in Missouri, 45 to 90% of PMP in Colorado, and 40% of PMP in Kansas.

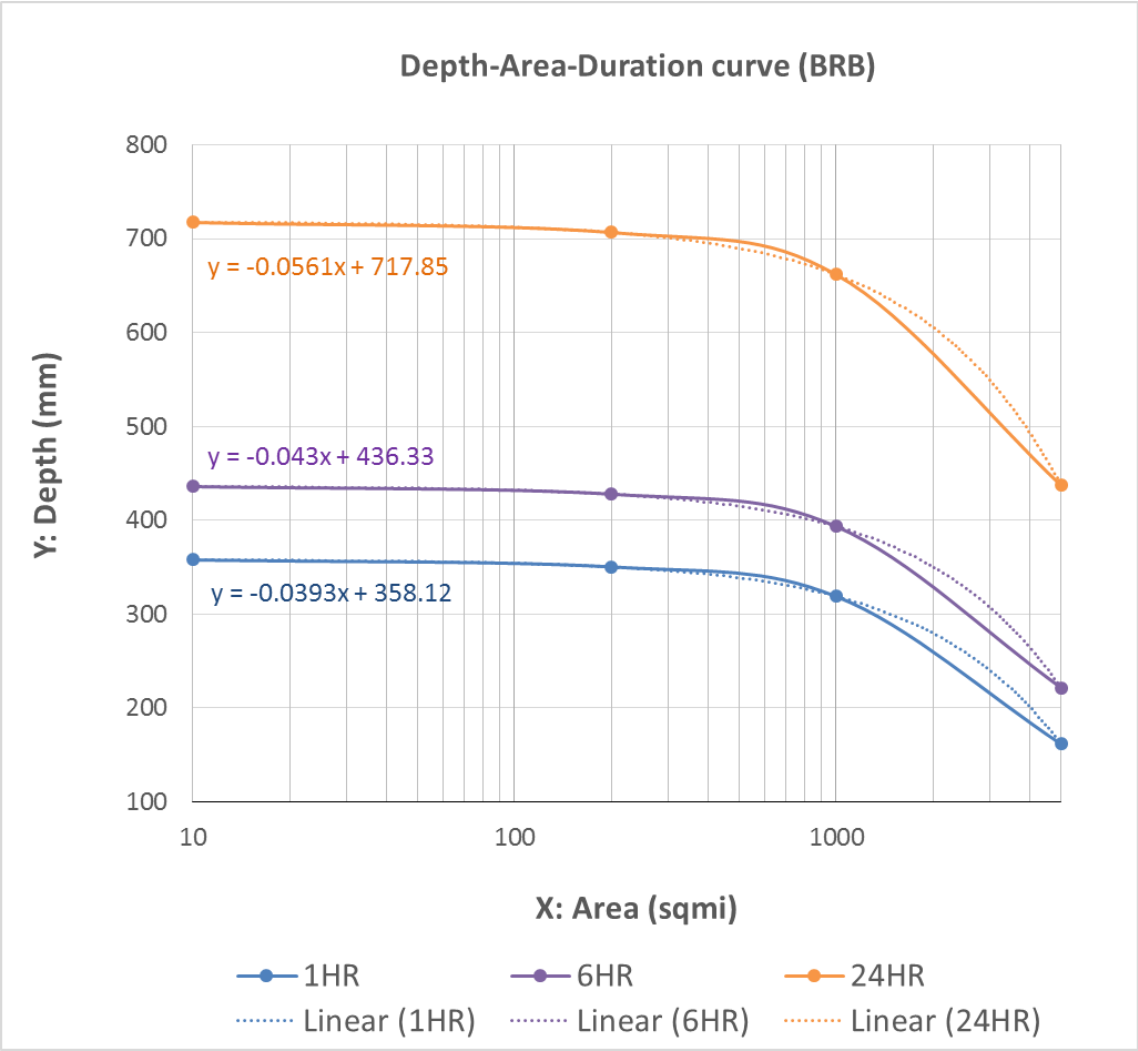

Figure II-7 Depth-Area-Duration curve for BRB

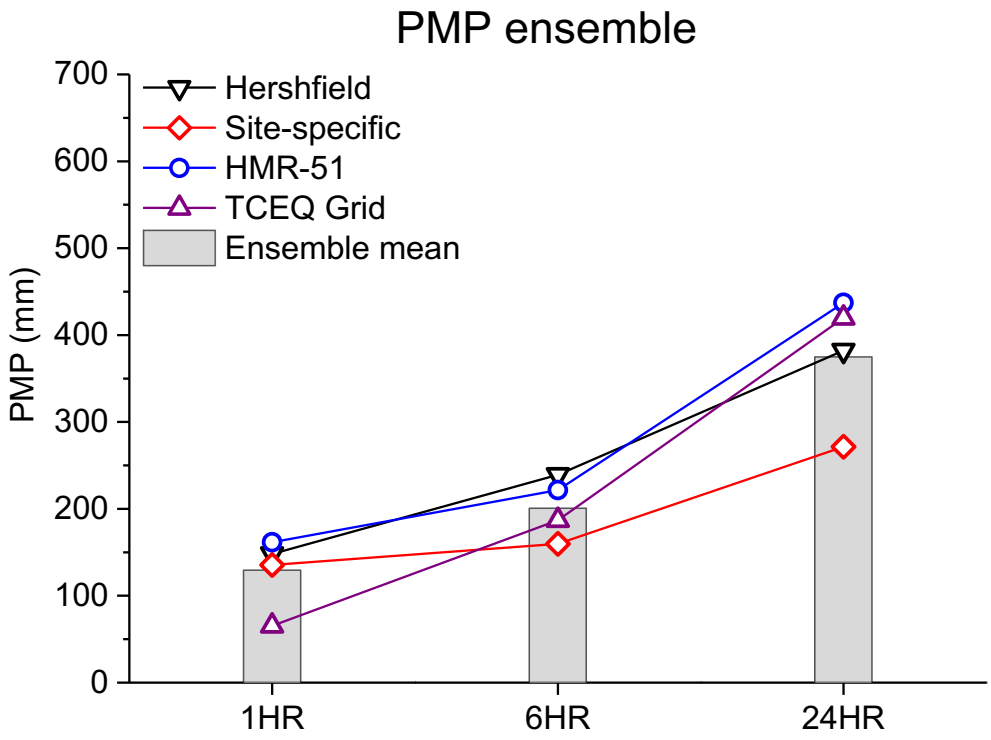

Figure II-8 Effect of PMP method selection in BRB

Table II-2 Design criteria from PMP ensembles in BRB

Criteria	PMP (mm)		
	1-HR	**6-HR**	**24-HR**
Severe Hazard (100% of PMP)	161.62	239.25	437.21
High Hazards (75% of PMP)	156.54	225.80	427.82
Significant Hazards (50% of PMP)	127.61	201.86	377.62
Low Hazards (25% of PMP)	98.67	177.93	327.42

2.7.2 Effect of topography

Many studies have suggested that the most appropriate values of frequency factor should be according to the climatic region of the study area (Casas et al., 2008; Dhar et al., 1981; Mejia and Villegas, 1979). Therefore, this study compared PMP values for different climatic zones using the site-specific method. The effect of topography at a particular location may vary, depending on the type of storm (TCEQ, 2016). In this study, the uncertainty due to the effect of topography was defined as the coefficient of variation of PMP values within climate zones. Because Texas, including BRB, has a spatial pattern with a decreasing precipitation gradient from east to west, that greatly influences land use and river flow (Rajsekhar et al., 2013).

Due to a decrease in moisture content from east to west by onshore flow and intermittent seasonal intrusions of continental air (Larkin and Bomar, 1983), a large precipitation gradient was captured under different climate zones in Texas. The National Climatic Data Center divides Texas into 10 climate divisions (TWDB, 2012). Each division represents regions with similar characteristics, such as vegetation, temperature, humidity, rainfall, and seasonal weather changes. They are commonly used to assess climate characteristics across Texas. There are seven climate zones from the upstream to the downstream of BRB. Since some climate zones only cover a small number of rain gauge stations, we re-grouped them into four zones according to their geographical position for the sake of convenience. The four zones consist of Zone 1 (High Plains), Zone 2 (Low Rolling Plains), Zone 3 (North Central and Edwards Plateau), and Zone 4 (East Texas, South Central, and Upper coast).

Each bar for a duration denotes the mean value of PMP within the same zone (Figure II-9a). Zone 2 had the largest PMP values among different zones, while Zone 1 had the smallest PMP in the group. Even though Zone 1 and Zone 2 were next to each other, their mean PMPs for each duration were considerably different. For example, the mean of 1-hour PMP in Zone 1 was 126.28 mm and the mean of the same duration PMP in Zone 2 was 144.33 mm which was 14% greater than in Zone 1. Also, the mean of 24-hour PMP in Zone 1 was 239.19 mm and the mean of the same duration PMP in Zone 2 was 284.04 mm which was 19% greater than in Zone 1. The PMP values varied in different climate zones without a certain pattern along the zones (e.g. upstream and downstream). The spatial distribution of precipitation in Texas, including BRB, resulted in the PMP gradients along with different climate zones.

The variability of PMPs under different zones were shown in each bar for a duration as the standard deviation of PMP within the same zone (Figure II-9b). The pattern of PMP variability was irregular for the results under different zones and durations. The maximum standard deviation was captured in Zone 1 for 24-hour PMP, while the minimum standard deviation was also obtained in the same zone for 1-hour PMP. In Zone 1 and Zone 4, the standard deviation increased as PMP duration increased, however, this relationship reversed in Zone 2. Even though there was no specific trend of its variability in different climate zones, there existed a topographical discrepancy. For all durations, the downstream of BRB tended to have large mean and standard deviation values. Because this region is relatively wetter than the upstream and receives more rainfall events, the downstream is also close to the Gulf of Mexico which frequently experiences floods. For

example, an average of four to five days of flooding has occurred each year in Harris county from 1996 to 2015 (NOAA, 2017).

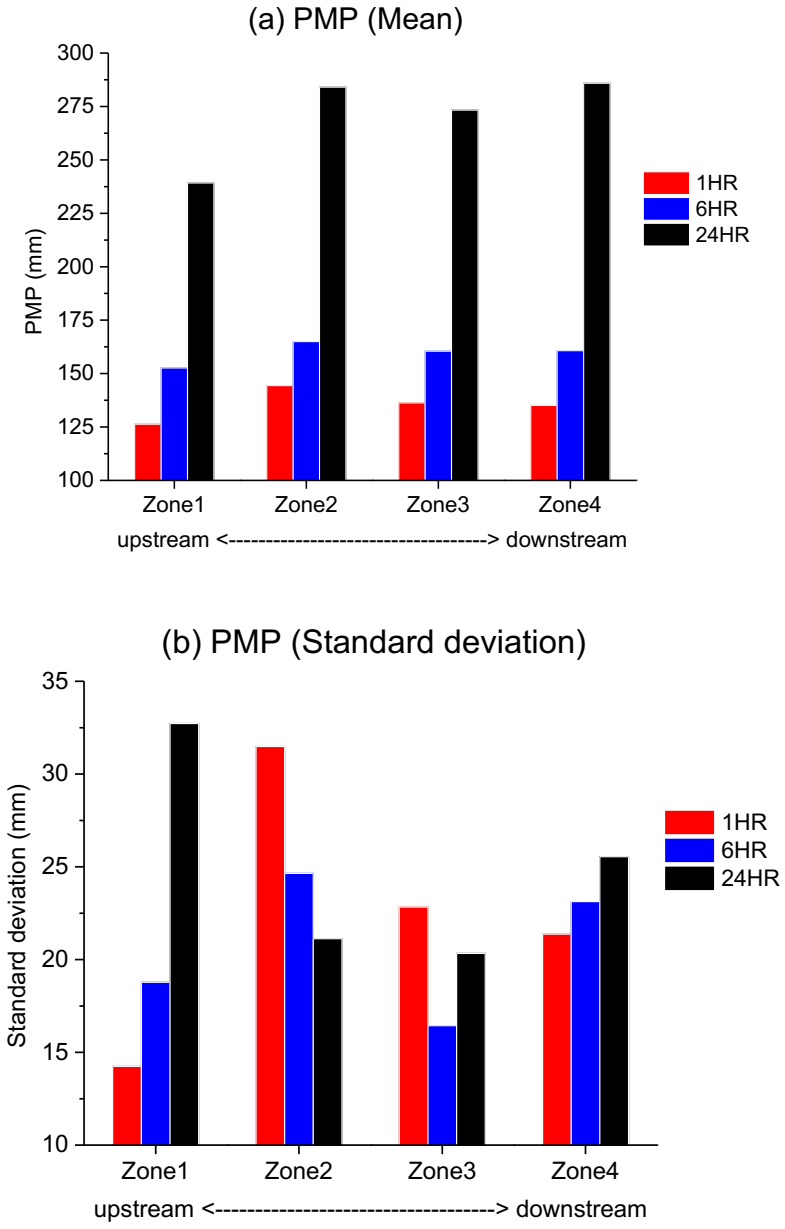

Figure II-9 Effect of topography on PMP estimation

2.7.3 Effect of non-stationarity (historical period)

The effect of non-stationarity was examined during the historical period, because the variability of annual maximum precipitation over time was observed (historical precipitation extremes in BRB). To examine any systematic change in the magnitude of precipitation, the record precipitation which can be the value from any station with the largest magnitude among stations every year in BRB was calculated. Each point denoted record precipitation in each year. There were 74 years of data length (1940-2013). First 37 years (P1: 1940-1976) and next 37 years (P2: 1977-2013) were separated to compare the mean of record precipitation between periods of the same data length. Figure II-10a showed that the mean of first period (P1) was 169.5 mm and the mean of next period (P2) was 189.0 mm. There was 19.5 mm of difference between two period mean values. To test whether these two mean values were statistically different, a two sample t-test (Snedecor and Cochran, 1989) was implemented with the null hypothesis that the population mean values were equal for the two samples. Then we rejected the null hypothesis and concluded that the two population means were different at the 0.10 significance level. In addition, the rank of each record precipitation value was calculated and took the average rank in each period (e.g. Rank 1 was the largest and Rank 74 was the smallest value). From figure II-10b, the average rank of the first period (P1) was 41.0 and of the next period (P2) was 33.8. The averaged rank also showed that the later period (P2) had a larger record of precipitation than the first 37 years (P1). Thus, there existed a systematic transition between two periods during the historical period in BRB. This may lead to a potential increase of PMP values in the future if non-stationarity persisted similar

to the historical period. Therefore, we examined the change of PMP (24-hour) between periods using the site-specific method.

There were 46-station precipitation data sets used in BRB. However, 6 stations did not have enough data during P1 for which we were unable to calculate PMP using the statistical method. Thus, 40 stations which had data for both periods were used in this PMP value comparison between P1 and P2. Statistics (mean and standard deviation) were calculated separately and PMPs were computed based on these two periods' statistics. Each station had a different trend of PMP change between the two periods (Figure II-11). For example, the largest increase of 396.6 mm (+121.1%) was captured at 'Stamford 2' station and the largest decrease of 225.0 mm (-58.1%) was observed at 'Indian Gap.' It was observed that the mean (+1.06 mm) and the standard deviation (+3.61 mm) of AMP in BRB increased from P1 to P2. The overall PMP increased from 390.4 mm to 412.7 mm (+22.31 mm) on average in BRB.

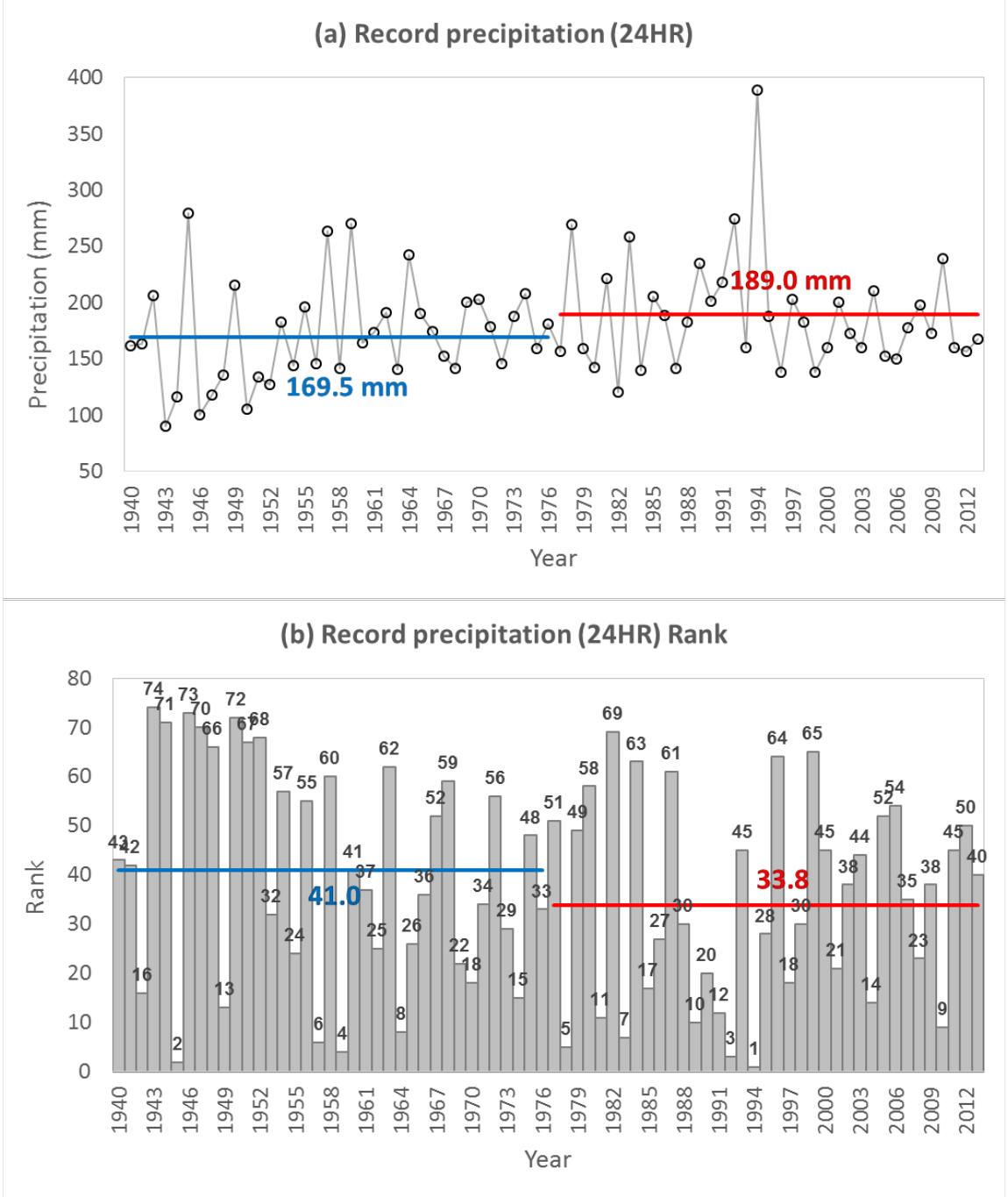

Figure II-10 Non-stationarity of record precipitation

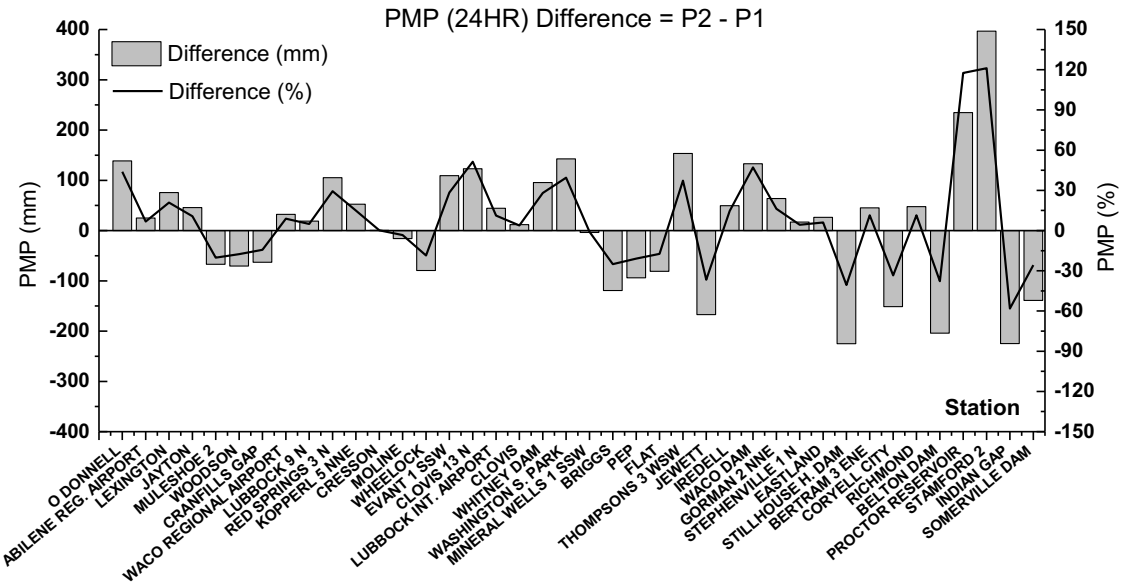

Figure II-11 Effect of climate change on PMP estimation

2.7.4 Relative contributions of sources of uncertainty

The uncertainty from each source was compared in terms of the PMP value change (Δ) for 1-, 6-, and 24-hour durations. The PMP value in this figure is the mean of all locations in BRB. For consistency of comparison, the site-specific method was set as the baseline and the maximum difference from each source of uncertainty was then estimated. In 'selection of method,' the difference between the maximum and minimum PMP values from different methods was calculated (MTH). In 'effect of topography,' the difference between zone 1 and zone 4 of PMP mean values was computed (TPO). In 'effect of non-stationarity,' PMP was calculated using the mean and standard deviation of AMP from Period 1 (1940-1976) and Period 2 (1977-2013) to see how much PMP will be potentially altered (NST). However, the change of PMP increased at 25 stations and the rest of them decreased from Period 1 to Period 2. To avoid canceling each other out and see how much they shifted, we calculated the absolute difference of PMP values between two periods and used the average of all stations from BRB. The total uncertainty was defined as the sum of uncertainties from the three sources (Δ = MTH + TPO + NST) where the site-specific method was set as a baseline. In other words, how much PMP estimated from the site-specific method was changed from three different uncertainty sources. Their percentage contributions were compared among the four sources of uncertainty within the total uncertainty (Figure II-12).

It was found that 'selection of method' showed a remarkable contribution to the uncertainty of PMP estimation. The second largest uncertainty contribution to PMP estimation was by 'effect of non-stationarity.' This implied that it was a more secure way

to adopt multiple PMP methods and to use up-to-date observations, because the uncertainty from these two sources considerably affected the estimation of PMP values. The least contribution (8.0% to 15.1%) was found from 'effect of topography.' There existed a discrepancy of PMP under different zones, however, the effect of climate zone within the same basin did not considerably affect the PMP estimation. Therefore, the uncertainty of PMP estimation was more sensitive to the existing observation statistics (mean and standard deviation) and the selection of method rather than the PMP estimation from different climate zones.

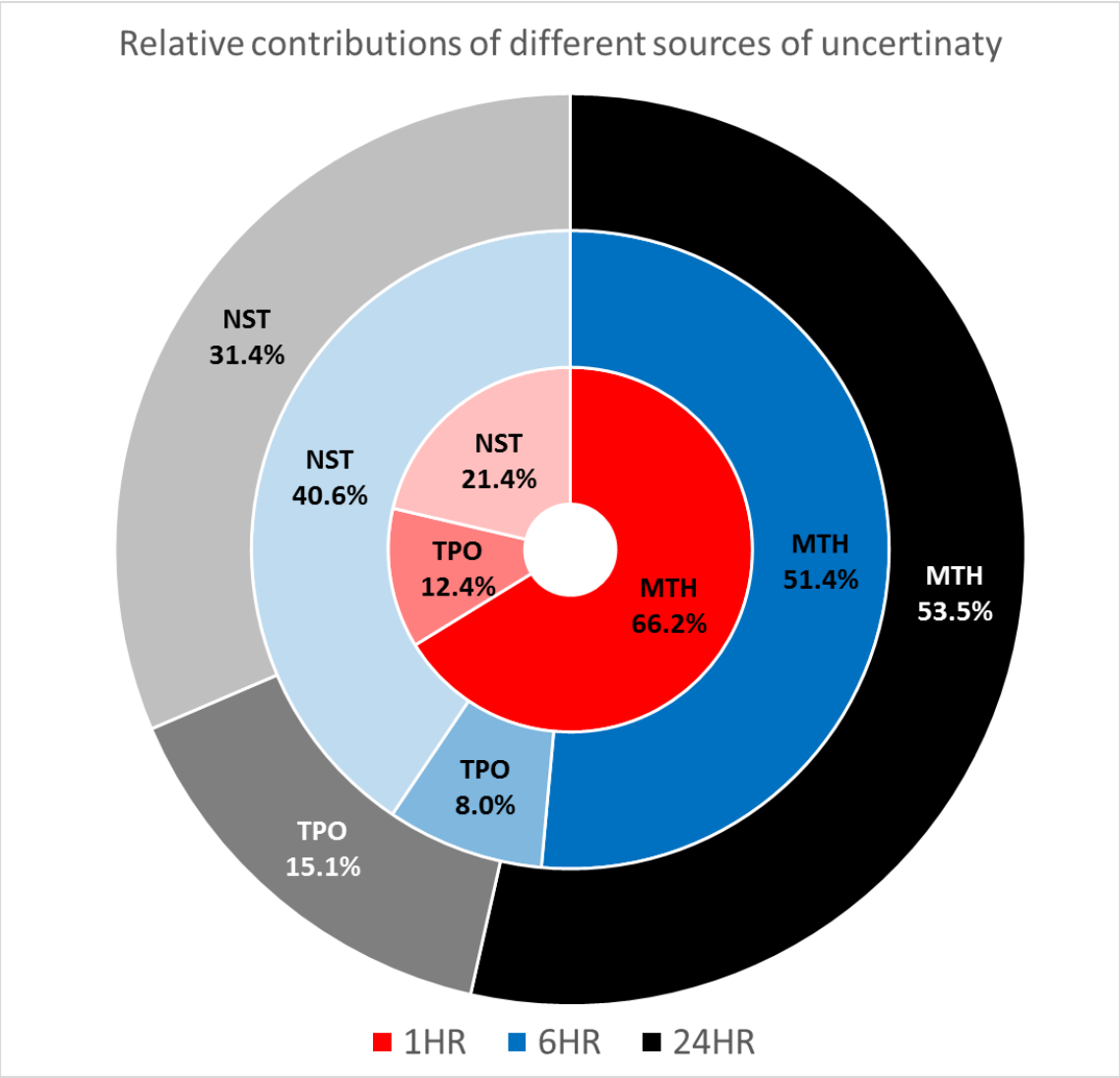

Figure II-12 Relative contributions of different sources of uncertainty

2.8 Conclusion

The estimation of PMP is a key consideration for dam safety. However, PMP calculation involves multiple sources of uncertainties, including climatic variables, non-stationarity, topography, and method of computation. Due to the inherent lack of precipitation data in the historical record and PMP calculation methods (HMR-51 and Hershfield), uncertainty exists in the estimation of PMP. To overcome the lack of available data, a simple statistical method (site-specific) which is computationally less expensive can produce a reliable and reasonable range of PMP values. The PMP estimate can be lower than HMR-51 Report when the proposed site-specific PMP method is used, which is likely to be economically beneficial for the design of hydraulic structures. Since PMP is the theoretical value and there is no true value for PMP, the uncertainty of PMP estimation from different methods is not negligible. We suggest to use the ensemble of PMP values (such as percentile of PMP) rather than using a single method. Under different climate zones, the pattern of PMP variability was irregular for the results and there existed a topographical discrepancy.

'Selection of method' is manageable (predictable) and 'effect of topography' does not change over time. Unlike the other two uncertainty sources, 'effect of non-stationarity' is not controllable. The contribution of each of the uncertainty sources to PMP estimation was found as 53.5% (selection of method), 31.4% (effect of non-stationarity), and 15.1% (effect of topography) in 24-hour PMP. The uncertainty of PMP estimation was more sensitive to the existing observation statistics and the selection of method rather than the PMP estimation from different climate zones within the same basin. Results showed that

extreme precipitation in Brazos River basin showed non-stationarity which affected PMP shift during the historical period. This implies that there is a potential increase of PMP values in the future if non-stationarity of extreme precipitation persists similar to the historical period.

We can only estimate PMP using historical observations and it is still challenging to predict future PMP using future scenarios. PMP estimation, including the most recent precipitation records, can help reduce the uncertainty from climate change and non-stationarity, while HMR-51 and Hershfield used outdated data which can cause misleading information for the current and future hydrometeorological conditions in designing flood–related projects. Unless the recent precipitation data are used in PMP estimation, it is likely to obtain misleading PMP information. By overlooking the impact of climate change and non-stationarity, the reliable estimation of PMP and the longer lifetime of dams cannot be ensured. Another limitation of this study is that our findings are site-specific results and may not be transferrable to other locations. However, Hershfield (global coverage) and site-specific (basin scale) methods still showed a disagreement in the estimated PMP. Even though our results are limited to site-specific, PMP estimation using adequate data for certain areas is required.

CHAPTER III

RELATIONSHIP BETWEEN EXTREME PRECIPITATION AND CLIMATIC CYCLES IN TEXAS

3.1 Synopsis

Texas has a spatial rainfall pattern with a decreasing gradient from east to west that greatly influences land use, vegetation, and river flow. This variation leads to major floods that cause huge losses of life and agricultural property. To minimize risk of failure, dams, reservoirs, nuclear power plants, and flood protection works are designed using Probable Maximum Precipitation (PMP) which is also used for rehabilitating old existing dams. PMP estimation has received significant attention recently, because meteorological extremes are projected to become more frequent, severe, and uncertain with climate change, and their controlling mechanisms seem to be global-scale climatic cycles. This study examines how global scale climatic indicators and regional precipitation extremes are related. First, statistically estimated PMPs (Hershfield and site-specific) 100-year precipitation obtained from distribution fitting are compared. Second, the impact of climatic cycles, including Atlantic Multidecadal Oscillation (AMO), North Atlantic Oscillation (NAO), Pacific Decadal Oscillation (PDO), Pacific North American Pattern (PNA), and Southern Oscillation Index (SOI), on extreme precipitation is investigated. Third, the effect of El-Niño and La-Niña on extreme precipitation is analyzed using El-Niño–Southern Oscillation Precipitation Index (ESPI). Finally, relations between geographical characteristics and precipitation extremes are quantified. Results show that

the annual cycle of monthly extreme precipitation is affected by warm and cold phases of climatic cycles. El-Niño years receive 16% more precipitation (72-hour) than do La-Niña years. At farther distance from the coastline, there is less precipitation and less variability in extremes. These findings help gain broader insights for understanding extreme meteorological events.

3.2 Introduction

Extreme precipitation events lead to disastrous floods which cause huge damages to infrastructure, livestock and agricultural systems, and disrupt the society (Durodola, 2019; Mishra and Singh, 2010; Papalexiou and Montanari, 2019). For example, storm water inundates urban areas, erodes soil, and carries wastes, such as chemicals and nutrients, into receiving water bodies (Mishra and Singh, 2010; Parker et al., 2010; Rosenzweig et al., 2002). To minimize the risk of failure due to extreme precipitation, major hydraulic structures, such as dams and reservoirs, nuclear power plants, and flood protection works, are designed, and old existing dams are rehabilitated, using Probable Maximum Precipitation (PMP). PMP is theoretically the maximum possible precipitation for a given duration under likely meteorological conditions. There did not seem to have been much attention paid to the assessment of PMP under changing climate (Beauchamp et al., 2013) until the World Meteorological Organization (WMO) report mentioned "PMP and climate change" which indicates that climate change could lead to an increase of PMP (WMO, 2009). It is generally accepted that climate change does have an impact on severe precipitation extremes and its effect should therefore be considered (Simonović, 2012).

Kunkel et al. (2013) examined the effect of potential climate change on PMP along with a significant future increase in mean and maximum precipitation. PMP values would increase in the future due to large atmospheric moisture content and moisture transport into storms.

In Texas, there have been severe extreme events in recent years, including hurricanes Bill, Cindy, Harvey, and Imelda. These events commonly passed through the southeastern part of Texas close to the coast. Precipitation of about 330 mm in 24 hours in 2015 (Bill), 474 mm in 5 days in 2017 (Cindy), and exceptionally within the same year, 1539 mm in 4 days in Houston area (Harvey) was observed. Hurricane Harvey was the severest extreme event in Texas. During August 25–30, 2017, hurricane Harvey struck Texas (particularly Houston) and generated extreme precipitation causing extensive flooding. The return period of the highest observed three-day precipitation amount (1043.4 mm at Baytown) was more than 9000 years (van Oldenborgh et al., 2017). The tropical storm originating from the western Caribbean and the southern Gulf of Mexico passed through South Texas in June 18-21, 2018. The record rainfall of 508 mm during 72 hours was measured at the Corpus Christi (NWS, 2018). The tropical storm Imelda with wind speed of 64 km/h caused catastrophic flooding in southeast Texas in September 17-19, 2019. A total amount of 1,102 mm was recorded in Jefferson County with five casualties (NCEI, 2019; Stanglin, 2019; Zelinsky, 2019). In terms of damage, floods caused an average of 82 deaths and $7.9 billion in property damage annually across the U.S. between 1985 and 2014 (Downton et al., 2005). Texas has the highest incidence of flood-related fatalities among all 50 states (Sharif et al., 2010) and is the only state that

has reported flood-related fatalities in every single year between 1959 and 2008 (Sharif et al., 2014).

National Centers for Environmental Information of National Oceanic and Atmospheric Administration (NOAA) reported that there was an increasing trend in precipitation and temperature in most of the basins in Texas (NOAA, 2018). It is found that more rapid intensification of extreme precipitation is captured in the tropics and subtropics mainly due to the effect of atmospheric circulation changes (Norris et al., 2019). Climate change (Pendergrass, 2018; Risser and Wehner, 2017; van Oldenborgh et al., 2017; Wang et al., 2018) and climatic cycles (Bhatia et al., 2019; Schlef et al., 2019) play a major role in increasing the intensity of precipitation. Recent climate modeling studies suggest that extreme precipitation events will be intensified during the 21st century at continental to global scales (Fischer and Knutti, 2016; Li et al., 2019; Pendergrass, 2018). Furthermore, extreme precipitation results from various pressure and sea surface temperature anomalies at annual to multi-decadal cycles (Hu et al., 2011; Quadrelli and Wallace, 2004; Renard and Lall, 2014) that are characterized by certain atmospheric or oceanic patterns of global scale climatic cycles (Guirguis et al., 2015; Tian et al., 2017; Trenberth et al., 2006). An increasing number of studies have investigated the variations in climatic cycles and related impacts on meteorological extremes in South America (Folland et al., 2001; Hill et al., 2011; Silva and Ambrizzi, 2006) and North America (Bhatia et al., 2019; Enfield et al., 2001; Hu and Feng, 2012). Kripalani and Kulkarni (2001) found that the climatic cycles were the leading drivers of precipitation extremes and their spatial and temporal variability. The climatic cycles have two different phases

(warm and cold) and their differences are known to remarkably affect the regional hydrologic cycle (Brugnara and Maugeri, 2019; López-Moreno et al., 2011; Mo, 2010; Tatli and Menteş, 2019). However, the effect due to different phases of climatic cycles on meteorological regimes has not been well documented for Texas.

The climatic cycles related to Atlantic and Pacific Oceans that are important for Texas are: Atlantic Multidecadal Oscillation (AMO), North Atlantic Oscillation (NAO), Pacific Decadal Oscillation (PDO), Pacific North American Pattern (PNA), and Southern Oscillation Index (SOI).

AMO is the multi–decadal scale oceanic temperature phenomenon (Kerr, 2000) which represents multi–decadal scale Sea Surface Temperature (SST) fluctuations in the Atlantic Ocean in mid– to high–latitude zones (Curtis, 2008). Texas is found to be strongly connected with AMO (Nogueira and Keim, 2010) and the weather stations with higher total precipitation or greater positive total precipitation anomaly are likely to receive extreme precipitation in the cold phase of AMO in the humid sub-tropical climate region (Bhatia et al., 2019).

NAO is a sub–annual to decadal scale low–frequency fluctuation in the strength of surface westerly climate across the northern hemisphere extratropical atmosphere on the large–scale movement of atmospheric mass (Greatbatch, 2000). It is based on the anomalies in sea level pressure between Icelandic low–pressure zone and subtropic atmospheric high–pressure system centered over the Azores (Ottersen et al., 2001). This climatic phenomenon results in negative precipitation anomalies in Texas (Parazoo et al., 2015). The cold and warm desert/semi-arid climate regions of Texas have been found to

be influenced by NAO (Bhatia et al., 2019) mainly due to the average temperature and temperature anomalies in the months of extremes.

PDO is the Pacific decadal variability in Northern Hemisphere climate, with temperature anomalies in the central North Pacific zone surrounded by anomalies of opposite sign in the Alaska gyre, off the coast of California, and toward the Tropics (Schneider and Cornuelle, 2005). In the critical summer season in Texas, PDO is closely correlated to streamflow of the Guadalupe and San Antonio River basins (Joseph et al., 2013).

PNA defines the anomalies of sea surface temperature and precipitation in the mid– to upper–tropospheric geopotential height fields over the North Pacific Ocean (Wallace and Gutzler, 1981). Cavazos (1999) found that a reverse PNA pattern was associated with summer precipitation events, and a positive connection between the PNA pattern and winter precipitation in northeastern Mexico and southeastern Texas.

SOI is the atmospheric component and is commonly considered as the key indicator of El-Niño–Southern Oscillation (Chiew and McMahon, 2002). It is computed by the normalized difference of the standardized sea level pressures between the eastern Pacific (Tahiti) and the western Pacific (Darwin) (Yan et al., 2011). There is a dry condition during high SOI years within the Gulf and Mexican region (Ropelewski and Halpert, 1989). Richman et al. (1991) found that the relation between low SOI values and positive Texas precipitation anomalies was confined to the eastern part of the state.

An index for the El Nino-Southern Oscillation (Benson) based on precipitation from Global Precipitation Climatology Project (GPCP) called the El-Niño–Southern

Oscillation Precipitation Index (ESPI) is introduced (Curtis and Adler, 2000). The ESPI is based on rainfall anomalies between the eastern tropical Pacific and the maritime continent. It is normalized to have zero mean and unit standard deviation and is used partly for feedback to El-Niño warming in the eastern Pacific, because large shifts in tropical convection change with exceptional latent heat release and large-scale atmospheric circulations affect global precipitation patterns (Curtis and Adler, 2003).

These indices have warm (positive) and cold (negative) phases. The warm phase of AMO has resulted in an increase in the number of active hurricane seasons (Goldenberg et al., 2001), leading to an overall enhancement of moisture transport and extreme precipitation events in the southeast U.S. (Li et al., 2011). During the cold phase of AMO, the monsoon rainfall of the southern U.S. is confined due to the recurrent northwesterly wind anomalies in the North American monsoon region (Hu and Feng, 2008). The warm phase of NAO is characterized by stronger Atlantic jet stream and northward shift of the storm track, resulting in tropical cyclones for the southeastern U.S. (Bell and Visbeck, 2009; Hurrell et al., 2003), while the southeastern U.S. is likely to experience colder and drier winter season in the cold phase of NAO due to the weakening of the aforementioned pressure centers and decrement in the pressure gradient across the North Atlantic. The winter precipitation phase in Texas is observed to be drier in the cold PDO and wetter in the warm PDO (Goodrich and Walker, 2011). The warm phase of PNA in winters is found to be wetter in the Southeastern U.S. (Leathers et al., 1991), and Henderson and Robinson (1994) found more precipitation in summertime than in wintertime in the cold phase of PNA. The warm phase (El-Niño) of SOI is characterized in the tropical Pacific Ocean

basin by anomalously warm waters, weak trade winds, low pressure, and heavy rains in the east, while high pressure and dry conditions are captured in the west (Curtis and Adler, 2000). The opposite sign refers to the cold phase (La-Niña).

The objective of this study therefore is to examine how global scale climatic indicators and regional precipitation extremes are related in Texas. First, statistically estimated PMPs and 100-year return period precipitation obtained from frequency distribution fitting are compared. Second, the impact of major Atlantic and Pacific Ocean based climatic cycles, including AMO, NAO, PDO, PNA, and SOI, on extreme precipitation is investigated for entire Texas. Third, the effect of El-Niño and La-Niña on the annual cycle of monthly extreme precipitation and annual maximum precipitation in different climate zones is analyzed. Finally, the relations of geographical characteristics to climate indices, precipitation extremes, and El-Niño and La-Niña effect are quantitatively evaluated.

3.3 Study area

Texas, the largest state in the contiguous United States (CONUS), contains a wide range of climates from arid to sub-tropical humid (Larkin and Bomar, 1983). The varied geographical characteristics with forests in the east, coastal plains, and the elevated plateaus in the south, and basins in the north and west, result in a wide variety of weather throughout the year (Benke and Cushing, 1996). The varied climate in Texas demonstrates itself in terms of large spatial and temporal variations in precipitation and temperature. It is greatly affected by physical features, including two competing systems between frontal

passages from northwest and moist air moving from the Gulf of Mexico (Hao and Singh, 2013; North and Schmandt, 1995). The annual mean precipitation in Southeast Texas is more than 1,400 mm, while Northwest Texas only receives about 400 mm (Lyons, 1990). There are two precipitation peaks in May and September (Lee et al., 2017) and most of the west Texas rivers flow only part of the year, while the east Texas rivers flow year-round (Geology, 1996). The annual mean temperature varies greatly with latitude from north to south. According to Bomar (1995), the average annual temperature (1961-1990) in the northern portion of the Texas High Plains is 13.2 ^{o}C, while it is 23.3 ^{o}C in Southern Texas. Overall, Texas has a spatial pattern with a decreasing rainfall gradient from east to west and a temperature gradient from north to south that greatly influence land use, vegetation, and river flow (Rajsekhar et al., 2013). Due to these large spatial and temporal variations of rainfall and temperature, hydrologic extreme events (such as droughts and floods) have led to unfavorable conditions for agricultural production (Guerrero, 2012) and water management. This is a critical issue for Texas, which has the largest farm area and the highest livestock production among the 50 states (Gleaton and Anderson, 2005). A total of 528,000 km^2 is occupied by farms and ranches which is about 76% of Texas surface area occupied by farms and ranches, and 22% of this area is crop land. For the crop land portion, about 57% is harvested, 10% is grassland, and 33% is either not harvested or fails to produce crops (National Agricultural Statistics Service, NASS, 2007). Figure III-1 shows locations of 217 rain gauge stations and climate zones used in this study. The climate zones divided by National Climatic Data Center (NCDC) is discussed in section 3.4.2.

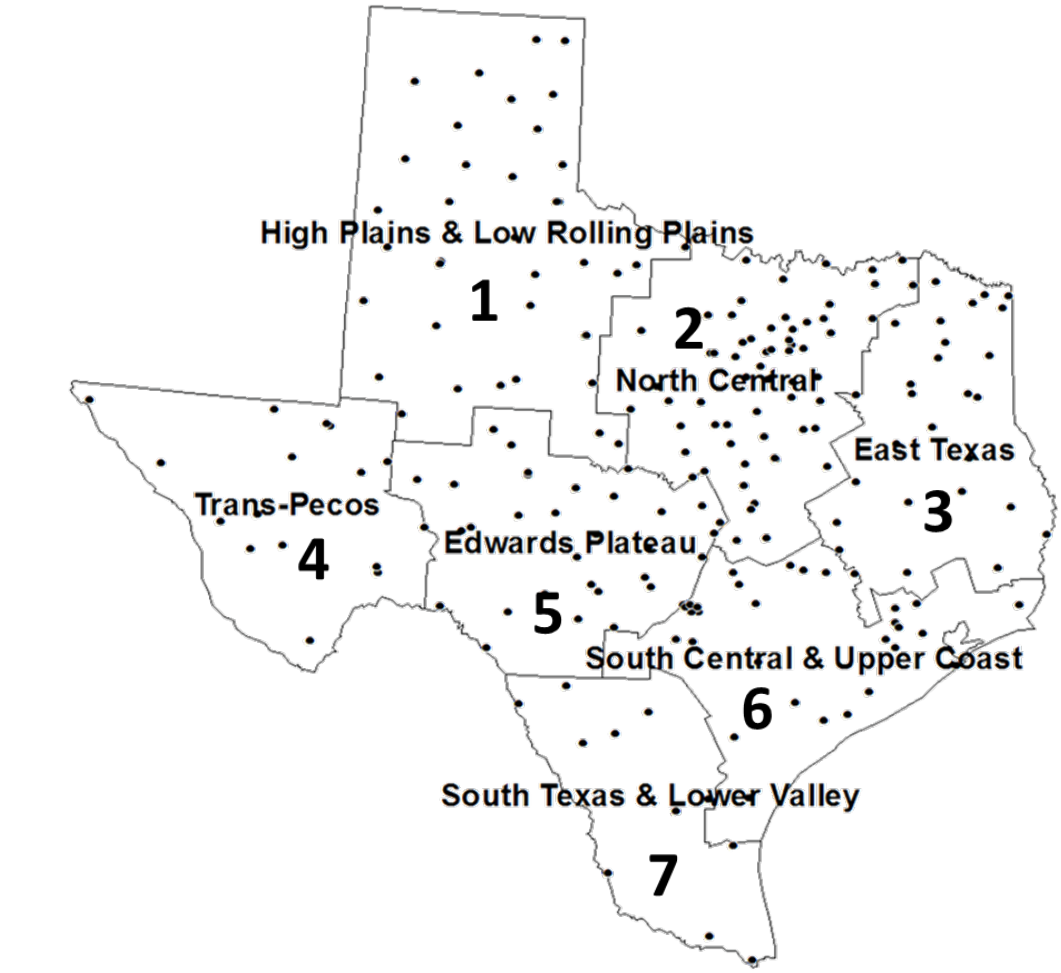

Figure III-1 Rain gauge stations and climate zones in Texas

3.4 Data

3.4.1 Precipitation

Hourly precipitation data (https://www.ncdc.noaa.gov/cdo-web/) were obtained from NOAA National Climatic Data Center (NCDC) to estimate PMP. A total of 217 gauge stations (Cooperative Observer Network; COOP) which have more than 30 years of data were selected (Figure III-1). From 1-hour duration precipitation data, 24-, 48-, and 72-hour precipitation data were generated. The maximum precipitation during certain durations was obtained from each year using moving window sum (Annual Maximum Precipitation; AMP). A period of 64 years (1950–2013) was determined, based on the available data of the overlapping period for climatic cycles from 1950. In order to meet National Weather Service quality standard, the Weather Forecast Office has monitored, reviewed, and taken corrective action on any COOP observations that do not meet the highest standards of quality. Precipitation reports are verified and corrected for each day, including past days, based on comparison with nearby reports or radar estimation (NWSI, 2017).

3.4.2 NCDC climate divisions

There are 344 climate divisions in the U.S. which are characterized on the basis of similar attributes of vegetation, rainfall, temperature, humidity, and seasonal weather changes from National Climatic Data Center (NCDC) (Karl and Koss, 1984; TWDB, 2012). Originally, there are 10 climate divisions lying within the Texas boundary, as shown in Figure III-1. For the convenience of analysis and comparison, these are

regrouped into seven zones as follows; Zone 1 (High Plains and Low Rolling Plains), Zone 2 (North Central), Zone 3 (East Texas), Zone 4 (Trans Pecos), Zone 5 (Edwards Plateau), Zone 6 (South Central and Upper Coast), and Zone 7 (South Texas and Lower Valley).

3.4.3 Climatic cycles and ENSO precipitation index

Monthly index of Atlantic Multidecadal Oscillation (AMO), North Atlantic Oscillation (NAO), Pacific Decadal Oscillation (PDO), and Pacific North American Pattern (PNA) were obtained from the Earth System Research Laboratory database (https://www.esrl.noaa.gov/psd/data/climateindices/) and monthly index of Southern Oscillation Index (SOI) was downloaded from Australian Government's Bureau of Meteorology database (http://www.bom.gov.au/climate/enso/). El Nino-Southern Oscillation Precipitation Index (ESPI) was obtained from Earth System Science Interdisciplinary Center (Essic) and Cooperative Institute Center and Cooperative Institute for Climate and Satellites (CICS) at University of Maryland, College Park (http://eagle1.umd.edu/GPCP_ICDR/espi.htm). Due to the availability of ESPI, this index was compared separately from other five climatic cycles. A brief summary of these climatic cycles is listed in Table III-1.

Table III-1 Climatic cycles and ENSO Precipitation Index

	Period	**Domain**	**Variables**
AMO	1856-2016	North Atlantic Ocean	Sea surface temperature Precipitation
NAO	1950-present	Iceland Low & Azores High	Pressure
PDO	1900-present	Northern Pacific Ocean	Sea surface temperature Sea level pressure
PNA	1950-present	N. Hemisphere mid-latitudes	Sea surface temperature Precipitation
SOI	1876-present	East and West Tropical Pacific	Sea surface pressure
ESPI	1979-present	Maritime Continent and Eastern tropical pacific	Precipitation

3.5 Methods

3.5.1 Site-specific method for Texas

The site-specific method was adopted from Chapter 2.5.4. Only part of Texas (BRB) was considered in previous chapter. However, entire Texas precipitation observations were considered for PMP estimation. *FFC* is the fitted curve for 24-, 48-, and 72-hour durations from the scatters of K_s values (Figure III-2). The calculated *B* values from *FFC* equation (4) were -0.0036 (24-hour), -0.0031 (48-hour), and -0.0026 (72-hour).

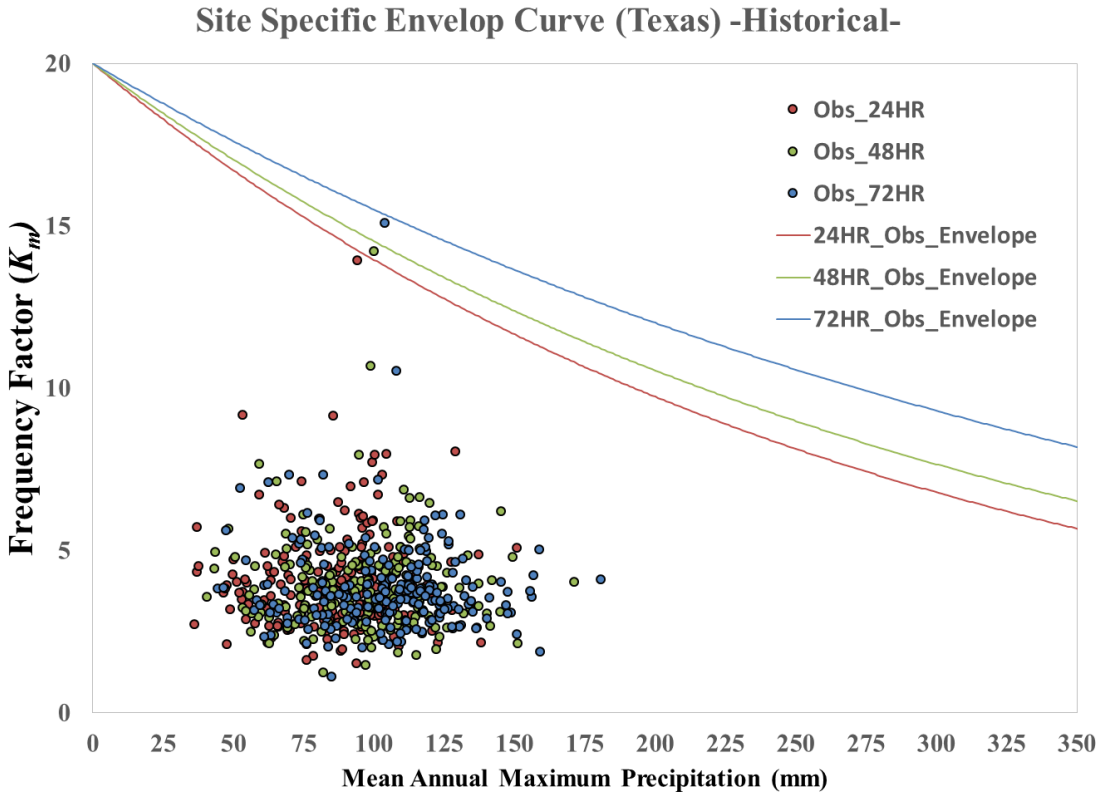

Figure III-2 Site-specific enveloping curve in Texas

3.5.2 Generalized Extreme Value (GEV) distribution

To estimate the return period of annual maximum precipitation series, it is important to select an appropriate frequency distribution. The generalized extreme value (GEV) distribution is one of the frequently employed probability distributions for modeling extreme values, including discharge and rainfall data to estimate magnitudes of maximum values corresponding to various return periods (Fowler and Kilsby, 2003; Katz et al., 2002; Mishra and Singh, 2010; Nguyen et al., 2002; Pangaluru et al., 2018). The GEV distribution (Hosking et al., 1985; Jenkinson, 1955) was selected for this study, because it was previously documented (Asquith, 1998) as appropriate for 1-day and greater durations in Texas. The GEV distribution incorporates Gumbel or type I ($\kappa = 0$), Fréchet or type II ($\kappa < 0$), and the Weibull or type III ($\kappa > 0$) distributions (Stedinger, 1993) as special cases. The cumulative distribution function of the GEV distribution can be written as

$$F(x) = \exp\left\{-\left[1 - \kappa\frac{(x-\xi)}{\alpha}\right]^{1/\kappa}\right\} \qquad \kappa \neq 0 \qquad (5)$$

$$F(x) = \exp\left\{-\exp\left[-\frac{(x-\xi)}{\alpha}\right]\right\} \qquad \kappa = 0 \qquad (6)$$

where $\xi + \alpha/\kappa \leq x < \infty$ for $\kappa < 0$, $-\infty < x < +\infty$ for $\kappa = 0$, and $-\infty < x \leq \xi + \alpha/\kappa$ for $\kappa > 0$. Three parameters are ξ = location, α = scale, and κ = shape. Considering x_1, x_2, …, x_n as the annual maxima of precipitation for given duration at each location, the method of maximum likelihood was adopted to estimate the parameters of the distribution selected to fit the data (Kotz and Nadarajah, 2000). If the set of $\{x_i\}$ is independent and identically

distributed from the GEV distribution, the log-likelihood function (Hosking et al., 1985) for a sample of x_n can be expressed as

$$\ln[L(\xi, \alpha, \kappa \mid x)] = -n\ln(\alpha) + \sum_{i=1}^{n}\left[\left(\frac{1}{\kappa} - 1\right)\ln(y_i) - (y_i)^{1/\kappa}\right] \tag{7}$$

$$y_i = \left[1 - \left(\frac{\kappa}{\alpha}\right)(x - \xi)\right] \tag{8}$$

The maximum likelihood estimation of the three parameters can be obtained by taking the first derivatives of $\ln[L(\xi, \alpha, \kappa \mid x)]$ with respect to each parameters and setting the derivatives zero as (Hosking, 1985):

$$\frac{1}{\alpha}\sum_{i=1}^{N}\left[\frac{1 - \kappa - (y_i)^{1/\kappa}}{y_i}\right] = 0 \tag{9}$$

$$-\frac{N}{\alpha} + \frac{1}{\alpha}\sum_{i=1}^{N}\left[\frac{1 - \kappa - (y_i)^{1/\kappa}}{y_i}\left(\frac{x_i - \xi}{\alpha}\right)\right] = 0 \tag{10}$$

$$-\frac{1}{\kappa^2}\sum_{i=1}^{N}\left\{\ln(y_i)\left[1 - \kappa - (y_i)^{1/\kappa}\right] + \frac{1 - \kappa - (y_i)^{1/\kappa}}{y_i}\kappa\left(\frac{x_i - \xi}{\alpha}\right)\right\} = 0 \tag{11}$$

3.5.3 Goodness of fit test

Three goodness of fit tests, including Chi-Square (C-S) test, Kolmogorov-Smirnov (K-S) test, and Anderson-Darling (A-D) test, were used. C-S test: The chi-square test is non-parametric and was used to determine whether a data sample came from a specified probability distribution, with parameters estimated from the data (Greenwood and Nikulin,

1996). The chi-square statistic (χ^2) is based on the grouping of data into *n* number of bins of equal probability as

$$\chi^2 = \sum_{i=1}^{n} \frac{(O_i - E_i)^2}{E_i} \tag{15}$$

where O_i is the observed frequency, and E_i is the expected frequency ($E_i = F(x_i) - F(x_{i-1})$). K-S test: The maximum difference $\left(D = max\left(D^{\pm}, D^{\mp}\right)\right)$ between the hypothesized distribution function and the empirical distribution (Conover, 1972) was computed. The test showed whether a sample came from the hypothesized distribution. Let $Z_{(i)} = F(x_i, \theta)$, where $F_n(x_i)$ indicates the empirical cumulative distribution function, x_i represents the order data, and θ is the parameter sets. Then,

$$D^{\pm} = max_i\left(\frac{i}{n - Z_i}\right), D^{\mp} = max_i\left(\frac{-(i-1)}{n}\right) \tag{16}$$

A-D test: The weighted square difference between the hypothesized and empirical distributions was calculated (Anderson and Darling, 1954) and a weight function was the test statistic (A):

$$A^2 = -n - \frac{1}{n}\sum_{i=1}^{n}(2i-1)\left\{\ln\left(F(x_i)\right) + \ln[1 - F(x_{n-i+1})]\right\} \tag{17}$$

The hypothesis testing for the chi-square goodness of fit test is set as null hypothesis that the data are consistent with given (GEV) distribution. 189 stations (24-hour), and 194 stations (48-hour), and 184 stations (72-hour) of total number of 217 stations indicated that the C-S goodness of fit test did not reject the null hypothesis at the 5% significant level. Likewise, 185 stations (24-hour), and 190 stations (48-hour), and 182 stations (72-

hour) for K-S test and 190 stations (24-hour), and 189 stations (48-hour), and 181 stations (72-hour) for A-D test did not reject the null hypothesis at the 5% significant level.

3.6 Results

3.6.1 PMP estimation and 100-year return period precipitation

PMP for 24-, 48-, 72-hour durations was calculated from the Hershfield and Site-specific methods. Figure III-3 shows the PMP values from the two methods at 217 stations. When the PMP values and the duration of PMP increased, the difference between two methods also increased. The overall estimation from the Hershfield method was larger than the values from the site-specific method. Because the Hershfield method has more possibility of including extreme observations from a large number (from 2645 stations in the U.S.) of data than the site-specific method does (from 217 stations in Texas). However, the Hershfield method does not contain recent observations, while site-specific does until 2013. Between the two methods, the difference was calculated as site-specific value minus Hershfield value in percentage. The site-specific PMP was 0.7% to 15.4% (24-hour), 5.1% to 22.2% (48-hour), and 6.3% to 27.8% (72-hour) lower than the Hershfield method (Figure III-3a, III-3b, and III-3c). Comparison of the values among the three durations shows that 24-hour had more linear relationship between two methods, while the non-dimensional comparison shows that 72-hour duration had nearly perfect (slope of 0.99) linear relationship (Figure III-3d, III-3e, and III-3f). The advantage of non-dimensional comparison was that the systemic error due to different durations (or amounts of PMP) was removed that we could compare PMPs relatively. Even though two methods resulted

in different PMP values themselves, they were systematically linearly related during the historical period in Texas. For every duration, the most difference was captured at the boundary of the coastline at Port Arthur, and the least difference was captured inland at Sanderson.

To compare with PMP, the annual maximum precipitation (AMP) and annual total precipitation (ATP) were calculated at each station and the spatially averaged value indicated 'mean of AMP and ATP.' Likewise, the 'standard deviation of AMP and ATP' were the average value from all stations (Table III-2). As the duration increased, the difference between two methods also increased as 7.3% for 24-hour, 12.5% for 48-hour, and 15.7% for 72-hour. From the GEV distribution fitting, the 100-year return period of AMP was calculated. The spatially averaged values were compared to two PMP estimates. The ratio of PMP from the Hershfield to the 100-year precipitation was 3.5 to 3.7 and the ratio of PMP from site-specific to 100-year precipitation was 3.1 to 3.3 in Texas. This finding (ratio) using statistical methods is similar to the previous studies using hydrometeorological PMP estimation (TCEQ, 2016). The ratio of both PMP values to mean of ATP was found to be 0.9 to 1.3. Specifically, the calculated 24-hour PMP values from both methods were close to the annual total precipitation in Texas on average.

Figure III-4 shows the ratio of annual maximum precipitation (AMP) to annual total precipitation (ATP) over time. The spatially averaged values of AMP over ATP from 1940 to 2013 were calculated for each year. For example, the value of 0.12 on the y-axis in 1950 means that annual maximum precipitation (24-hour) was 12% of annual total precipitation for 271 stations averaged. The largest ratio was captured in 1947 as 0.20 (for

24 hours), 0.24 (for 48 hours), and 0.26 (for 72 hours), while the least ratio was found in 1992 as 0.10 (for 24 hours), 0.11 (for 48 hours), and 0.13 (for 72 hours). The most extreme case was in 1947, amounting to 26% (48 mm) of total precipitation (288 mm) within 72 hours. Figure III-5 indicates what the return period of PMP value would be if the PMP really occurred. The PMP values and their return periods were calculated from the GEV distribution fitting. Since the National Research Council estimates the return period of PMP in the U.S. in the range of 10^5 to 10^9 years as the upper bound of extreme precipitation (NRC, 1994), the return periods of PMP from the two methods were counted as a histogram (Figure III-5). Most PMP values fell into the return period range of 10^5 and 10^6 years. The return period of PMP was at least 1,000 years. Those longer durations of return period seemed much higher, however, a recent study by van Oldenborgh et al. (2017) found that the return period of the largest observed 72-hour precipitation amount of Hurricane Harvey was greater than 9,000 years. Also Kao et al. (2019) highlighted that the 72-hour precipitation during Hurricane Harvey in the Houston area exceeded up to 25 mm from its PMP values in HMR-51.

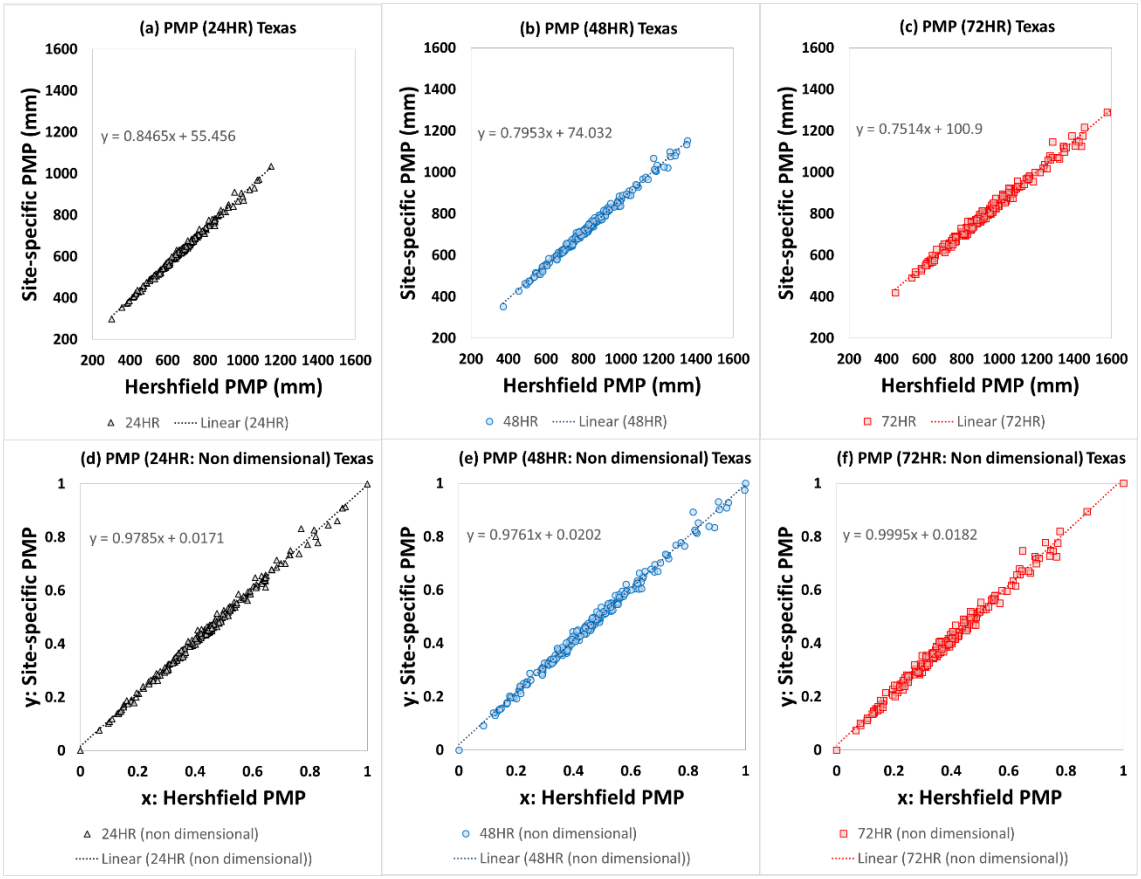

Figure III-3 Hershfield and site-specific PMP estimation in Texas

Table III-2 AMP, ATP, PMP, and 100-year precipitation in Texas

	24-hour	48-hour	72-hour
Mean of AMP	86.0 mm	97.4 mm	104.5 mm
Standard deviation of AMP	38.2 mm	43.4 mm	46.4 mm
Mean of ATP	693.14 mm		
Standard deviation of ATP	227.41 mm		
PMP Hershfield (H)	677.9 mm	819.6 mm	928.8 mm
PMP Site-specific (S)	629.3 mm	725.8 mm	801.9 mm
Difference = (S-H)/S	-7.3%	-12.5%	-15.7%
100-year precipitation (GEV distribution)	189.2 mm	230.9 mm	251.2 mm
Ratio of PMP Hershfield to 100-year precipitation	3.6	3.5	3.7
Ratio of PMP Site-specific to 100-year precipitation	3.3	3.1	3.2
Ratio of PMP Hershfield to Mean of ATP	1.0	1.2	1.3
Ratio of PMP Site-specific to Mean of ATP	0.9	1.0	1.2

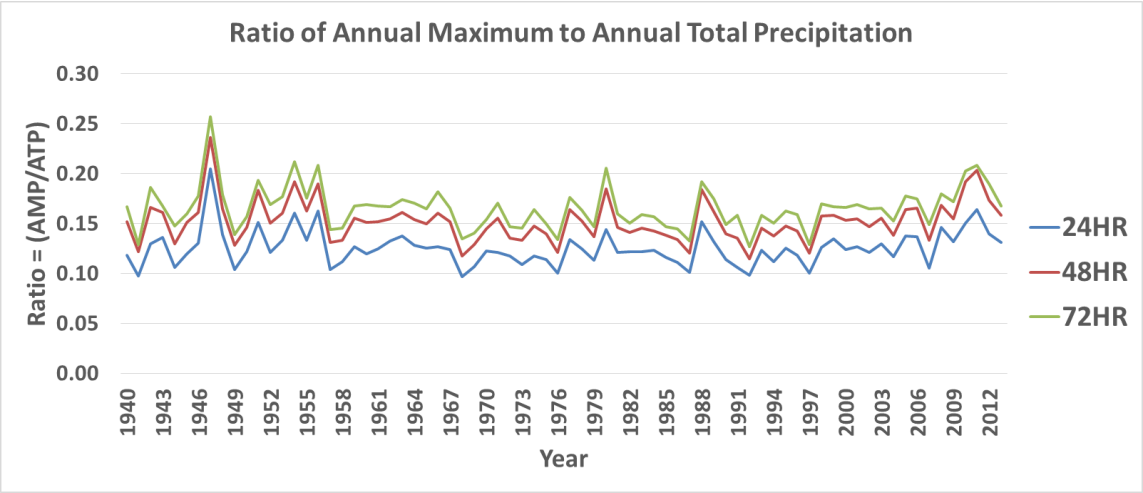

Figure III-4 Ratio of annual maximum to annual total precipitation in Texas

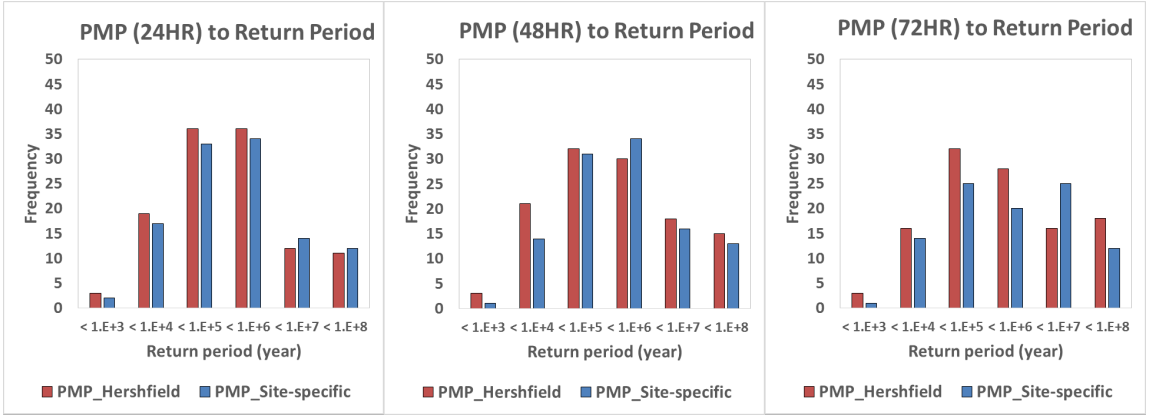

Figure III-5 Return period of PMP values

3.6.2 Spatial distributions of PMP and extreme precipitation

The map of AMP, standard deviation of AMP, ratio of AMP to ATP, record precipitation, PMP, 100-year precipitation at each station for 72-hour duration, and ATP, was constructed, as shown in Figure III-6. The mapped spatial distribution was driven from the point values using the inverse distance weighting method (Philip and Watson, 1982; Watson, 1985) in ArcGIS interpolation mapping tool. ATP (Figure III-6a) and AMP for 72 hours (Figure III-6c) had similar spatial patterns that three climate zones (2, 3, and 6) in the east received a large amount of precipitation, while zone 4 showed the driest condition for annual maximum and annual total precipitation. The 100-year return period of precipitation from the GEV distribution (Figure III-6b) showed a similar spatial pattern as ATP and AMP. Moreover, zone 7 (Southcentral and Lower Valley) had a large amount of 100-year precipitation. Even though zone 7 had a smaller amount of annual maximum and total precipitation, this zone had less frequent but more extreme precipitation, because the standard deviation of AMP (Figure III-6g) was found to be high in this zone. Likewise, the record precipitation (the observed amount with the largest value among AMPs within the period of 1940 to 2013 from each station) showed a similar pattern as the 100-year return period precipitation. In other words, zone 7 normally had small amounts of precipitation throughout the years, however, there was unpredictable extreme precipitation due to more variability.

The spatial distributions of PMP estimated from the Hershfield and site-specific methods were nearly identical (Figure III-6e and III-6f). The range of PMP values was 446 mm to 1739 mm for the Hershfield method and 419 mm to 1389 mm for the site-

specific method. A large amount of PMP was found along the Gulf coast, including zones 3, 6, and 7. The PMP values from zone 7 were not expected to be high, based on low AMP (Figure III-6c). Since PMP is a function of mean and standard deviation of AMP, the high standard deviation of AMP (Figure III-6g) caused the larger amount of PMP in zone 7. The ratio of annual maximum (72-hour) to annual total precipitation was calculated (Figure III-6h). The ratio of AMP to ATP in the wetter regions of east (as low as 6%) was likely to be less than in the west drier regions (as high as 18%). Since this ratio did not consider the temporal variation of extreme values, such as standard deviation of AMP, it could be hazardous to assess the extreme events solely by relying on the ratio of AMP to ATP. Likewise, the higher ratio did not guarantee the possibility of severe events. Therefore, the PMP estimation including both mean and standard deviation of AMP was a more secure way to evaluate extreme events.

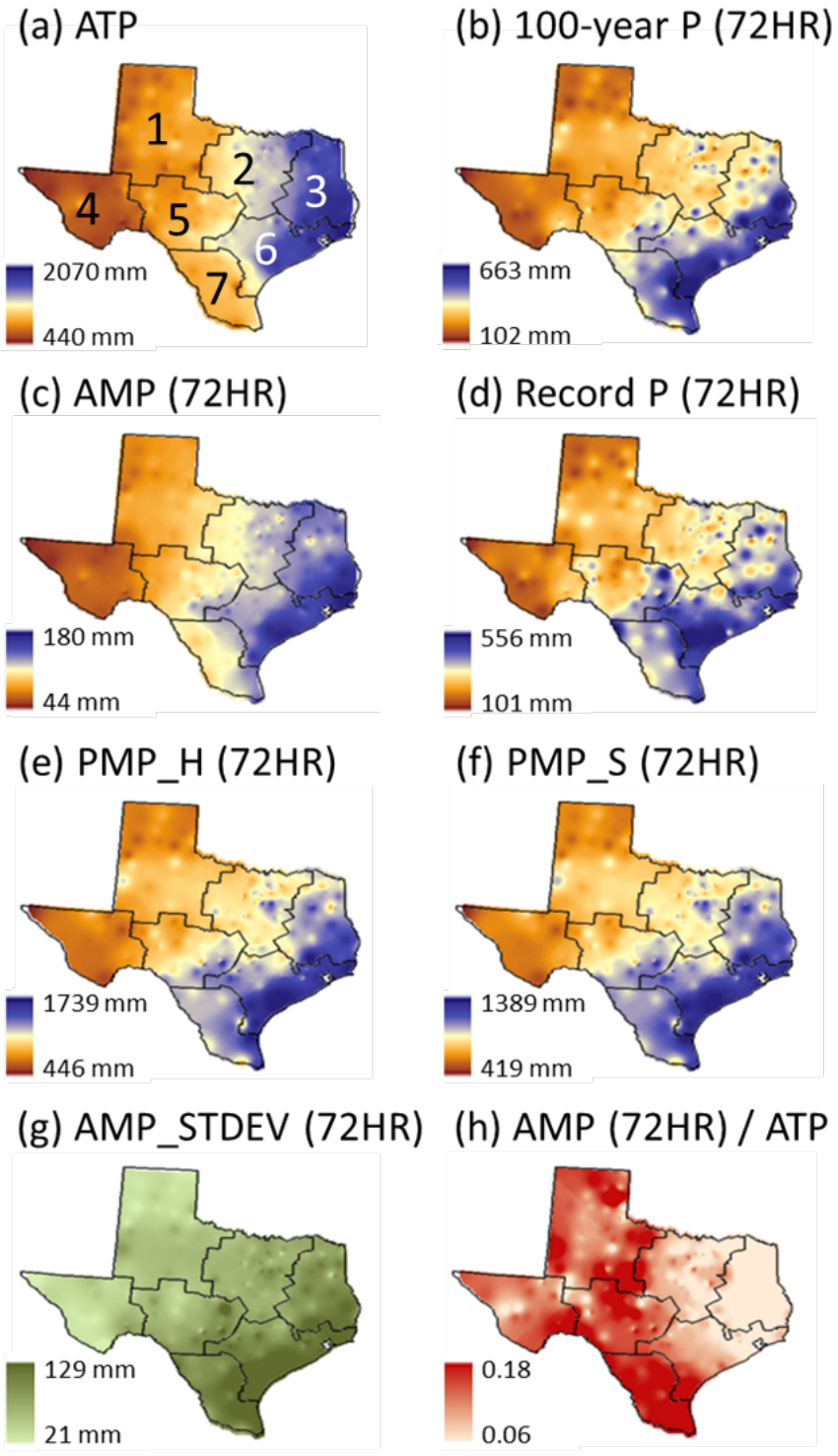

Figure III-6 Spatial distribution of PMP and extreme precipitation statistics

3.6.3 Climatic cycles and extreme precipitation

The maximum 72-hour precipitation records were obtained for each month and the average for all 217 stations from 1950 to 2013 (Figure III-7a) was obtained. The 12-month average of 72-hour precipitation was 38.3 mm and the total amount was 459.3 mm. There were two precipitation peaks in May (50.4 mm) and September (50.5 mm). The following months (June and October) also received large amounts of precipitation. Within those four months, about 42% of the total amount of precipitation was observed. The winter season (December, January, and February) received only 19% of the total amount of precipitation.

To identify the impact of warm phase (positive index) and cold phase (negative index) on monthly extreme precipitation, indices and 72-hour precipitation of corresponding months were collected and the averaged values were plotted, as shown in Figure III-7b (AMO), III-7c (NAO), III-7d (PDO), III-7e (PNA), and III-7f (SOI). The bar charts in the figures are the absolute difference between precipitation records of the two phases (hereafter called 'delta'). From June to October, delta was smaller than for other seasons for AMO and NAO. There was a sudden transition between May (maximum delta) and June (minimum delta) for AMO. The values of winter and spring (from December to May) delta were largely affected by the different phases of AMO. NAO had a similar pattern of the annual cycle of delta as AMO did except for January, because both climatic cycles had the same domain over Atlantic Ocean. Both PDO and PNA had the largest delta in October, and more precipitation was captured in the warm phase of PDO and cold phase of PNA in this month. There was a sudden transition from September to December for PDO. PNA had a similar pattern of the annual cycle of delta as PDO did. This was also

because both climatic cycles had the same domain over Pacific Ocean. SOI had a unique pattern in that the large delta was captured during precipitation peak months. For example, more precipitation was captured in June (due to the cold phase of SOI) and in September (due to the warm phase of SOI).

The average of each month's delta is shown in the top left corner of each figure in climatic cycles. In Texas, the Pacific group (PDO = 50 mm and PNA = 52 mm) was more sensitive to the effect of warm and cold phases of climatic cycle than the Atlantic group (AMO = 36 mm and NAO = 34 mm) was. Overall, August had the smallest delta for all five climatic cycles. The largest delta, on average, was observed for PNA, and NAO had the least delta. Therefore, the annual cycle of monthly extreme precipitation was notably altered in warm and cold phases of different climatic cycles.

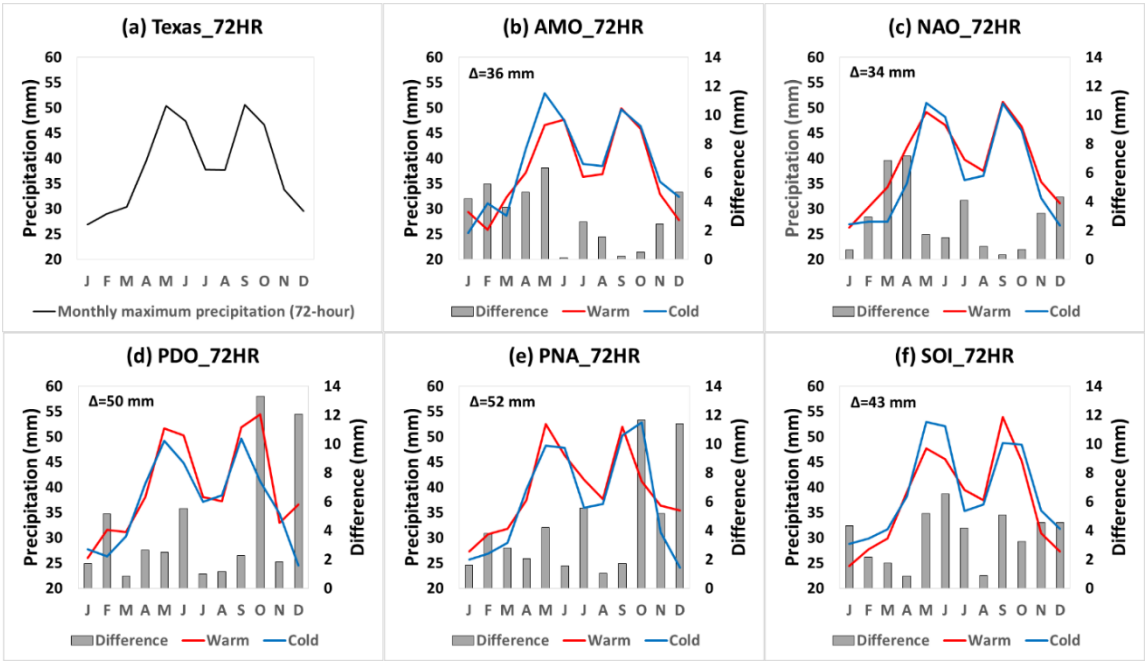

Figure III-7 Annual cycle of monthly maximum precipitation (72-hour) and its relation to climatic cycles under different phases.

3.6.4 Effect of ENSO on extreme precipitation

To investigate the El-Niño and La-Niña effect on the annual cycle of monthly extreme precipitation in Texas, ESPI was used for comparison between two phases (1979-2013). Since ESPI calculation was based on precipitation anomalies, it was appropriate for this analysis to focus on extreme precipitation. Figure III-8a shows the effect of El-Niño and La-Niña on monthly extreme 72-hour precipitation. The El-Niño months received 11% more precipitation than La-Niña months did. For example, the El-Niño months received 41.2 mm and the La-Niña months received 37.0 mm. However, the annual cycle of monthly maximum precipitation showed a significant variation between the two phases. The bar chart in the figures is the absolute difference between El-Niño and La-Niña. Their difference was large from October to December, however, the preceding two months (August and September) had nearly no difference (only up to 0.3 mm) between the two phases. Under the El-Niño condition, two peak months received more precipitation (15% more in May and 24% more in October) than under the La-Niña condition.

ESPI was reclassified into four groups to separate the strong and mild signals of El-Niño and La-Niña. The index above 1 was strong El-Niño (SEL), between 0 and 1 was mild El-Niño (MEL), between -1 and 0 was mild La-Niña (MLN), and below -1 was strong La-Niña (SLN). The precipitation values of the corresponding months are plotted as shown in Figure III-8b. Notably, there was more precipitation during the cold season (December to March) in Texas under strong El-Niño. Because El-Niño is characterized by temperature anomaly (e.g. above-average sea surface temperature) along the equator in the Pacific Ocean. This phenomenon allows to shift the weather patterns over parts of the

world, including the U.S. During a typical El Niño, Texas experienced a wetter-than-average weather pattern and a cooler-than-normal weather pattern due to the southern part of the jet stream moving over the state. The weather pattern in Texas had already persisted for several weeks and it's likely it will continue from January through the spring months. Historically, El-Niño weather pattern has been responsible for a very wet and stormy spring in 2015 (including record flooding in May) and a wet spring in 2016 (Ramon, 2019). Likewise, there was less precipitation during the cold season under strong La-Niña in Texas. The maximum value (57.7 mm) was captured in May under mild El-Niño and the minimum values (22.4 mm) were observed in February under strong La-Niña. During peak months, Mild La-Niña brought less precipitation and its variation of annual cycle was less evident among four groups of El-Niño and La-Niña signals.

The results from Figure III-8a were divided into seven groups to investigate the effect of El-Niño and La-Niña on the annual cycle of monthly extreme precipitation (72-hour) in different climate zones (Figure III-9). Every zone had two precipitation peaks except for Zone 4 (the driest region of Texas). The delta in Zone 4 was found to be the smallest among zones. From June to October, the effect of El-Niño and La-Niña was less evident in Zone 1. The effect of El-Niño and La-Niña was noticeable during October through December in Zone 2. El-Niño brought more precipitation (+14.1%) than did La-Niña in Zone 5. Their difference was larger, especially during peak months. There was a sudden transition of delta during two consecutive months (December and January) in Zone 7. The zones along the coastline (Zones 3, 6, and 7) had similar patterns of the annual cycle. However, Zone 3 and Zone 6 received more precipitation than did Zone 7. Also,

delta was larger in Zone 3 and Zone 6. These zones are more sensitive to El-Niño and La-Niña cycles and especially Zone 6 (where major cities of Texas are located) have suffered from floods every year since 1999 (Erdman, 2019).

The El-Niño year and La-Niña year were defined from ESPI. Since this index is given as monthly time step, the average value of indices from each year denotes El-Niño year (positive) and La-Niña year (negative). The corresponding annual maximum precipitation (72-hour) was selected, respectively, as El-Niño year AMP (Figure III-10a) and La-Niña year AMP (Figure III-10b) for each station. The spatially averaged value of AMP was 91.9 mm during El-Niño years and was 79.5 mm during La-Niña years. Under both conditions, the eastern part of Texas received more precipitation than the western part. In El-Niño years, the maximum value was observed at the city of Victoria (182.35 mm). In El-Niño years, the maximum values were observed at Port Arthur (186.22 mm). Both stations are close to the Gulf of Mexico and belong to climate zone 6. Figure III-10c shows the difference between El-Niño years and La-Niña years. Blue color indicates more El-Niño year precipitation and red color shows more La-Niña year precipitation. About 67% of stations received more precipitation during El-Niño years. The difference between two conditions was more evident in the eastern part of Texas. The average difference between two conditions was 12.4 mm. El-Niño years were wetter than normal conditions and they typically kept Texas out of a drought, while El-Niño could help keep hurricanes development.

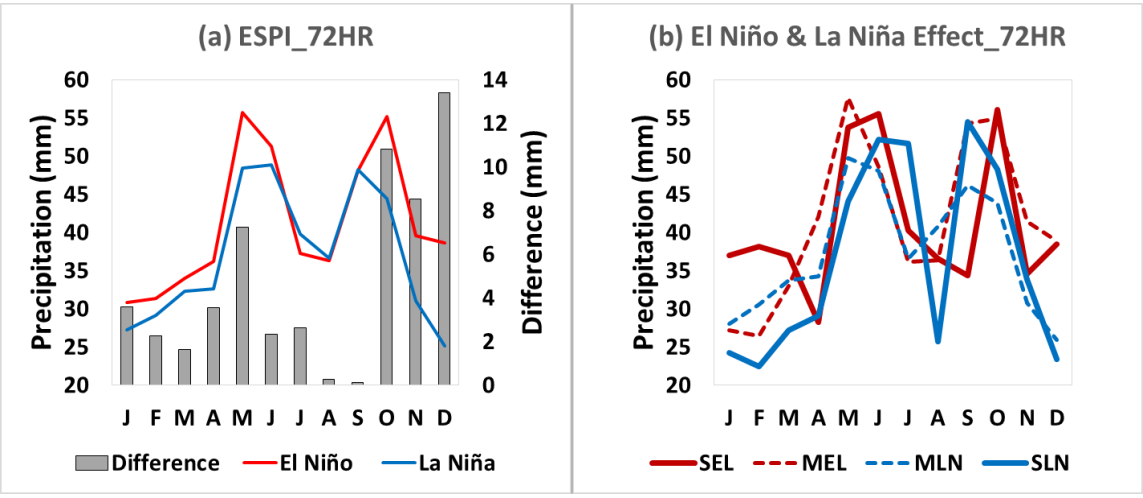

Figure III-8 Effect of El-Niño and La-Niña on the annual cycle of monthly extreme precipitation (72-hour).

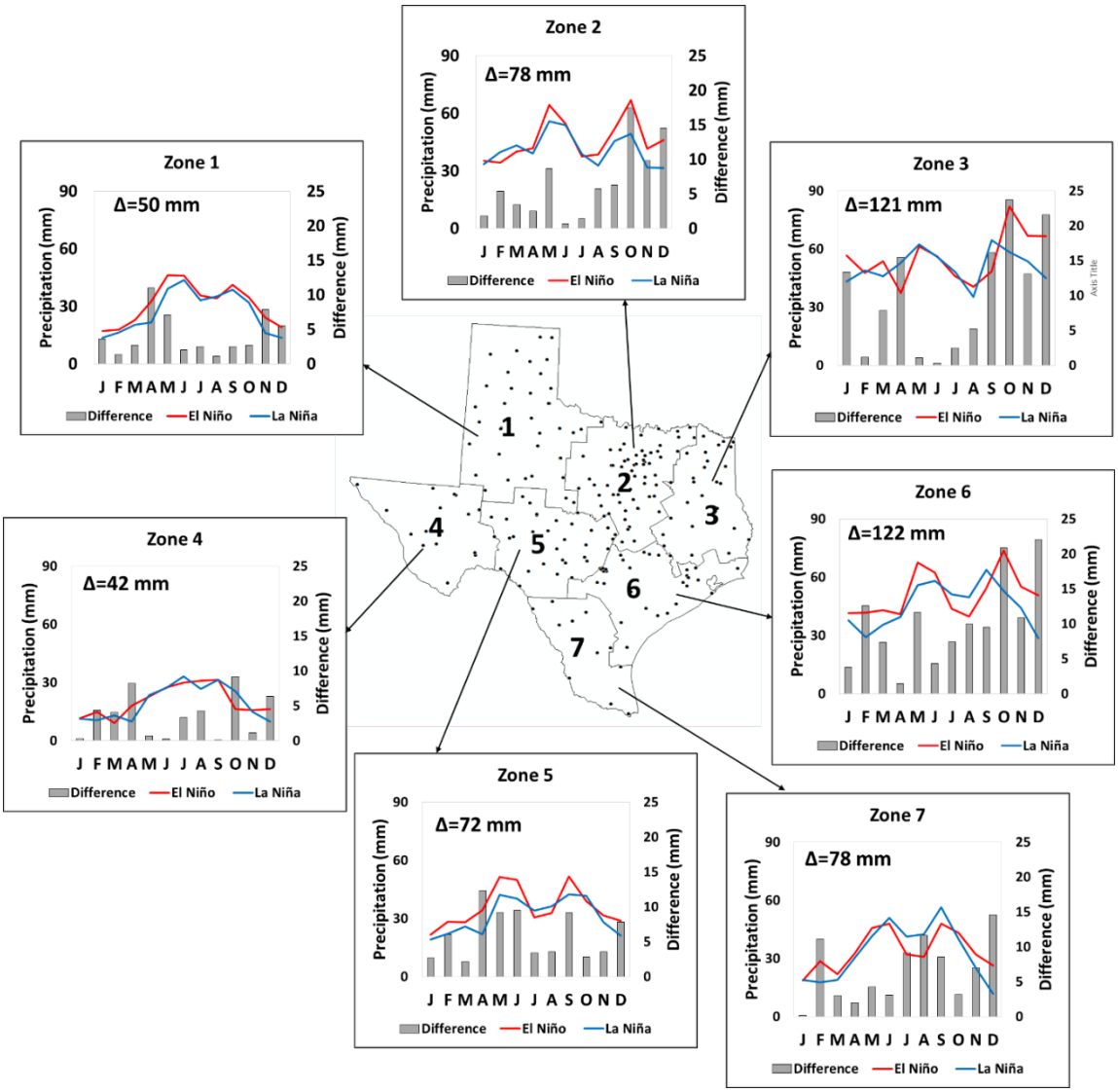

Figure III-9 Effect of El-Niño and La-Niña on the annual cycle of monthly extreme precipitation (72-hour) in different climate zones.

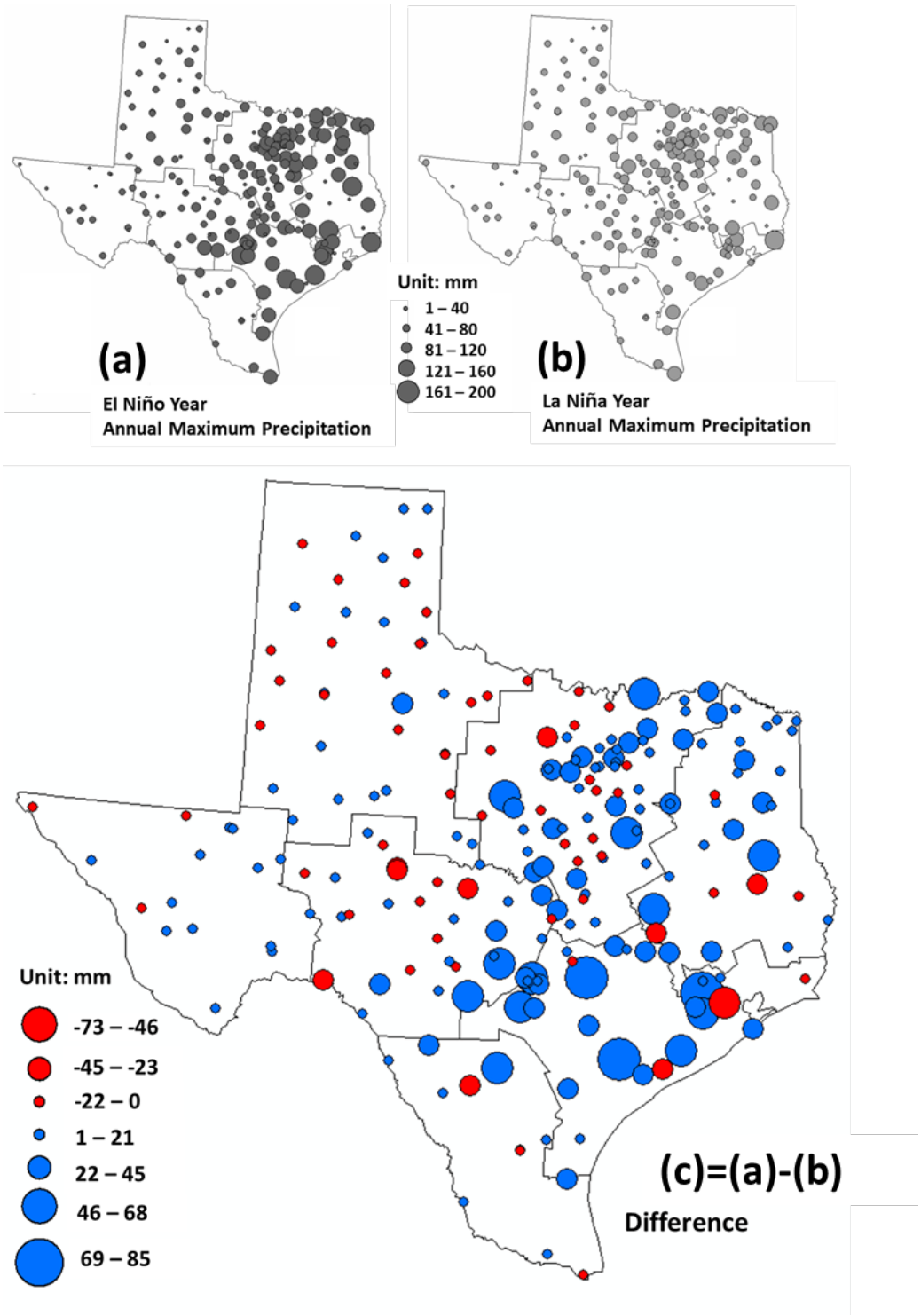

Figure III-10 Effect of El-Niño and La-Niña on annual extreme precipitation (72-hour)

3.6.5 Geographical characteristics of extreme precipitation

The foregoing discussion showed that the effect of El-Niño and La-Niña on extreme precipitation in Texas was substantially related to the location of stations. Geographically, the southeastern part of Texas (close to the Gulf of Mexico) was more sensitive and responsive to El-Niño and La-Niña. To quantitatively estimate the relationship between extreme precipitation and distance from the coastline, the shortest length between gauge stations and the coastline was calculated using ArcGIS tool. Both El-Niño year (R^2 = -0.46) and La-Niña year (R^2 = -0.31) precipitations were negatively correlated to the distance from the coastline (Figure III-11a and III-11b). The difference between two conditions was more remarkable within the distance of 200 km from the coastline (Figure III-11c). In addition, PMP and 100-year precipitation (72-hour) had a higher correlation than did the El-Niño and La-Niña relationship. Not only the mean precipitation had an increasing precipitation gradient from west to east, but also the maximum precipitation had a distinct relationship with the distance from the coastline. The stronger correlation was observed for PMP (R^2 = -0.75) than for 100-year return period precipitation (R^2 = -0.68) in Texas (Figure III-11d and III-11e). In terms of annual precipitation variability, the standard deviation of AMP was also found to be smaller as the distance farther from the coastline (Figure III-11f). More precipitation brought more variability of annual maximum precipitation. The maximum standard deviation of annual maximum precipitation was captured at Alice Airport about 45.4 km from the coastline. At this station, the maximum value of 100-year precipitation (664.5 mm) was estimated among 217 stations.

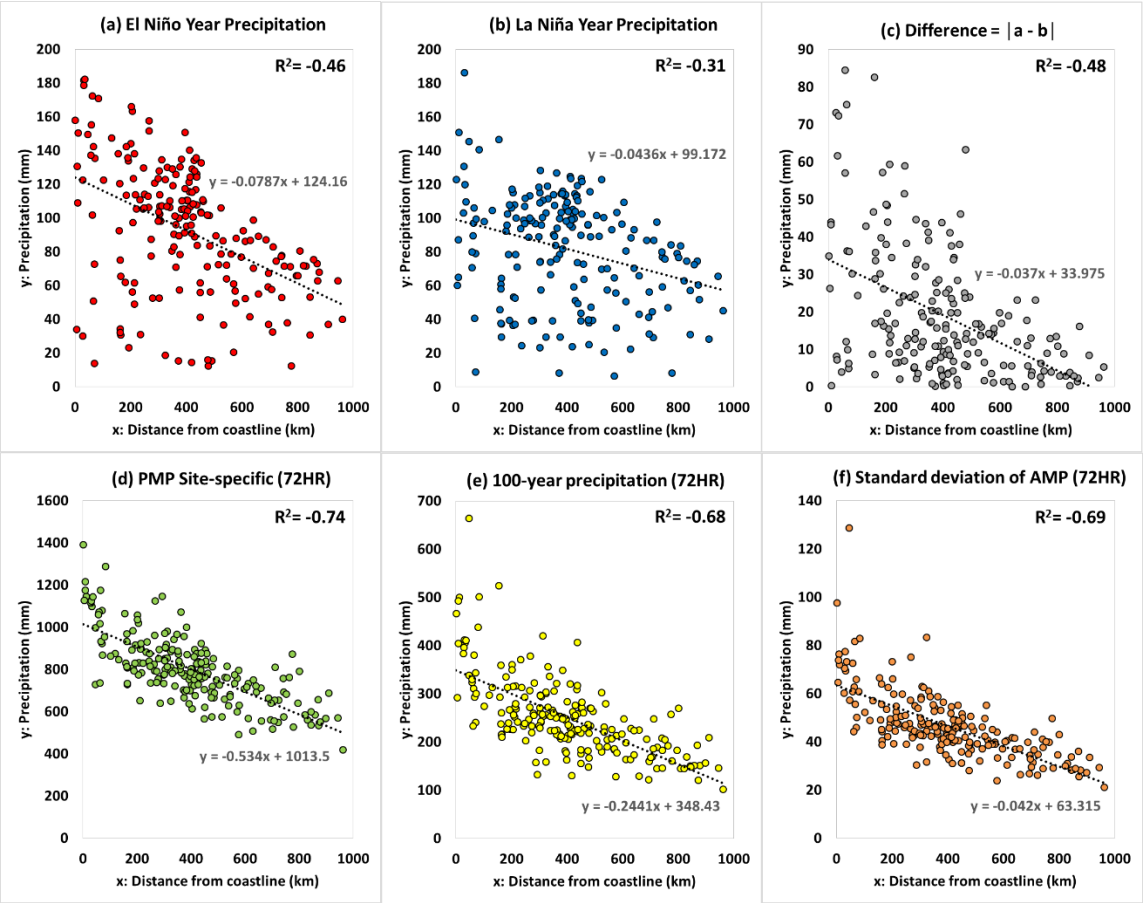

Figure III-11 Geographical characteristics of extreme precipitation (72-hour)

3.7 Conclusion

PMP was estimated by two statistical approaches (Hershfield method and site-specific method) and was about 3.1 to 3.7 times larger than the 100-year return period AMP in Texas. It is handy to estimate PMP values roughly from 100-year return period AMP. The site-specific PMP was more conservative, about 7-15% lower than the Hershfield PMP. It is still being debated as to which method is more accurate or more reliable, but at least the site-specific method, including more recent observations, can be more reasonable than the method using outdated data. A recent study of Kao et al. (2019) suggested that the current PMP needs to be updated to protect communities and environment from possible risk of flooding. PMP is not an impractical number, because the value close to PMP actually occurred recently in Texas. It was shown that the estimation of PMP, including both mean and standard deviation of AMP, was a more secure way to evaluate extreme events than AMP and ATP themselves, as shown by the frequency distribution of extreme events.

The warm and cold phases of climatic cycles affect the annual cycle of monthly extreme precipitation which maintains two precipitation peaks in May-June and September-October with different peak values. Using ESPI, El-Niño years receive about 16% more precipitation (72-hour) annually than La-Niña years. In Zone 6 (Southcentral and Upper Coast) the El-Niño and La-Niña dominantly affect the annual cycle of monthly maximum precipitation (72-hour). In Texas, 145 out of 217 stations received more precipitation during El-Niño years from 1950 to 2013, because in El-Niño years Texas experiences a wetter than average weather pattern due to the southern branch of the jet

stream moving over the state which intensifies storms. There is a geographical relationship between climate indices and precipitation extremes (PMP and AMP). At farther distances from the coastline, less precipitation and less variable extremes are captured, and the correlation with distance is more evident in El-Niño years (R^2 = -0.46) than in La-Niña years (R^2 = -0.31). From a geographical aspect, Texas is influenced by several factors that can potentially contribute to extreme precipitation. The adjacency of the region to the Gulf of Mexico is the main reason of more extremes along with the coast line. The large amount of moisture moves directly into the inland areas and it is converted into rainfall on the ground. A driving factor is the eastern North Pacific Ocean provided mid-level moisture which can contribute to the tropical cyclones. The boundary between two different masses (fronts) can be a key mechanism of generating upward motion in the atmosphere with heavy rainfall and unstable atmosphere (TCEQ, 2016).

The global scale climatic indicators (AMO, NAO, PDO, PNA, SOI, and ESPI) can provide regional response to meteorological extreme events. It is important to understand the change of climatic cycles, because the historical extreme events show various responses in different phases of climatic cycles and there is a particular geographical pattern of precipitation extremes under El-Niño and La-Niña. These findings can raise the community's awareness for broader insights into understanding meteorological extreme events.

CHAPTER IV

THE EFFECT OF ROSSBY WAVE BREAKING AND CLIMATIC CYCLES ON EXTREME PRECIPITATION IN TEXAS

4.1 Synopsis

Relationship between extreme precipitation and the climatic cycles has been investigated in a variety of region globally. However, the linkage between extreme precipitation and Rossby Wave breaking has not been documented, especially over Texas which experiences flooding every year. Rossby Wave (RW) breaking was defined as a detection of Potential Vorticity (PV) and was obtained from ERA-Interim products. This study focused on the following steps of analyses. First, how often and how severe Rossby Wave (RW) visited Texas were calculated. Second, the relationship between RW and extreme precipitation was investigated. Third, how El-Niño and La-Niña affected extreme precipitation while considering the RW occurrence. Fourth, the relationship between climatic cycles and extreme precipitation was identified. Fifth, the joint event of climatic cycles and RW on extreme precipitation was calculated in terms of the number of events and the precipitation depth. Finally, precipitation characteristics (number of rain days, duration, depth, and intensity of precipitation events) were grouped under different zones of RW frequency. It was found that the extreme precipitation was largely affect by ESPI and SOI which directly indicated the El-Niño and La-Niña effects among climatic cycles. Texas commonly received more precipitation under no Rossby Wave conditions. Precipitation characteristics commonly have eastern to western (large to small) pattern in

terms of magnitude. These findings can contribute to understanding the extreme precipitation event with the joint effect of climatic cycles and atmospheric phenomenon.

4.2 Introduction

Extreme precipitation leads to a significant natural disaster from global to regional scale, for example, it causes flooding which threatens human life and agricultural productivity (Ashley and Ashley, 2008; Gochis et al., 2015; Špitalar et al., 2014; White et al., 2019). Floods are usually triggered by heavy rainfall during a short period of time (Dong et al., 2011). Flooding depends on a number of factors, such as the magnitude and intensity of rainfall, antecedent soil moisture conditions, topography of the affected landscape, soil type, and land use (Collier, 2007; Funk, 2006). Flooding has caused an average of 82 deaths and annually $7.9 billion loss in property damage in the U.S. between 1985 and 2014 (Downton et al., 2005). Texas has the highest incidences of flood related fatalities among all 50 states (Sharif et al., 2010) and is also the only state that has reported flood-related fatalities in every single year during that same period (Lee et al., 2017; Sharif et al., 2014).

Rapid intensification of extreme precipitation is captured in the tropics and subtropics due to the effect of atmospheric circulation changes (Norris et al., 2019). Climatic cycles (Bhatia et al., 2019; Schlef et al., 2019) constitutes a key role in increasing the intensity of precipitation. Extreme precipitation results from various pressure and sea surface temperature anomalies at annual to multi-decadal cycles (Hu et al., 2011; Quadrelli and Wallace, 2004; Renard and Lall, 2014) that are explained by atmospheric or oceanic

patterns of global scale climatic cycles (Guirguis et al., 2015; Tian et al., 2017; Trenberth et al., 2006). The global scale climatic cycles are the major mechanisms of precipitation regimes, such as the precipitation intensity and extreme events (Gerlitz et al., 2016; Jones and Carvalho, 2014; Marani and Zanetti, 2015). Recent studies have investigated the relationship between climatic cycles and precipitation which helps understand the changing regional hydro-climatic regimes (Bhatia et al., 2019; Bhatia et al., 2020; Renard and Lall, 2014). However, the effect due to different phases of climatic cycles on meteorological regimes has not been well documented for Texas.

In addition to the relationship between climatic cycles and extreme precipitation, the study of extreme precipitation developed from a complex three-dimensional flow evolution that greatly affects surface sensible weather has recently been conducted such as Rossby Wave breaking (Hanley and Caballero, 2012; Moore et al., 2019; Sprenger et al., 2013). Heavy precipitation is likely to occur in the mixture of deep rising of warm moist air and poleward transport in airstreams within warm conveyor belts (Carlson, 1980; Harrold, 1973; Pfahl et al., 2014). Rossby Wave may occur when a wave strengthens and undergoes a nonlinear evolution with a rapid and irreversible deformation of potential vorticity (Holton, 1973; McIntyre and Palmer, 1983). High potential vorticity air can serve as channels for tropical to extratropical air mass exchange (Papin et al., 2017). The extratropical tropopause was characterized by bands of strong gradients of potential vorticity on isentropic surfaces (Hoskins et al., 1985). They concurred with jet stream and functioned as wave guides for Rossby Wave propagation (Schwierz et al., 2004). Rossby wave in the Earth's atmosphere was simple to monitor as large scale meanders of the jet

stream. When these deviations became greatly pronounced, the cold or warm air masses got detached, and became low-strength cyclones and anticyclones, respectively, and produced weather patterns at mid-latitudes (Kaspi and Schneider, 2011). Recent studies have investigated the linkage between extreme precipitation events and Rossby Wave breaking in the United States (Hu et al., 2017; Moore et al., 2019; Ryoo et al., 2013).

In this study, the impact of major Atlantic and Pacific Ocean based climatic cycles, including Atlantic Multidecadal Oscillation (AMO), North Atlantic Oscillation (NAO), Pacific Decadal Oscillation (PDO), Pacific North American Pattern (PNA), Southern Oscillation Index (SOI), and El-Niño–Southern Oscillation Precipitation Index (ESPI) on extreme precipitation in Texas was linked with Rossby Wave breaking. Rossby Wave frequency in Texas was first calculated. The number of events and how extreme precipitation were affected under the joint events of climatic cycles and Rossby Wave was investigated. Precipitation characteristics (number of rain days, duration, depth, and intensity of precipitation events) were examined under different zones of RW frequency.

4.3 Data

4.3.1 Precipitation

A total of 217 gauge stations which have more than 30 years of data were selected (Figure IV-1). Hourly precipitation data (https://www.ncdc.noaa.gov/cdo-web/) was imported from NCDC. The number of rain days and precipitation duration, depth, and intensity were selected for analysis of precipitation characteristics. The number of rain days was the temporal mean (1979-2013) of rain days per year at each station. Duration

(hour) was the temporal mean of maximum duration of precipitation events per year at each station. Depth (mm) was the temporal mean of maximum depth of precipitation events per year at each station. Intensity (mm/hour) was the temporal mean (1979-2013) of maximum intensity of precipitation events per year at each station. A period of 35 years (1979–2013) was determined, based on the available data of the overlapping period for climatic cycles and Rossby Wave data.

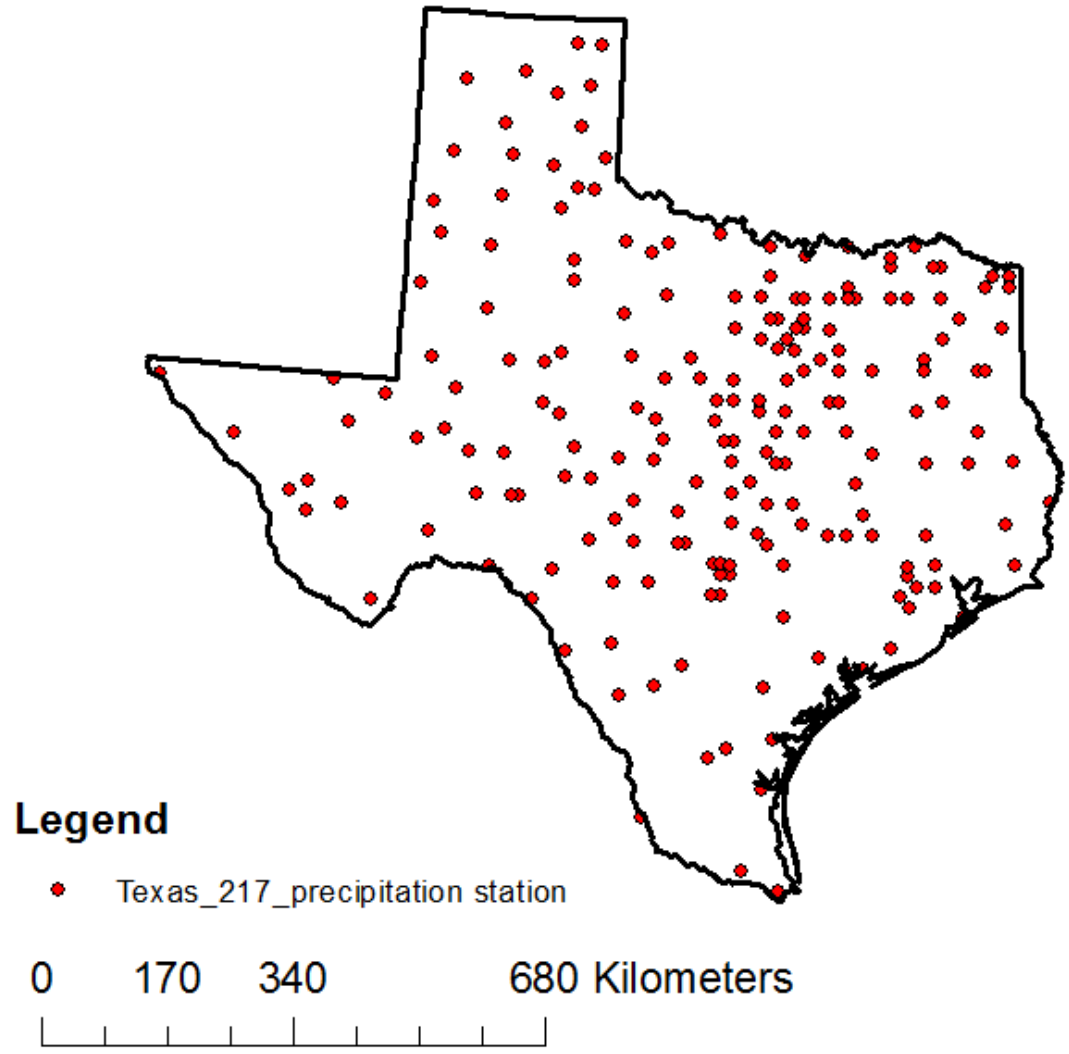

Figure IV-1 Rain gauge stations in Texas (1979-2013)

4.3.2 Rossby wave breaking

Rossby Wave (RW) breaking was defined as a detection of Potential Vorticity (PV) and was constructed by the method of Wernli and Sprenger (2007). The occurrence of RW breaking was defined as high PV (> 2 Potential Vorticity Unit; 1PVU= 10^{-6} $K \cdot kg^{-1}m^2s^{-1}$) at the field of the 300-, 315-, 320-, and 350-K isentropic surface. In this study, 320-K level of vertical coordinate was selected based on the European Centre for Medium-Range Weather Forecasts (ECMWF) Reanalysis pressure and isentropic level (https://rda.ucar.edu/datasets/ds627.1/docs/Pressure_and_isentropic_levels/). The level of 320-K was about 8500 m height. The ECMWF interim reanalysis (ERA-Interim) provided the PV products to identify the RW at monthly scale (Dee et al., 2011). PV data was available at 0.125 degree resolution (finest gird) globally from 1979 to current. The range of PVU is between -8 and +8. Figure IV-2 shows the example of PVU in January 1979.

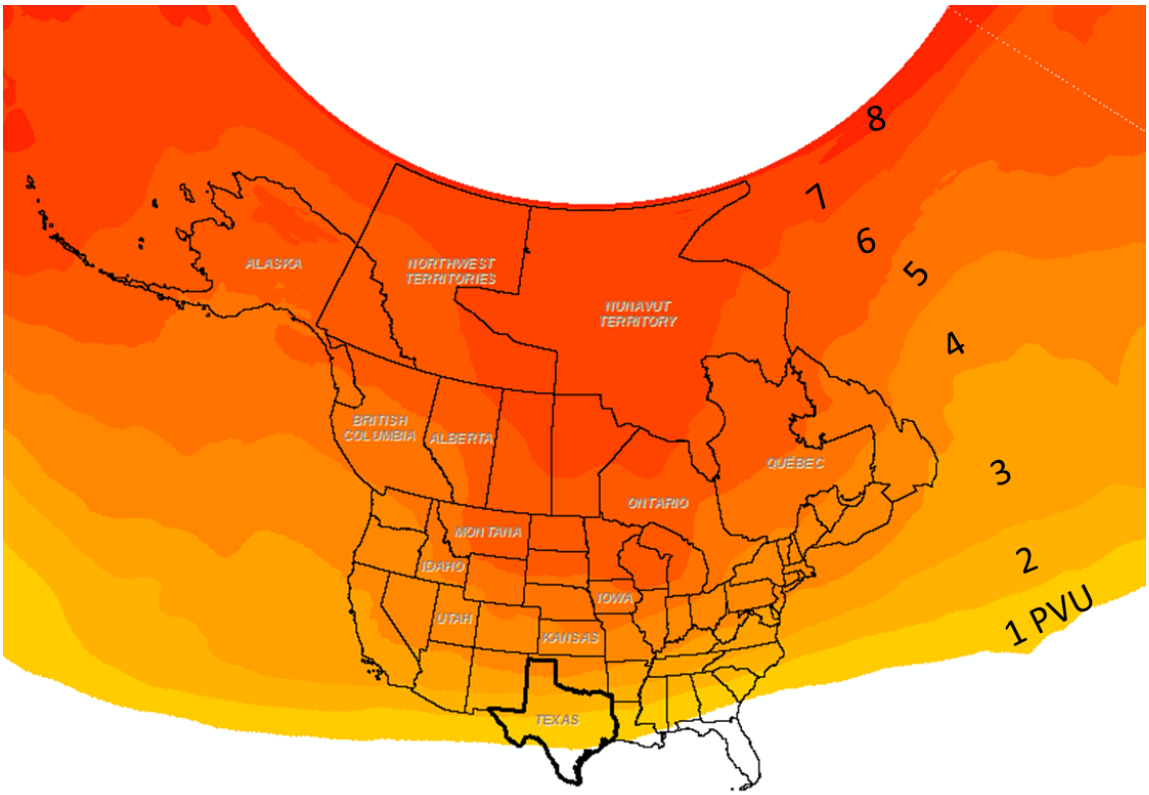

Figure IV-2 Potential vorticity in January 1979

4.4 Analysis

4.4.1 Rossby Wave in Texas

The percentage of areal extent of Rossby Wave (Figure IV-3a) and the intensity of RW (Figure IV-3b) over Texas were calculated at monthly time step. RW visited Texas every year, however, its coverage varied year to year. Before 1999, several years reached the full coverage of RW over Texas. After 2000, there was no month having a full coverage of RW. The largest annual coverage was found in 1992, and the least annual coverage was detected in 2006. The mean of annual coverage of RW was 38.4% from 1979 to 2013. The intensity of RW was calculated based on the PVU values. More than 2 PVU was considered as RW. The maximum annual intensity of 3.06 PVU was captured in 1992, however, the maximum monthly intensity was found in February 1998. The minimum annual intensity of 2.21 PVU was detected in 2006 and the minimum monthly intensity was found in May 1987. From 1979 to 2013, the mean of annual intensity of RW was 2.56 PVU.

From the monthly time series of RW coverage and intensity, it was found that certain months did not have RW. The annual cycle of monthly coverage (Figure IV-4a) and intensity of RW (Figure IV-4b) was calculated during 35 years (1979-2013). There were variations in each year, but commonly there was no RW visiting in June, July, August, and September (summer season). March and October were barely covered by less intense Rossby Wave. Throughout the years (on average of 35 years), Rossby Wave had common annual cycle of its coverage and intensity. During the relatively cold and cool

seasons in Texas, Rossby Waves were captured dominantly. The maximum coverage and intensity of RW were found in February.

The frequency of RW was calculated as the number of months with RW occurrence divided by total length of duration (Figure IV-5). Total length of duration was 35 years times 12 months = 420 months. The frequency was calculated from each grid cell at $1/8^{th}$ degree. The southern part of Texas, including gulf coast, rarely experienced Rossby Wave. The far northern part of Texas had Rossby Wave frequency up to 50% of total duration. This RW frequency map is further used in chapter 4.2.6 for the RW effect on precipitation characteristics.

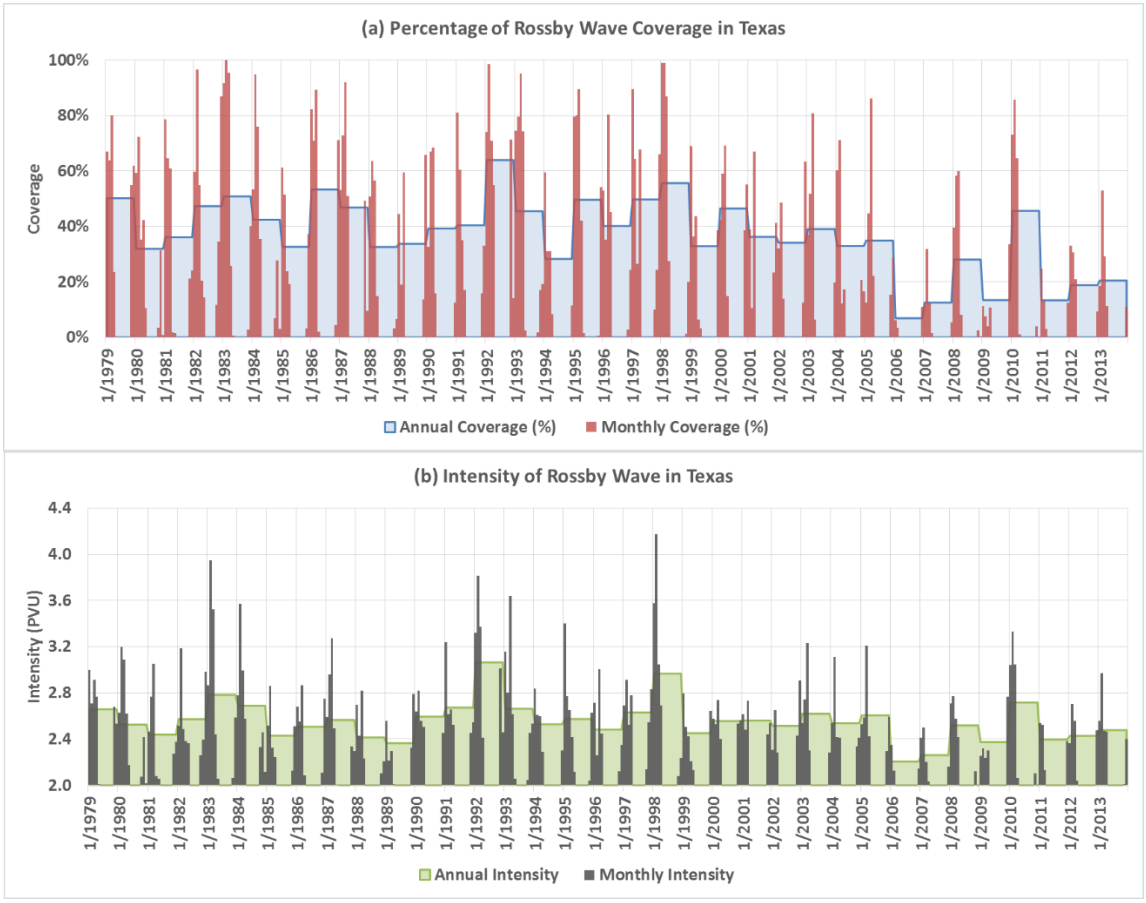

Figure IV-3 Percentage and intensity of Rossby Wave coverage in Texas (1979-2013)

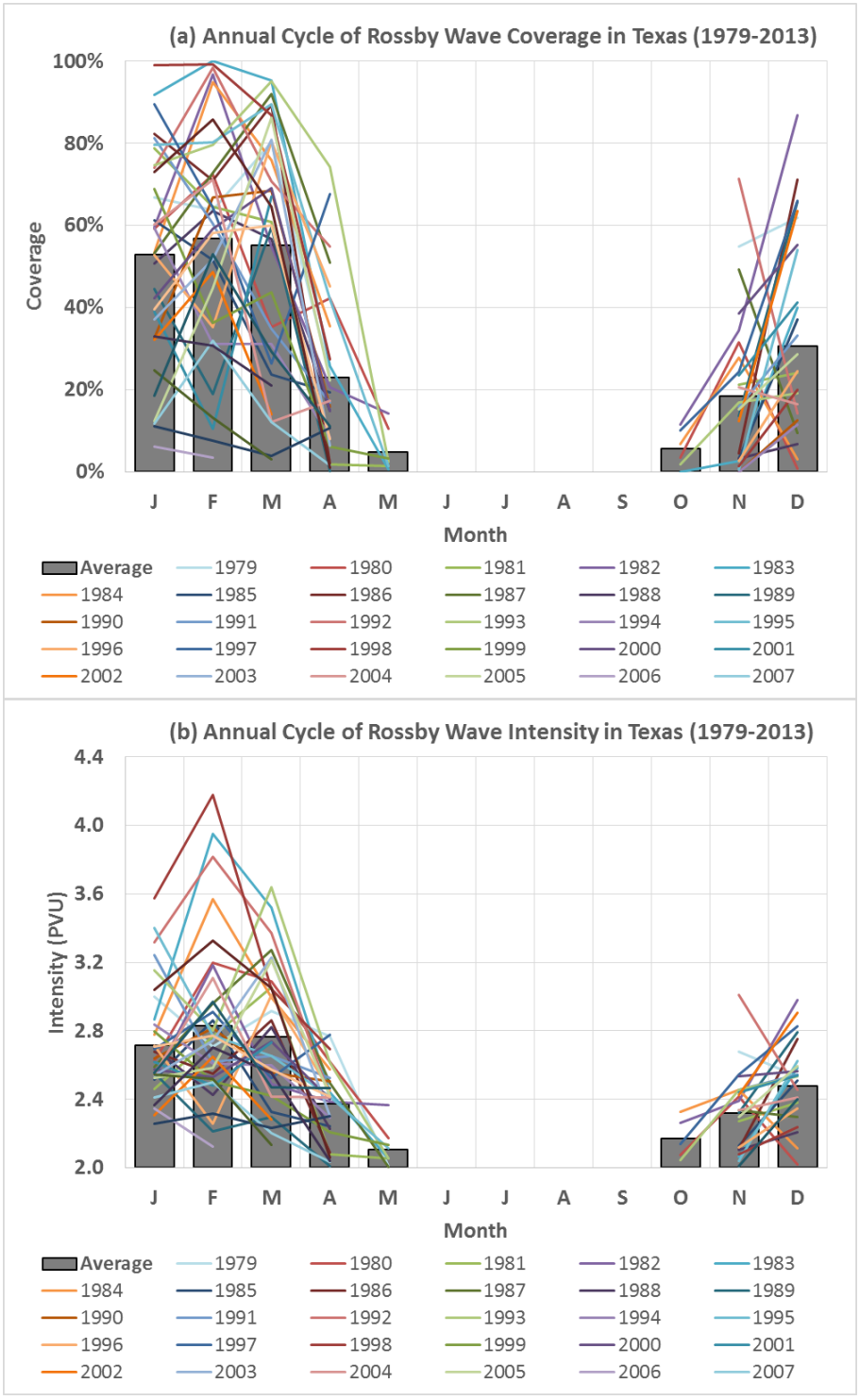

Figure IV-4 Annual cycle of monthly coverage and intensity of Rossby Wave in Texas

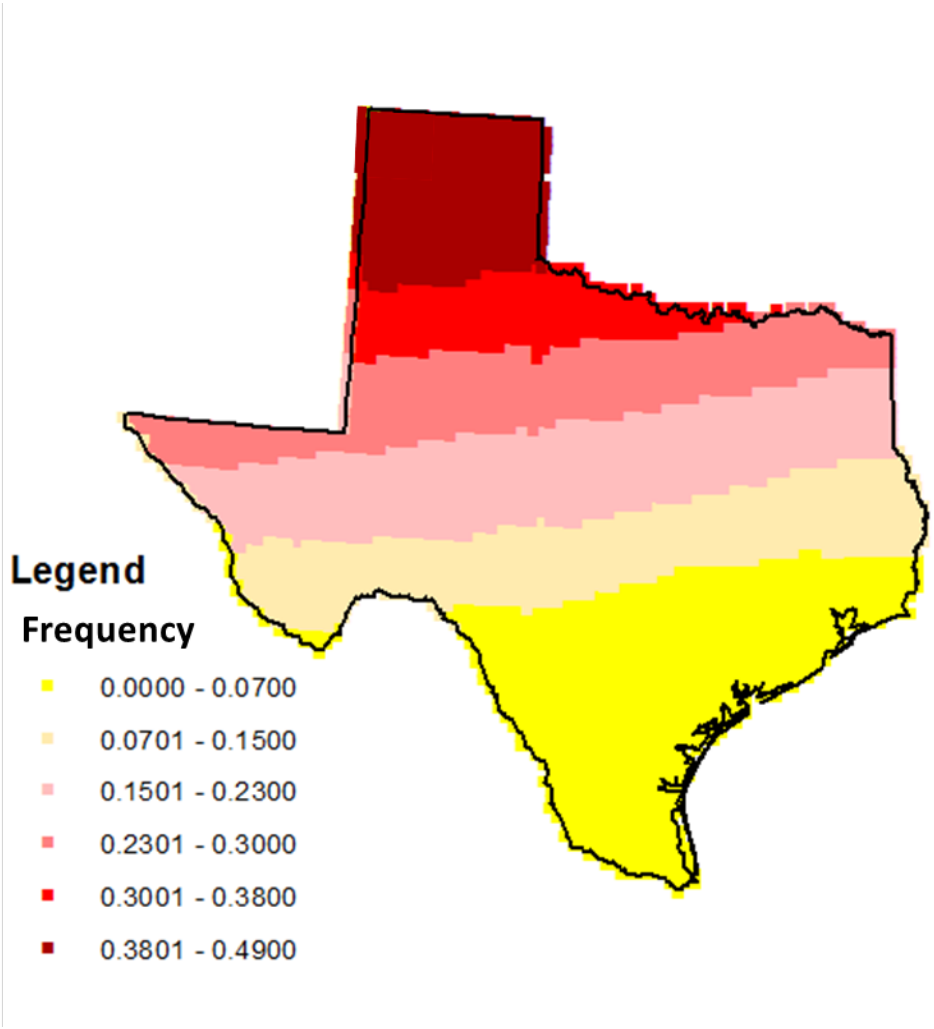

Figure IV-5 Frequency of Rossby Waves in Texas (1979-2013)

4.4.2 Rossby wave and extreme precipitation

The monthly coverage of RW and the 72-hour maximum precipitation (217-station average) in that month was calculated (Figure IV-6a) and its annual mean value was plotted (Figure IV-6b). Between RW coverage and maximum precipitation, there was no correlation found. The average of 72-hour maximum precipitation in no Rossby Wave months (42.68 mm) was larger than the amount in Rossby Wave months (33.27 mm). About 28.3% more precipitation received when there was no Rossby Wave. Rossby Wave generally brought drier condition than normal months without Rossby Wave. There was no trend found in the time series of monthly and annual mean of maximum precipitation with and without RW.

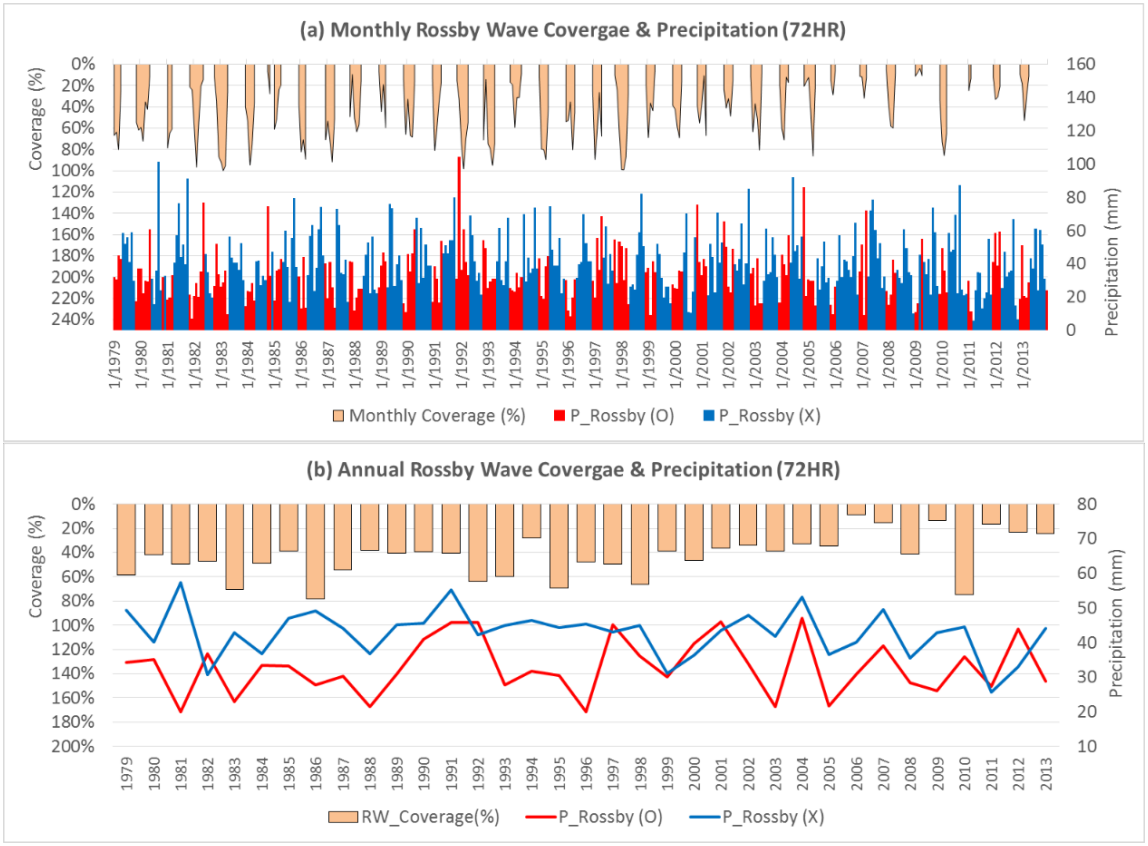

Figure IV-6 Time series of Rossby Wave coverage and precipitation

4.4.3 Rossby wave, El-Niño and La-Niña

The El-Niño–Southern Oscillation Precipitation Index (ESPI) and Rossby Wave were compared over time in Texas. Since ESPI and RW are monthly indices and variables, each month was grouped as either El-Niño month or La-Niña month. On average (1979-2013), all months' average of RW coverage was 38.4 % and of RW intensity was 2.56 PVU. El-Niño months had more intense and larger coverage of RW than in La-Niña months (Table IV-1). The total number of months of RW was 178 and no RW was 242. Historically, there was no RW in June, July, August, and September. Every year in January Texas was under RW. La-Niña dominantly occurred (246 months), while the number of El-Niño was 174 months. The number of months with La-Niña was larger every year (Table IV-2). During 420 months, 173 months (41.2%) were under El-Niño and 247 months (58.8%) were under La-Niña condition. The average values of monthly maximum precipitation under El-Niño was 40.81 mm and under La-Niña was 37.2 mm. Texas received about 9.7% more precipitation between 1979 and 2013. Historically, La-Niña brought slightly drier condition than El-Niño condition. Each month was classified as four different cases as shown in table IV-3. Historically, 'no Rossby Wave and La-Niña' condition dominantly occurred. The wettest condition was 'no Rossby Wave & El-Niño,' whereas the driest condition was 'Rossby Wave & La-Niña.' From this table, Rossby Wave again brought drier condition than normal months without Rossby Wave. Figure IV-7 shows the monthly occurrence of the joints events (four cases in Table IV-3). June, July, August, and September were never Rossby Wave months during 35 years. November was the only month having four different cases. The most extreme case was defined as

'above 90th percentile of 72-hour precipitation' from the 217 station averaged monthly extreme time series (Table IV-4). The joint event of 'no Rossby Wave & El-Niño' was most frequent (21 months) and 'Rossby Wave & El-Niño' was least frequent (3 months). In terms of the magnitude of extreme events, 'Rossby Wave & El-Niño' months experienced large amounts of precipitation (86.31 mm). The relationship among Rossby Wave, El-Niño, and La-Niña apparently showed the different amounts and frequency of extreme precipitation.

Table IV-1 Rossby wave, El-Niño and La-Niña

	All months	**El-Niño months**	**La-Niña months**
Coverage of RW	38.4 %	44.5 %	33.3 %
Intensity of RW	2.56	2.64	2.45

Table IV-2 Occurrence of Rossby wave, El-Niño and La-Niña

Number of month	J	F	M	A	M	J	J	A	S	O	N	D	Total
RW	35	34	32	25	2	0	0	0	0	3	16	31	178
NRW	0	1	3	10	33	35	35	35	35	32	19	4	242
El-Niño	15	14	16	14	14	13	14	15	16	12	15	16	174
La-Niña	20	21	19	21	21	22	21	20	19	23	20	19	246

Table IV-3 Joint events of Rossby Wave, El-Niño, and La-Niña on precipitation

Case	(1)	(2)	(3)	(4)
	RW & El-Niño	RW & La-Niña	No RW & El-Niño	No RW & La-Niña
Number of months	86	92	88	155
Number of months (%)	20.5 %	21.9 %	21.0 %	36.9 %
Precipitation	35.39 mm	31.30 mm	46.10m	40.76 mm

Table IV-4 Extreme combination of joint events on precipitation

Case	(1)	(2)	(3)	(4)
	RW & El-Niño	RW & La-Niña	No RW & El-Niño	No RW & La-Niña
Number of months	3	5	21	14
Precipitation	86.31 mm	72.94 mm	71.78mm	75.68 mm

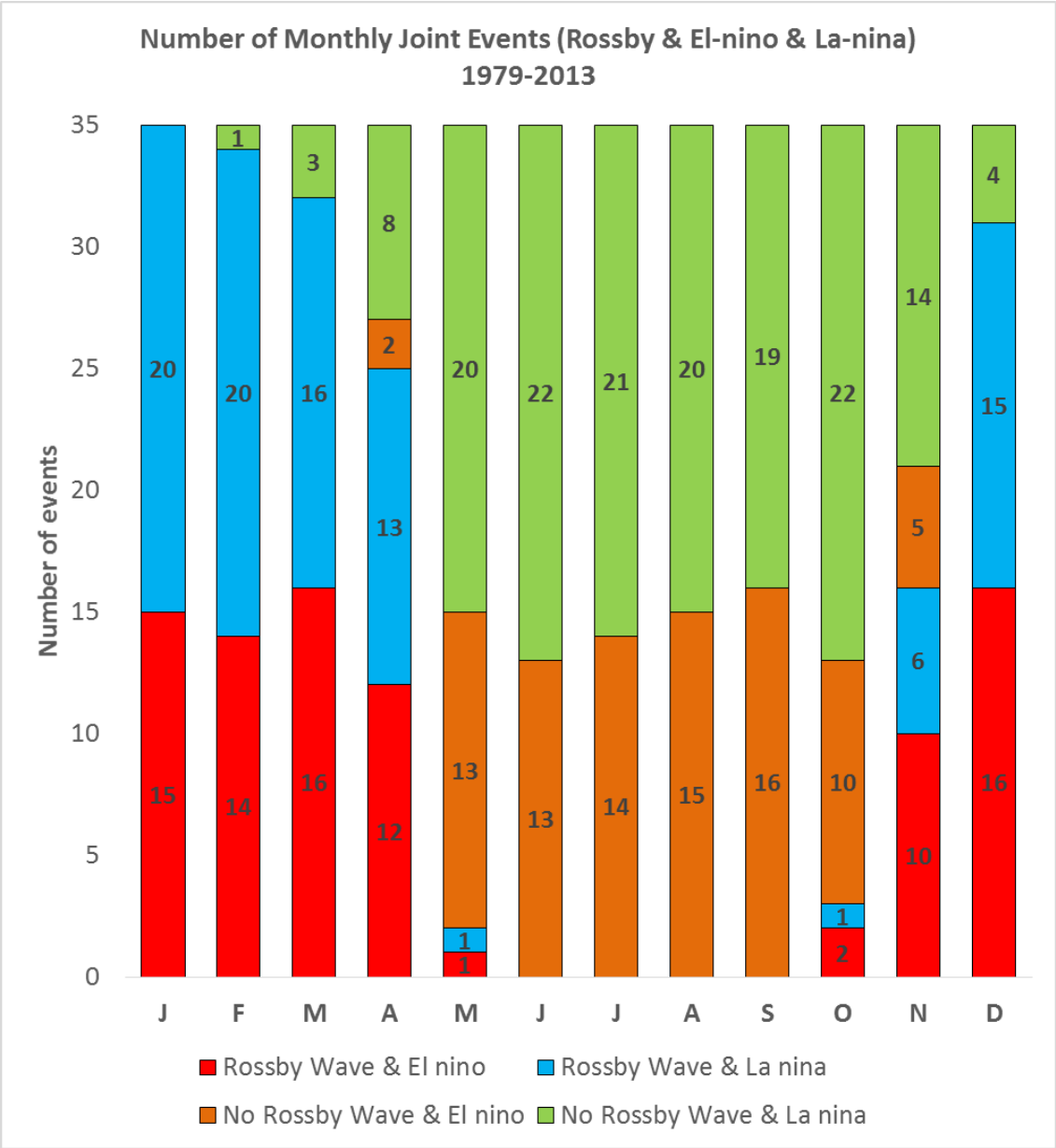

Figure IV-7 Number of monthly joint events (Rossby Wave, El-Niño, and La-Niña)

4.4.4 Climatic cycles and extreme precipitation

The monthly 72-hour maximum precipitation under different climatic indices were calculated (Figure IV-8). Each bar indicates the mean of monthly maxima over time. The mean of monthly maximum precipitation was 38.72 mm and its bias was between -1.63 mm and 2.11 mm. Extreme precipitation was largely affected by ESPI and SOI which directly indicated the El-Niño and La-Niña effects. ESPI (+) and SOI (-) indicated El-Niño. ESPI (-) and SOI (+) indicated La-Niña. PNA had the least effect of monthly extreme precipitation in Texas, because its impact was limited in the western part of the U.S.

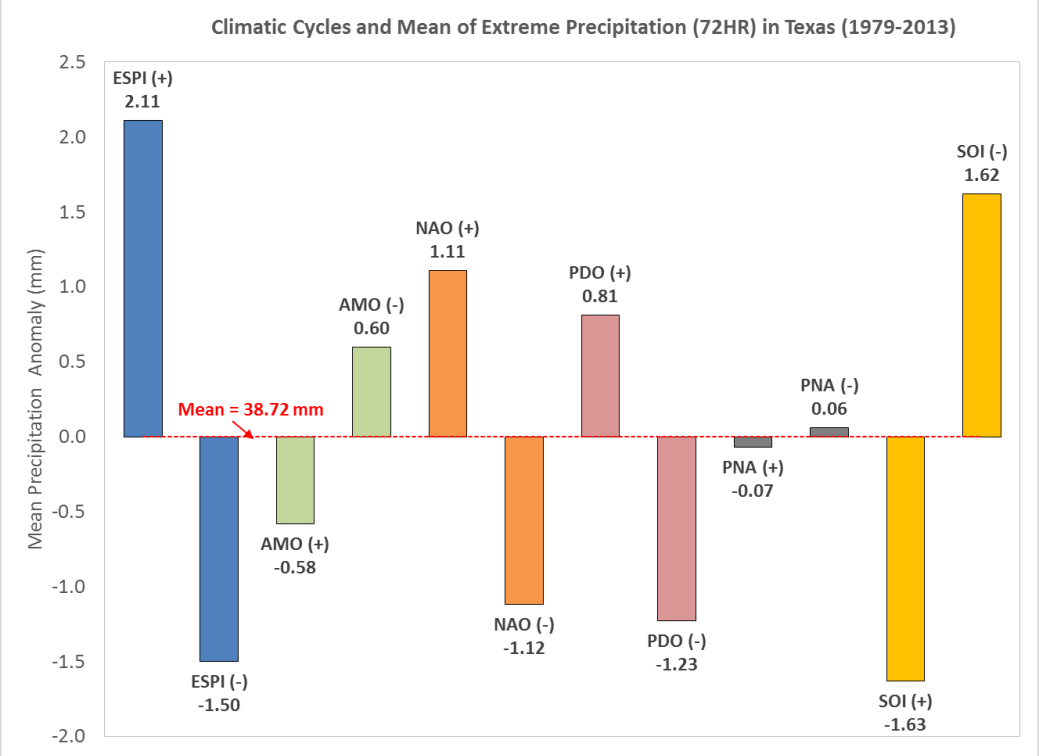

Figure IV-8 Climatic cycles and extreme precipitation

4.4.5 Joint events of climatic cycles and Rossby Wave on extreme precipitation

Under each climatic cycle, each month was classified in four different cases as (1) + index & Rossby Wave, (2) + index & no Rossby Wave, (3) - index & Rossby Wave, and (4) – index & no Rossby Wave. The number of months and how extreme precipitation were affected under each case of joint events (Climatic Cycle and Rossby Wave).

Under climatic cycles, the maximum number of joint events in each case were commonly under no Rossby Wave (Figure IV-9). Even though 'no Rossby Wave months' were limited to four months (June, July, August, and September), there were more joint events than in other 8 months. Among climatic cycles, La-Niña (negative ESPI) and no Rossby Wave had the maximum number of events (154 months out of 420 months, 36.7 %). In terms of precipitation amount, Texas commonly received more precipitation under 'no Rossby Wave (NRW)' under each climatic cycle (Figure IV-10). Rossby Wave brought drier condition in Texas. The wettest condition was 'El-Niño (positive ESPI) and no Rossby Wave'. The maximum precipitation difference between RW and NRW was found in positive ESPI (10.71 mm). The minimum precipitation difference between RW and NRW was found in negative PDO (2.97 mm). Among climatic cycles, ESPI was the most sensitive to the existence of Rossby Wave on extreme precipitation. Therefore, the effect of El-Niño and La-Niña under Rossby Wave on extreme precipitation was evident in Texas during the historical period.

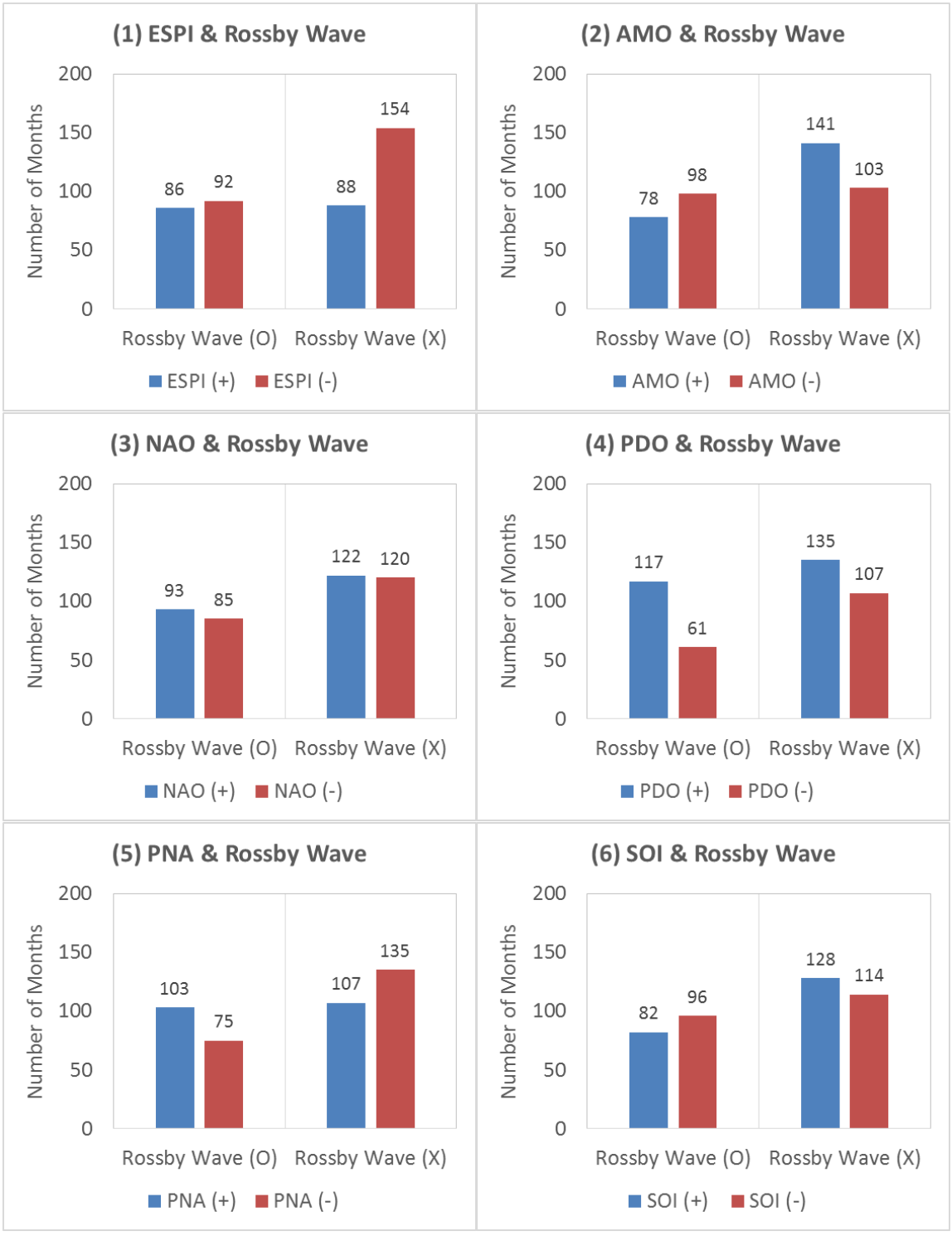

Figure IV-9 Number of joint events (Climatic Cycles and Rossby Wave)

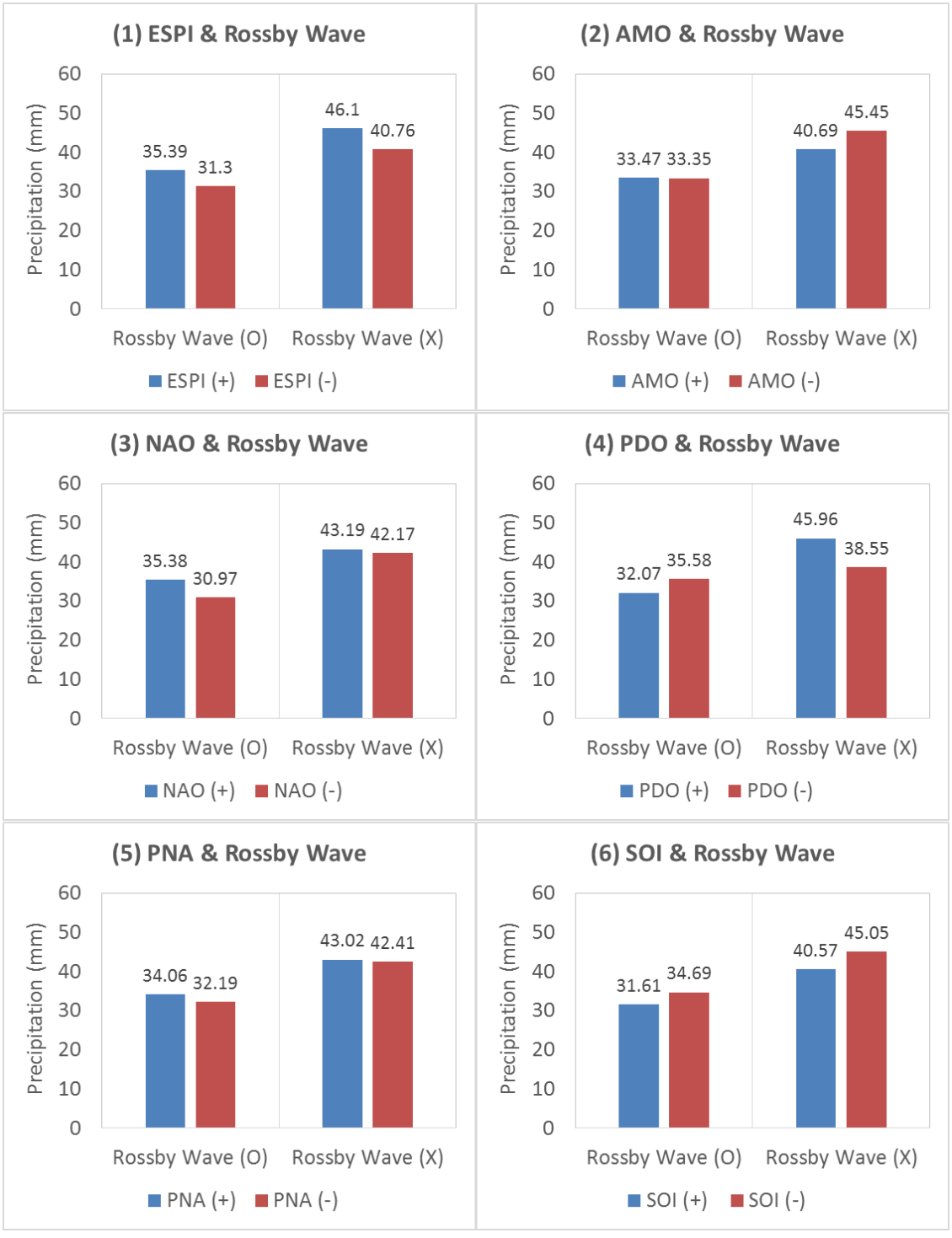

Figure IV-10 Extreme precipitation in joint events (Climatic Cycles and Rossby Wave)

4.4.6 Rossby Wave and precipitation characteristics

Precipitation characteristics in this analysis had four aspects, including of the number of rain days, duration, depth, and intensity of precipitation. The number of rain days was calculated for each station in every year. The duration, depth, and intensity were calculated from precipitation events which were independently selected from the time series of hourly precipitation in every year at each station. The Rossby Wave frequency map from figure IV-5 was used for developing the scatter plot of relationship between RW frequency and precipitation characteristics. Each station matched each the grid cell of frequency. In figure IV-11, the correlation between precipitations characteristics were not strong (R^2 of -0.22 to -0.51). However, four characteristics had adverse relation to the frequency of RW. Among the four aspects, the Rossby Wave frequency and precipitation depth were moderately correlated (R^2 = -0.51). There were five zones under different Rossby Wave frequency to see the relationship between Rossby Wave and precipitation characteristics (Figure IV-12). The four characteristics commonly have eastern to western (large to small) pattern in terms of their magnitude. We could find a pattern under different Rossby Wave frequency zones (Figure IV-13). Very North (High Frequency of Rossby Wave zone: ~0.5) had the least values of statistics of all characteristics. Very South (Low Frequency of Rossby Wave zone: ~0.1) had the largest values of all statistics. The average depth difference between RW frequency zone 1 and zone 2 was 34 mm (64.8 %). Not only correlation between RW frequency and precipitation depth but also the magnitude under different RW frequency zones was remarkable. The frequency of Rossby Wave evidently affects precipitation characteristics.

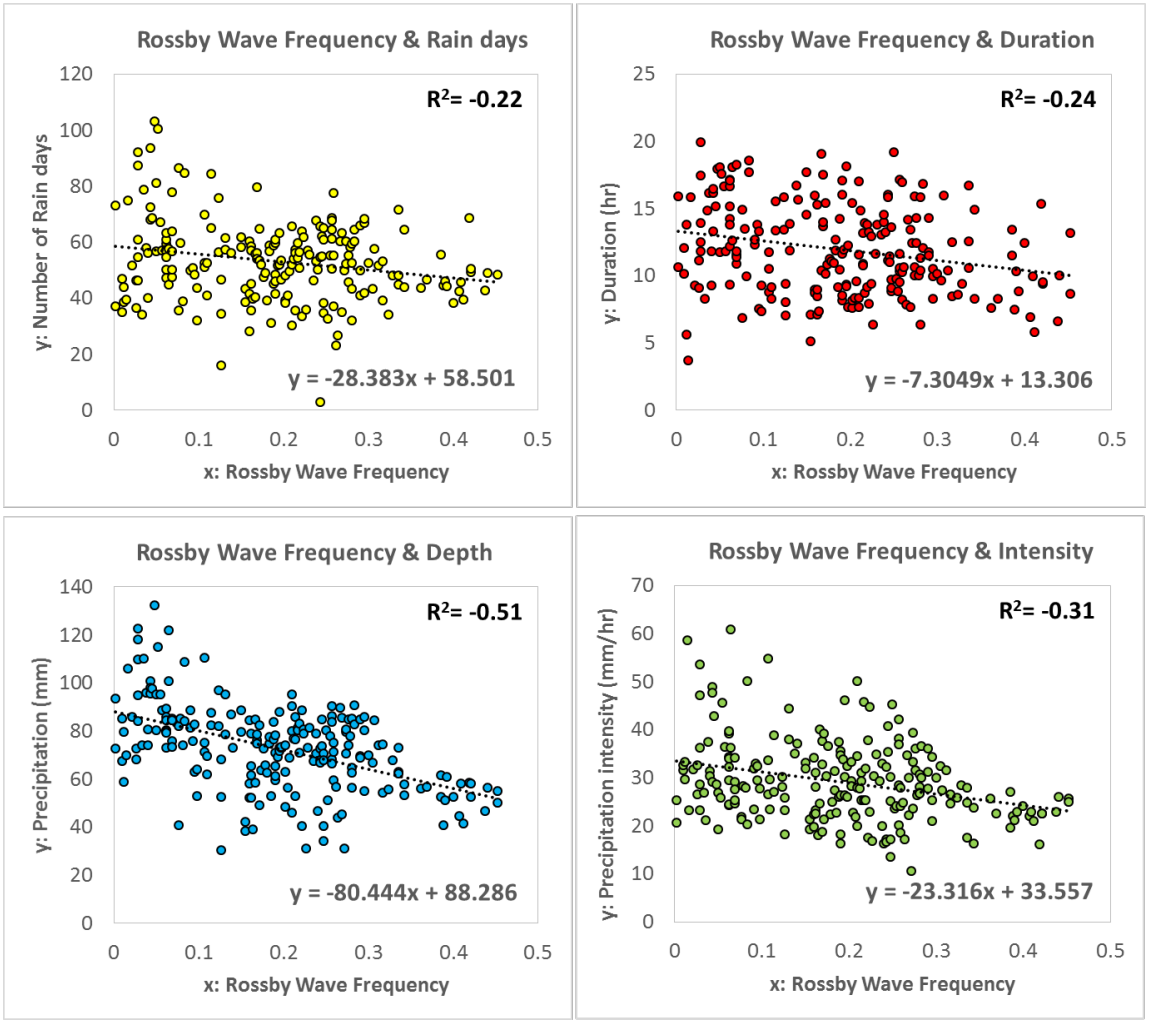

Figure IV-11 Rossby Wave frequency and precipitation characteristics in Texas

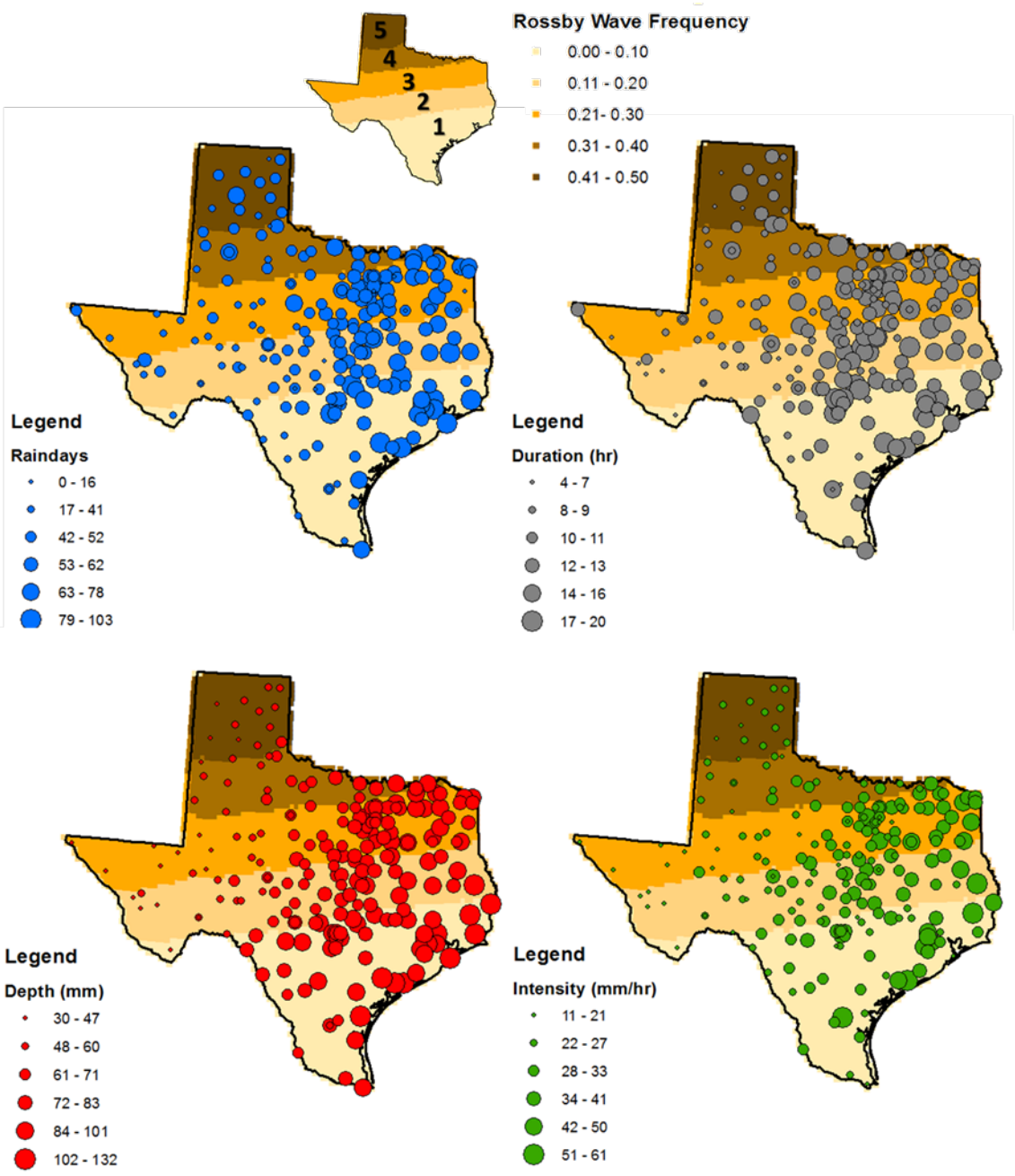

Figure IV-12 Spatial distribution of rain days, duration, depth, and intensity of precipitation

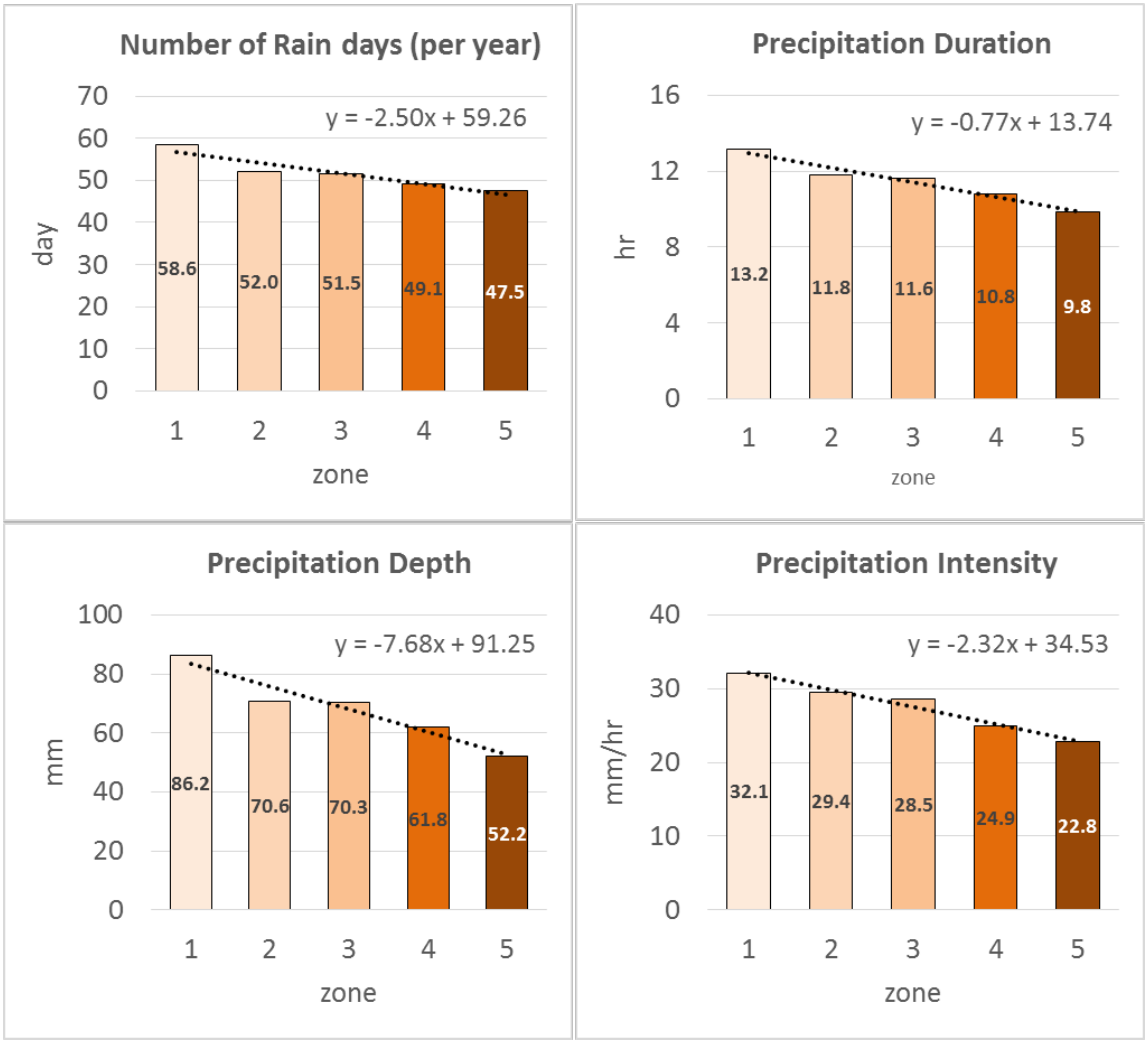

Figure IV-13 Precipitation characteristics under different Rossby Wave frequency zones.

4.5 Conclusion

Rossby Wave (RW) breaking was defined as a detection of Potential Vorticity (PV) and PV was a variable that was explained by the absolute vorticity (circulation) and the thickness of a column of air. By using ERA-Interim PV products, we could calculate the areal extent and the intensity of Rossby Wave over Texas from 1979 and 2013. RW visited Texas every year, however its coverage varied year to year. The mean of annual coverage of RW was 38.4 % and the mean of annual intensity of RW was 2.56 PVU in Texas. From the monthly time series of RW coverage and intensity, it was found that June, July, August, and September did not have RW. There was a spatial pattern in frequency of RW in North (High Frequency: ~0.5) and South (Low Frequency: ~0.1). The average of 72-hour maximum precipitation in no Rossby Wave months (42.68 mm) was 28.3% larger than the amount in Rossby Wave months (33.27 mm). However, there was no trend found in the time series of monthly and annual mean of maximum precipitation with and without RW.

ESPI and RW were monthly indices and variables, each month were grouped as either El-Niño months or La-Niña months. The El-Niño months had more intense (2.76 PVU) and larger coverage (44.5 %) of RW than in La-Niña months (2.45 PVU, 33.3 %). Historically, no Rossby Wave and La-Niña condition frequently occurred (37 % of duration). Extreme precipitation was largely affected by ESPI and SOI which directly indicated the El-Niño and La-Niña effects among climatic cycles. Texas commonly received more precipitation under ‘no Rossby Wave (NRW)’ under each climatic cycle. The effect of El-Niño and La-Niña under Rossby Wave on extreme precipitation was

evident in Texas. Rossby Wave frequency and precipitation depth were moderately correlated (R^2 = -0.51). Precipitation characteristics (number of rain days, duration, depth, and intensity of precipitation) commonly have eastern to western (large to small) pattern of its magnitude.

The effect of Rossby Wave was more significant than the effect of El-Niño and La-Niña on extreme precipitation in Texas. Rossby Wave had month-to-month variation, while the El-Niño and La-Niña had multi year-to-year cycles. Figure IV-14 shows three stages of Rossby Wave and air mass development. Throughout the year, the Gulf coast was under no Rossby Wave with the warm mass of tropical air. It remained relatively humid in all stages which resulted in more precipitation along the Gulf coast. The stage (a) was winter to spring months (December-January-February-March) with the average RW coverage of 48.9 %. Due to the intrusion of cold polar air mass, Texas experienced dry and humid weather at the same time by location. The average 72-hour maximum precipitation was 28.9 mm with the driest condition among three stages. The stage (b) was transition months between seasons (April and November). Due to strong warm tropical air mass, the coverage of RW decreased on average by 20.6% in Texas. Only the panhandle area of Texas was under Rossby Wave with cold mass of polar air and dryness. The average 72-hour maximum precipitation was 36.6 mm which had more amount than stage (a). The stage (c) was summer season from May to October. During this time, Rossby Wave was barely captured with the average coverage of 1.7 % of Texas. The warm mass of tropical air dominantly developed with more humidity from the ocean. Therefore, the amount of average 72-hour precipitation was the largest (45.1 mm) among the stages. The

effect of Rossby Wave was evident in the monthly cycle of precipitation extremes. These findings will contribute to understanding the climatology of precipitation, in addition to the joint effect of climatic cycle and atmospheric phenomenon of Rossby Wave.

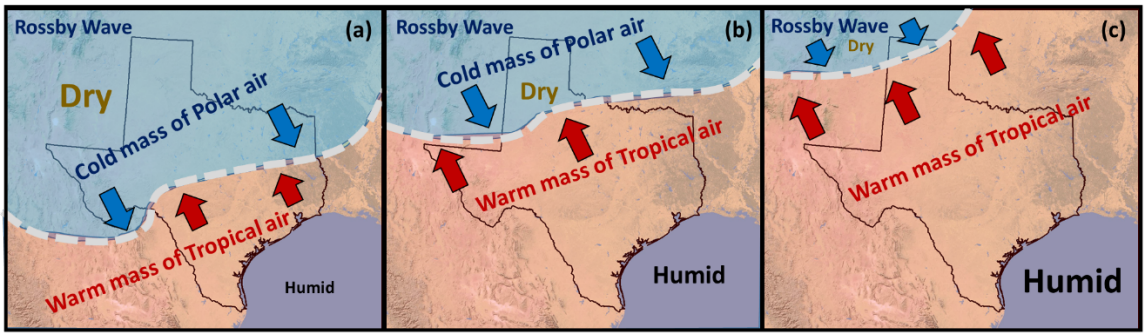

Dec-Jan-Feb-Mar (Winter-Spring)
Avg. occurrence: 33 of 35 months
Avg. coverage: 48.9 %
Avg. 72-hour precipitation: 28.9 mm

Apr & Nov (Transition)
Avg. occurrence: 20.5 of 35 months
Avg. coverage: 20.6 %
Avg. 72-hour precipitation: 36.6 mm

May-Jun-Jul-Aug-Sep-Oct (Summer)
Avg. occurrence: 0.8 of 35 months
Avg. coverage: 1.7 %
Avg. 72-hour precipitation: 45.1 mm

Figure IV-14 Rossby Wave and air mass developing in Texas

CHAPTER V

FUTURE PROBABLE MAXIMUM PRECIPITATION ESTIMATION USING CLIMATE PROJECTION SCENARIOS

5.1 Future climate projections of extreme precipitation

For future climate scenarios, the statistically downscaled climate projections from the Coupled Model Intercomparison Project Phase 5 (CMIP5) (Maurer, 2007; Reclamation et al., 2013) was adopted. Bias-Correction and Spatial Disaggregation (BCSD) are implemented to generate the gridded CMIP5 data (Wood et al., 2004). Future projections are available under Representative Concentration Pathway (RCP) +2.6w/m^2, +4.5w/m^2 +6.0w/m^2, and +8.5w/m^2 scenarios. In this study, 16 CMIP5 models were selected to project future climate change based on the data availability and two extreme RCPs of 2.6 and 8.5 were selected (Table V-1). Annual maximum precipitation and record precipitation were calculated from 217 precipitation stations which had more than 30 year data in Texas.

Each station had 1 set of historical annual maximum precipitation (AMP) series (1940-2013) and 16 sets of future AMP series (2020-2099) for two RCPs. The temporal mean of AMP and maximum of AMP (record precipitation) were scatter plotted in figure V-1 and figure V-2. The mean of AMP during historical period was 101.65 mm, future RCP 2.6 was 87.27 mm, and RCP 8.5 was 88.14 mm. The maximum of AMP during historical period was 249.01 mm, future RCP 2.6 was 209.26 mm, and RCP 8.5 was 219.50 mm.in Texas. Between historical and future periods, the drier condition was

projected in terms of CMIP5 ensemble means for both mean and maximum of AMP cases. RCP 8.5 scenarios had more precipitation than RCP 2.6 in the future. Even though there was more precipitation during the historical period, comparison of maxima (Figure V-2) indicated that there were a more chance of large maximum precipitation than in the historical period.

Table V-1 CMIP5 models

Model	Center
bcc-csm1-1	Beijing Climate Center, China Meteorological Administration
canesm2	Canadian Centre for Climate Modelling and Analysis
ccsm4	National Center for Atmospheric Research
csiro-mk3-6-0	Commonwealth Scientific and Industrial Research Organization in collaboration with the Queensland Climate Change Centre of Excellence
gfdl-cm3	Geophysical Fluid Dynamics Laboratory
gfdl-esm2g	
gfdl-esm2m	
ipsl-cm5a-lr	Institute Pierre-Simon Laplace
ipsl-cm5a-mr	
miroc5	Atmosphere and Ocean Research Institute, National Institute for Environmental Studies, and Japan Agency for Marine-Earth Science and Technology
miroc-esm	
miroc-esm-chem	
mpi-esm-lr	Max Planck Institute for Meteorology
mpi-esm-mr	
mri-cgcm3	Meteorological Research Institute
noresm1-m	Norwegian Climate Centre

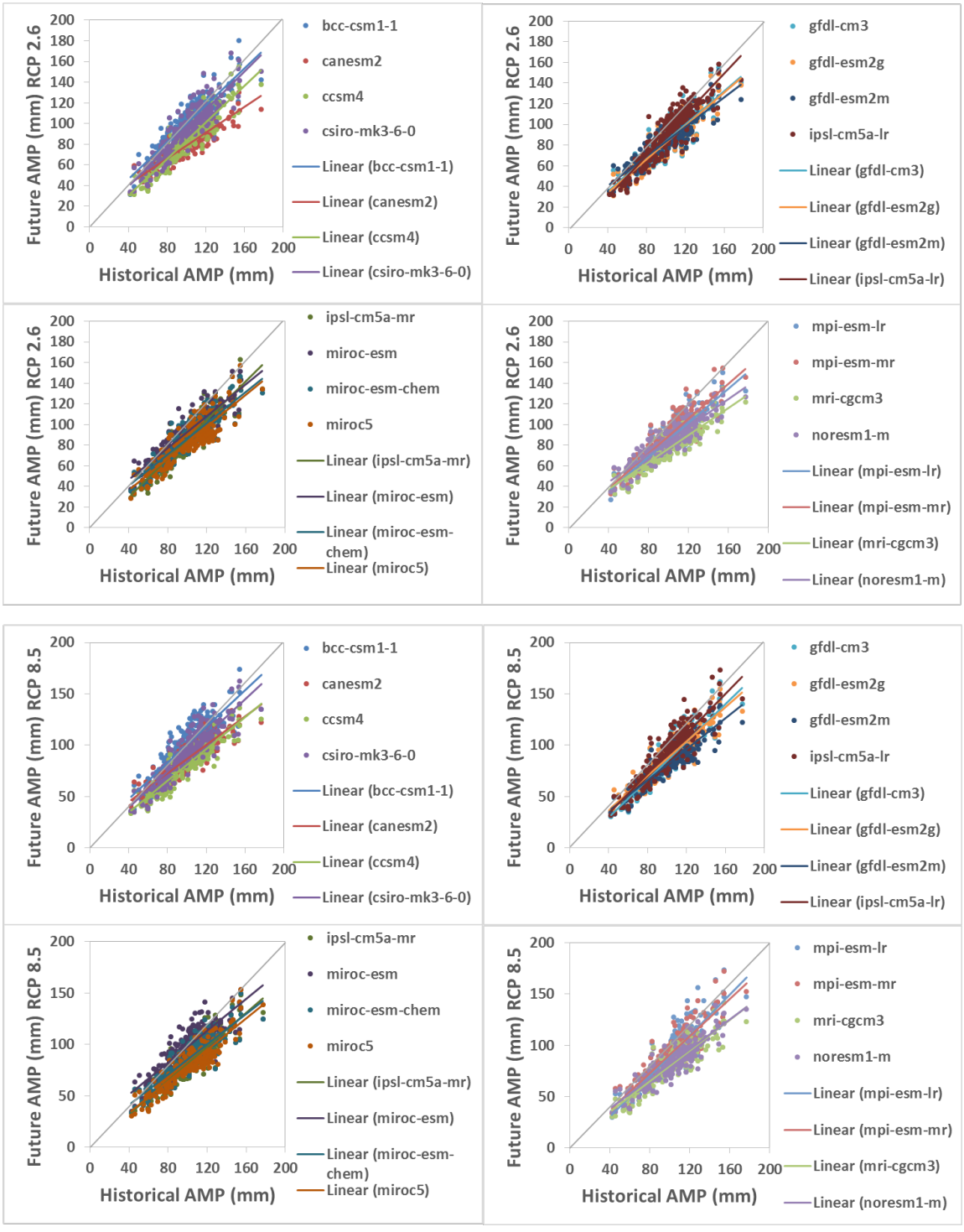

Figure V-1 Historical and future mean of AMP series (72-HR)

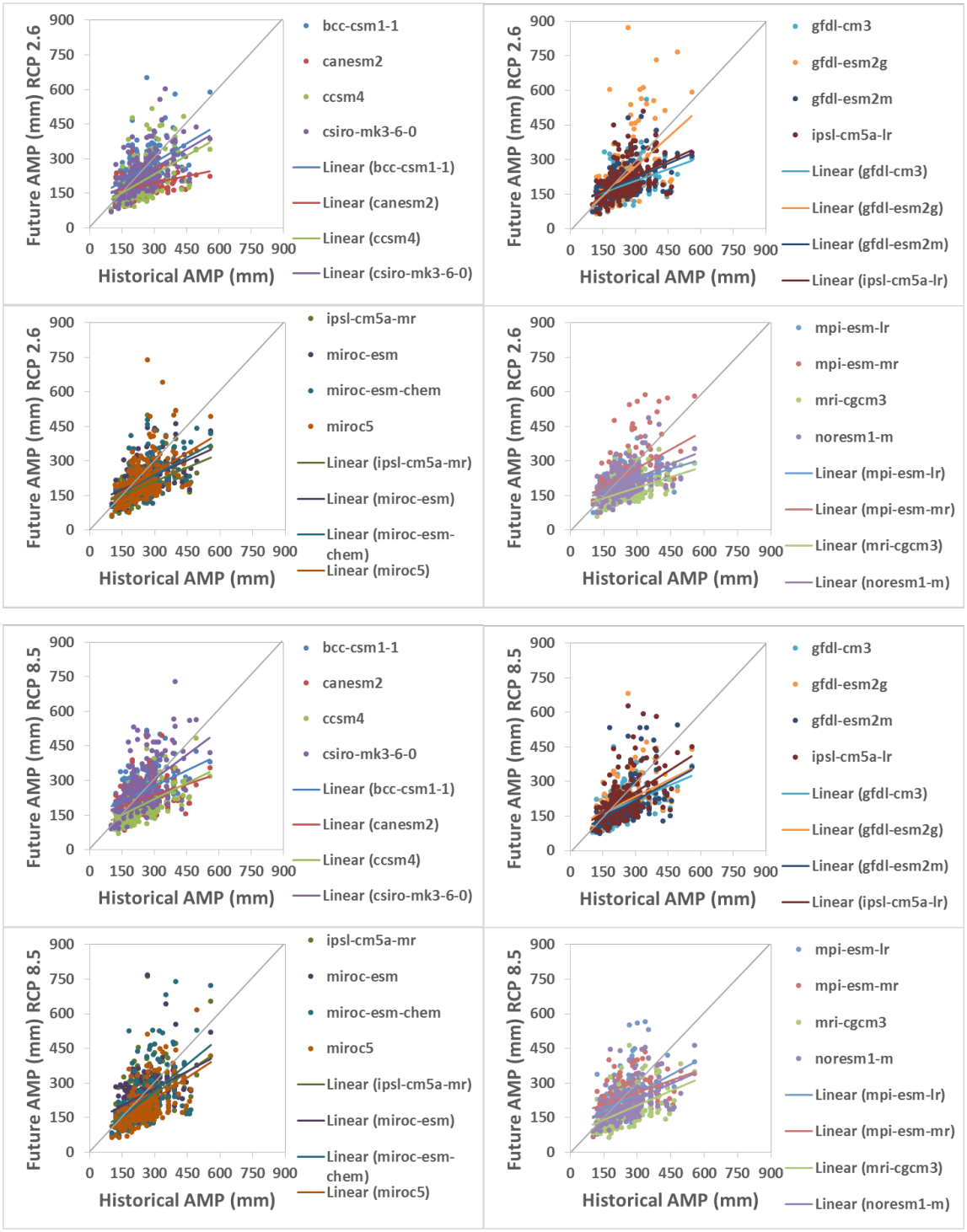

Figure V-2 Historical and future maximum of AMP series (72-HR)

5.2 Future PMP estimation

Using Hershfield and site-specific method, future PMP was estimated using projected future precipitation values (Figure V-3). Because PMP estimation depends on the available observations, it was sensitive to maximum precipitation and the shape of frequency factor curve was very dependent on the existence of maxima. Bold lines were historical PMPs in red with Hershfield method and blue with site-specific method. 16 red lines were future PMP estimation using Hershfield and 16 blue lines were future PMP of site-specific method. There were several stations with large values of future PMP than in historical PMP.

The number of stations (out of 217) more than historical PMP under two RCPs and two PMP estimation methods were calculated (Figure V-4). In RCP 2.6, the average number of stations more than historical PMP was 41 in Hershfield method and 48 in site-specific method. However, site-specific method (49) had the number of stations more than historical PMP in RCP 8.5 than Hershfield method (47). In both RCPs, bcc-csm1-1 had the most extreme cases among 16 CMIP5 scenarios.

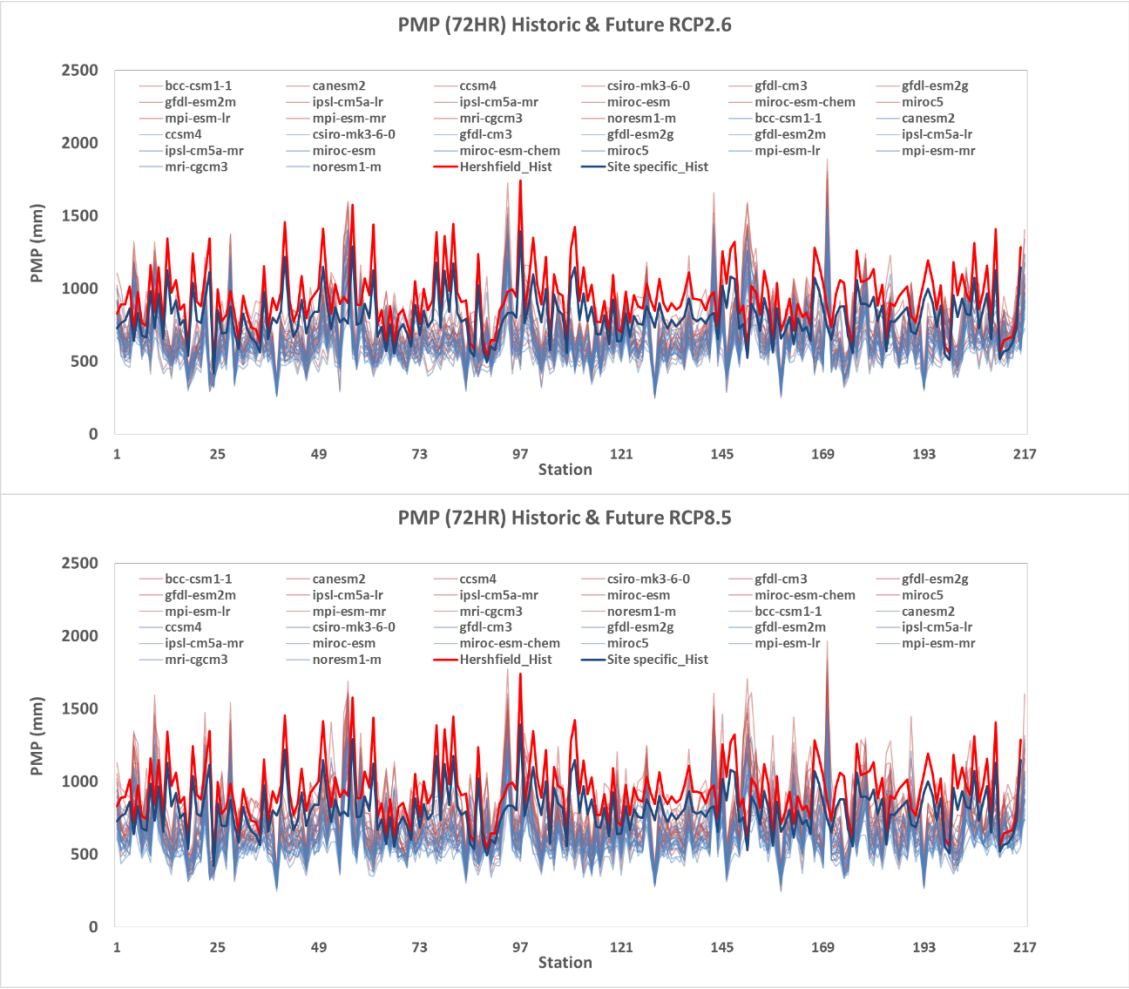

Figure V-3 PMP historical and future RCP 2.6 and RCP 8.5

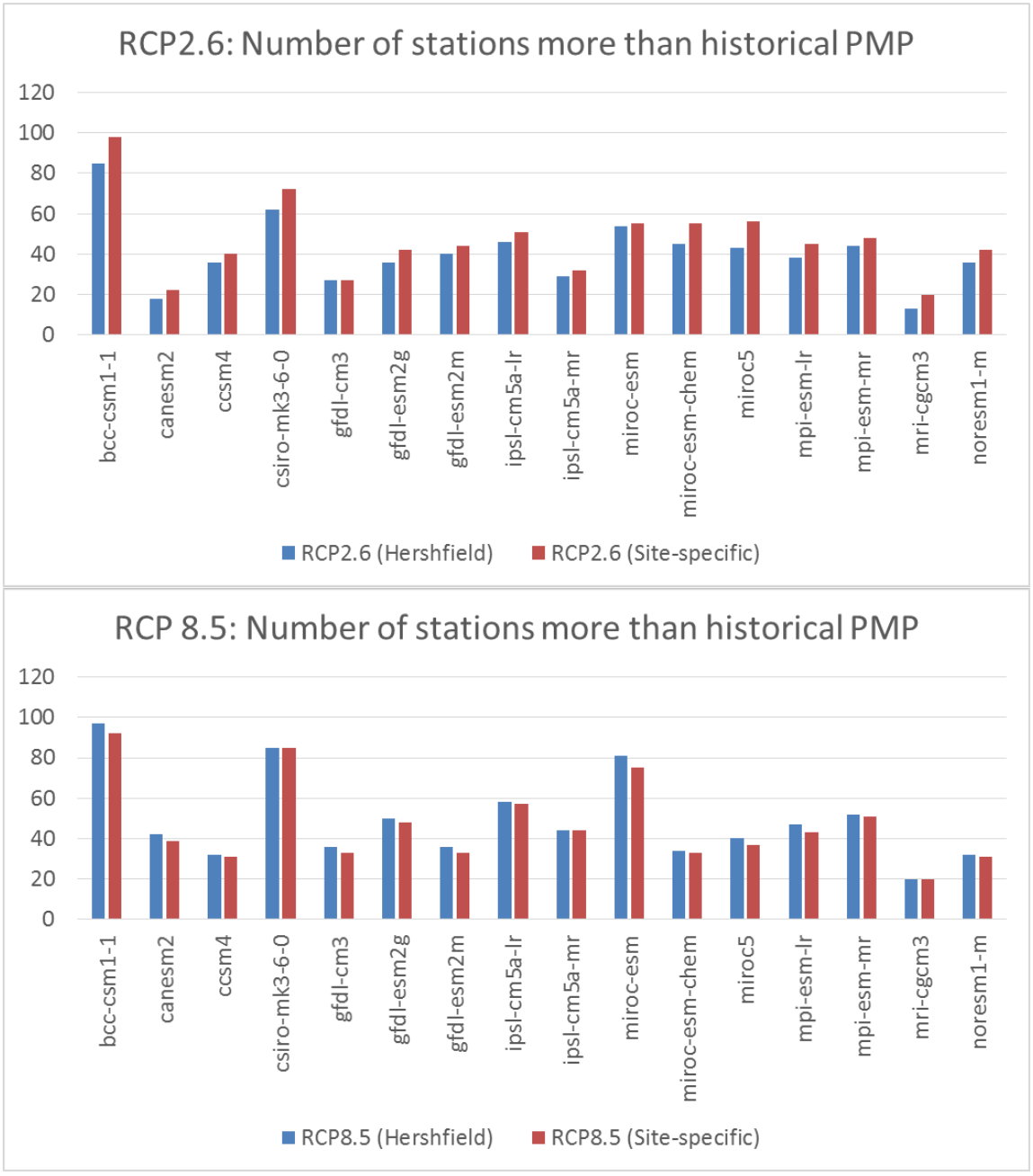

Figure V-4 Comparison between historical and future PMPs

CHAPTER VI

CONCLUSIONS

6.1 Conclusion

This dissertation explored the relationship between extreme precipitation and climatic cycles under climate change in Texas. The estimation of PMP is a key consideration for dam safety. However, There is no universal definition of PMP and its calculation involves multiple sources of uncertainties, including non-stationarity, topography, and method of computation. Among sources of uncertainties, the selection of method had the largest contribution. During the historical period, the non-stationarity of extreme precipitation was captured. This entailed that there was a likelihood of PMP increase in the future if non-stationarity of extreme precipitation continues similarly as the historical period. We emphasized that uncertainty analysis of PMP estimation was limited to site-specific PMP estimation so using adequate data for certain area was required. The warm and cold phases of climatic cycles affected the annual cycle of monthly extreme precipitation which maintained two precipitation peaks. The El-Niño years received about 16% more precipitation annually than did the La-Niña years. El-Niño and La-Niña dominantly affected the annual cycle of monthly maximum precipitation in Southcentral and Upper Coast. In Texas, 67% stations received more precipitation during El-Niño years from 1950 to 2013 due to the southern branch of the jet stream moving over the state which intensifies storms. At farther distances from the coastline, less precipitation and less variable extreme precipitation was captured. The historical extreme events showed various

responses in different phases of climatic cycles. These findings could raise the community's awareness for broader insights into understanding meteorological extreme events. Potential Vorticity was a measure of Rossby Wave and was widely used in recent studies. From the calculation of areal extent and intensity of Rossby Wave, RW visited Texas every year, however its coverage and intensity varied year to year. It was found that June, July, August, and September never had RW. There was 28.3% more precipitation in no Rossby Wave months than in Rossby Wave months. The El-Niño months had more intense and larger coverage of RW than has La-Niña months. The joint event of no Rossby Wave and La-Niña condition dominantly occurred. Precipitation characteristics (number of rain days, duration, depth, and intensity of precipitation) also showed a pattern under different RW frequency zones. These findings will contribute to understanding the climatology of precipitation, in addition to the joint effect of climatic cycle and atmospheric phenomenon of Rossby Wave. Through this study, we explored the broader insights of precipitation extremes by looking at different aspects of natural phenomenon such as climatic cycles and Rossby Wave in Texas. Global scale climatic indices and Rossby Wave could explain the regional behavior of extreme precipitation. Our findings will be possibly useful for water resources management and planning.

6.2 Recommendations

We propose further research, and specifically, we suggest the following:

- Extend the study domain to a continental and global scale, especially for uncertainty analysis of PMP estimation, because our findings were site specific and the sources of uncertainty contribution may not be same or similar to Brazos River basin in Texas.
- Due to the availability of hourly precipitation which are available until 2013 with quality control, PMP estimation needs to be updated every couple of decades. Because 1970s reports still used for dam safety practice, we found PMP was sensitive to observations including extreme values.
- This study was solely focused on hourly precipitation for climatology. Storm events are a complex phenomenon of climatology and atmospheric circulation. Thus, more variables, such as wind speed, sea surface temperature, and atmospheric pressure data, could lead to more robust results.
- PMP is the key component for the estimation of probable maximum flood (PMF). Comprehensive analysis of PMP and PMF would be beneficial for storm water management.
- Climatic cycles and Rossby Wave were jointly investigated in terms of precipitation characteristics. An independent analysis for the contribution of each phenomenon is recommended.

REFERENCES

Anderson, T.W., Darling, D.A., 1954. A test of goodness of fit. Journal of the American statistical association, 49(268): 765-769.

Ashley, S.T., Ashley, W.S., 2008. Flood fatalities in the United States. Journal of Applied Meteorology and Climatology, 47(3): 805-818.

Asquith, W.H., 1998. Depth-duration frequency of precipitation for Texas. Water-Resources Investigations Report, 98: 4044.

Bass, B., Juan, A., Gori, A., Fang, Z., Bedient, P., 2016. 2015 Memorial Day Flood Impacts for Changing Watershed Conditions in Houston. Natural Hazards Review, 18(3): 05016007.

Beauchamp, J., Leconte, R., Trudel, M., Brissette, F., 2013. Estimation of the summer-fall PMP and PMF of a northern watershed under a changed climate. Water Resources Research, 49(6): 3852-3862.

Bell, I., Visbeck, M., 2009. North Atlantic Oscillation.

Benke, A.C., Cushing, C.E., 1996. Rivers of North America.

Benson, M.A., 1973. Thoughts on the design of design floods. IN: FLOODS AND DROUGHTS.

Bhatia, N., Singh, V.P., Lee, K., 2019. Variability of extreme precipitation over Texas and its relation with climatic cycles. Theoretical and Applied Climatology. DOI:10.1007/s00704-019-02840-w

Bhatia, N., Singh, V.P., Lee, K., 2020. Sensitivity of extreme precipitation in Texas to climatic cycles. Theoretical and Applied Climatology: 1-10.

Bomar, G.W., 1995. Texas weather. University of Texas Press.

Breeding, S.D., 1948. Texas floods of 1940. US Government Printing Office.

Brugnara, Y., Maugeri, M., 2019. Daily precipitation variability in the southern Alps since the late 19th century. International Journal of Climatology, 39(8): 3492-3504. DOI:10.1002/joc.6034

Carlson, T.N., 1980. Airflow through midlatitude cyclones and the comma cloud pattern. Monthly Weather Review, 108(10): 1498-1509.

Casas, M.C., Rodríguez, R., Nieto, R., Redaño, A., 2008. The estimation of probable maximum precipitation. Annals of the New York Academy of Sciences, 1146(1): 291-302.

Casas, M.C., Rodríguez, R., Prohom, M., Gázquez, A., Redaño, A., 2011. Estimation of the probable maximum precipitation in Barcelona (Spain). International Journal of Climatology, 31(9): 1322-1327.

Cavazos, T., 1999. Large-Scale Circulation Anomalies Conducive to Extreme Precipitation Events and Derivation of Daily Rainfall in Northeastern Mexico and Southeastern Texas. Journal of Climate, 12(5): 1506-1523. DOI:10.1175/1520-0442(1999)012<1506:lscact>2.0.co;2

Chan, J.C., Zhou, W., 2005. PDO, ENSO and the early summer monsoon rainfall over south China. Geophysical Research Letters, 32(8).

Chavan, S.R., Srinivas, V., 2015. Probable maximum precipitation estimation for catchments in Mahanadi river basin. Aquatic Procedia, 4: 892-899.

Chavan, S.R., Srinivas, V., 2017. Regionalization based envelope curves for PMP estimation by Hershfield method. International Journal of Climatology, 37(10): 3767-3779.

Chiew, F.H.S., McMahon, T.A., 2002. Global ENSO-streamflow teleconnection, streamflow forecasting and interannual variability Hydrological Sciences Journal, 47(3): 505-522. DOI:10.1080/02626660209492950

Chow, V.T., 1951. A general formula for hydrologic frequency analysis. Eos, Transactions American Geophysical Union, 32(2): 231-237.

Chow, V.T., Maidment, D.R., Mays, L.W., 1988. Applied hydrology.

Collier, C., 2007. Flash flood forecasting: What are the limits of predictability? Quarterly Journal of the royal meteorological society, 133(622): 3-23.

Collier, C., Hardaker, P., 1996. Estimating probable maximum precipitation using a storm model approach. Journal of hydrology, 183(3-4): 277-306.

Conover, W.J., 1972. A Kolmogorov goodness-of-fit test for discontinuous distributions. Journal of the American Statistical Association, 67(339): 591-596.

Council, N.R., 2000. Risk analysis and uncertainty in flood damage reduction studies. National Academies Press.

Curtis, S., 2008. The Atlantic multidecadal oscillation and extreme daily precipitation over the US and Mexico during the hurricane season. Climate Dynamics, 30(4): 343-351. DOI:10.1007/s00382-007-0295-0

Curtis, S., Adler, R., 2000. ENSO indices based on patterns of satellite-derived precipitation. Journal of Climate, 13(15): 2786-2793.

Curtis, S., Adler, R.F., 2003. Evolution of El Niño-precipitation relationships from satellites and gauges. Journal of Geophysical Research: Atmospheres, 108(D4). DOI:10.1029/2002jd002690

Dee, D.P. et al., 2011. The ERA-Interim reanalysis: Configuration and performance of the data assimilation system. Quarterly Journal of the royal meteorological society, 137(656): 553-597.

Dhar, O., Kulkarni, A., Rakhecha, P., 1981. Probable maximum point rainfall estimation for the southern half of the Indian peninsula. Proceedings of the Indian Academy of Sciences-Earth and Planetary Sciences, 90(1): 39-46.

Dong, X. et al., 2011. Investigation of the 2006 drought and 2007 flood extremes at the Southern Great Plains through an integrative analysis of observations. Journal of Geophysical Research: Atmospheres, 116(D3).

Dooge, J.C., 1986. Looking for hydrologic laws. Water Resources Research, 22(9S).

Douglas, E.M., Barros, A.P., 2003. Probable maximum precipitation estimation using multifractals: application in the eastern United States. Journal of Hydrometeorology, 4(6): 1012-1024.

Downton, M.W., Miller, J.Z.B., Pielke Jr, R.A., 2005. Reanalysis of US National Weather Service flood loss database. Natural Hazards Review, 6(1): 13-22.

Durodola, O.S., 2019. The Impact of Climate Change Induced Extreme Events on Agriculture and Food Security: A Review on Nigeria. Agricultural Sciences, 10(4): 487-498.

Enfield, D.B., Mestas-Nuñez, A.M., Trimble, P.J., 2001. The Atlantic Multidecadal Oscillation and its relation to rainfall and river flows in the continental U.S. Geophysical Research Letters, 28(10): 2077-2080. DOI:10.1029/2000gl012745

Erdman, J., 2019. Is Houston the Nation's Flood Capital?, SEVERE WEATHER. weather.com.

Essic, J., 2005. National Land Cover Dataset.

FEMA, 2004. Federal guidelines for dam safety, selecting and accommodating inflow design flood for dams.

FEMA, F.E.M.A., 2012. Summary of Existing Guidelines for Hydrologic Safety of Dams.

Field, C.B. et al., 2012. IPCC 2012. Managing the risks of extreme events and disasters to advance climate change adaptation. A special report of the intergovernmental panel on climate change.

Fischer, E.M., Knutti, R., 2016. Observed heavy precipitation increase confirms theory and early models. Nature Climate Change, 6(11): 986.

Folland, C.K., Colman, A.W., Rowell, D.P., Davey, M.K., 2001. Predictability of Northeast Brazil Rainfall and Real-Time Forecast Skill, 1987–98. Journal of Climate, 14(9): 1937-1958. DOI:10.1175/1520-0442(2001)014<1937:ponbra>2.0.co;2

Fowler, H., Kilsby, C., 2003. A regional frequency analysis of United Kingdom extreme rainfall from 1961 to 2000. International Journal of Climatology: A Journal of the Royal Meteorological Society, 23(11): 1313-1334.

Funk, T., 2006. Heavy convective rainfall forecasting: A look at elevated convection, propagation, and precipitation efficiency, Proc. 10th Severe Storm and Doppler Radar Conf.

Geology, B.o.E., 1996. RIVER BASIN MAP OF TEXAS. In: Texas, R.B.o. (Ed.), University of Texas, Austin, TX. Bureau of Economic Geology.

Gerlitz, L. et al., 2016. A statistically based seasonal precipitation forecast model with automatic predictor selection and its application to central and south Asia. Hydrol. Earth Syst. Sci., 20(11): 4605-4623. DOI:10.5194/hess-20-4605-2016

Gleaton, C.S., Anderson, C.G., 2005. Facts about Texas and US agriculture. Texas Cooperative Extension Department of Agricultural Economics, The Texas A&M University System, College Station, Texas.

Gochis, D. et al., 2015. The great Colorado flood of September 2013. Bulletin of the American Meteorological Society, 96(9): 1461-1487.

Goldenberg, S.B., Landsea, C.W., Mestas-Nuñez, A.M., Gray, W.M., 2001. The Recent Increase in Atlantic Hurricane Activity: Causes and Implications. Science, 293(5529): 474-479. DOI:10.1126/science.1060040

Goodess, C.M., 2013. How is the frequency, location and severity of extreme events likely to change up to 2060? Environmental science & policy, 27: S4-S14.

Goodrich, G.B., Walker, J.M., 2011. The influence of the PDO on winter precipitation during high-and low-index ENSO conditions in the eastern United States. Physical Geography, 32(4): 295-312.

Greatbatch, R.J., 2000. The North Atlantic Oscillation. Stochastic Environmental Research and Risk Assessment, 14(4): 213-242. DOI:10.1007/s004770000047

Greenwood, P.E., Nikulin, M.S., 1996. A guide to chi-squared testing, 280. John Wiley & Sons.

Guerrero, B., 2012. The Impact of Agricultural Drought Losses on the Texas Economy, 2011. Briefing paper, updated, 4(2): 2012.

Guilbert, J., Betts, A.K., Rizzo, D.M., Beckage, B., Bomblies, A., 2015. Characterization of increased persistence and intensity of precipitation in the northeastern United States. Geophysical Research Letters, 42(6): 1888-1893.

Guirguis, K., Gershunov, A., Cayan, D.R., 2015. Interannual variability in associations between seasonal climate, weather, and extremes: wintertime temperature over the Southwestern United States. Environmental Research Letters, 10(12): 124023.

Hamed, K.H., Rao, A.R., 1998. A modified Mann-Kendall trend test for autocorrelated data. Journal of hydrology, 204(1-4): 182-196.

Hanley, J., Caballero, R., 2012. The role of large-scale atmospheric flow and Rossby wave breaking in the evolution of extreme windstorms over Europe. Geophysical Research Letters, 39(21).

Hansen, E.M., Schreiner, L.C., Miller, J.F., 1982. Application of probable maximum precipitation estimates: United States east of the 105th meridian, 55. US Department of Commerce, National Oceanic and Atmospheric Administration.

Hao, Z., Singh, V.P., 2013. Entropy-based method for extreme rainfall analysis in Texas. Journal of Geophysical Research: Atmospheres, 118(2): 263-273. DOI:10.1029/2011jd017394

Harrold, T., 1973. Mechanisms influencing the distribution of precipitation within baroclinic disturbances. Quarterly Journal of the Royal Meteorological Society, 99(420): 232-251.

Henderson, K.G., Robinson, P.J., 1994. Relationships between the Pacific/North American teleconnection patterns and precipitation events in the south-eastern USA. International Journal of Climatology, 14(3): 307-323.

Hendrickson Jr, K., 2002. Handbook of Texas online: Brazos River. Texas State Historical Association.

Hershfield, D.M., 1961a. Estimating the probable maximum precipitation. Journal of the hydraulics Division, 87(5): 99-116.

Hershfield, D.M., 1961b. Rainfall frequency atlas of the United States. Technical paper, 40.

Hershfield, D.M., 1965. Method for estimating probable maximum rainfall. Journal (American Water Works Association), 57(8): 965-972.

Hill, K., Taschetto, A., England, M., 2011. Sensitivity of South American summer rainfall to tropical Pacific Ocean SST anomalies. Geophysical Research Letters, 38(1).

Holton, J.R., 1973. An introduction to dynamic meteorology. American Journal of Physics, 41(5): 752-754.

Hosking, J.R., 1985. Algorithm as 215: Maximum-likelihood estimation of the parameters of the generalized extreme-value distribution. Journal of the Royal Statistical Society. Series C (Applied Statistics), 34(3): 301-310.

Hosking, J.R.M., Wallis, J.R., Wood, E.F., 1985. Estimation of the generalized extreme-value distribution by the method of probability-weighted moments. Technometrics, 27(3): 251-261.

Hoskins, B.J., McIntyre, M.E., Robertson, A.W., 1985. On the use and significance of isentropic potential vorticity maps. Quarterly Journal of the Royal Meteorological Society, 111(470): 877-946.

Hu, H. et al., 2017. Linking atmospheric river hydrological impacts on the US West Coast to Rossby wave breaking. Journal of Climate, 30(9): 3381-3399.

Hu, Q., Feng, S., 2008. Variation of the North American summer monsoon regimes and the Atlantic multidecadal oscillation. Journal of Climate, 21(11): 2371-2383.

Hu, Q., Feng, S., 2012. AMO-and ENSO-driven summertime circulation and precipitation variations in North America. Journal of Climate, 25(19): 6477-6495.

Hu, Q., Feng, S., Oglesby, R.J., 2011. Variations in North American summer precipitation driven by the Atlantic Multidecadal Oscillation. Journal of Climate, 24(21): 5555-5570.

Hurrell, J.W., Kushnir, Y., Ottersen, G., Visbeck, M., 2003. An overview of the North Atlantic oscillation. The North Atlantic Oscillation: climatic significance and environmental impact, 134: 1-35.

Iizumi, T. et al., 2013. Prediction of seasonal climate-induced variations in global food production. Nature climate change, 3: 904-908.

Jakob, D., Smalley, R., Meighen, J., Taylor, B., Xuereb, K., 2008. Climate change and probable maximum precipitation. Proceedings of Water Down Under 2008: 109.

Jenkinson, A.F., 1955. The frequency distribution of the annual maximum (or minimum) values of meteorological elements. Quarterly Journal of the Royal Meteorological Society, 81(348): 158-171.

Jennings, A.H., 1950. World's greatest observed point rainfalls. Monthly Weather Review, 78(1): 4-5.

Jones, C., Carvalho, L.M.V., 2014. Sensitivity to Madden–Julian Oscillation variations on heavy precipitation over the contiguous United States. Atmospheric Research, 147-148: 10-26. DOI:https://doi.org/10.1016/j.atmosres.2014.05.002

Joseph, J.F., Falcon, H.E., Sharif, H.O., 2013. Hydrologic Trends and Correlations in South Texas River Basins: 1950–2009. Journal of Hydrologic Engineering, 18(12): 1653-1662. DOI:doi:10.1061/(ASCE)HE.1943-5584.0000709

Kao, S.-C., DeNeale, S.T., Watson, D.B., 2019. Hurricane Harvey Highlights: Need to Assess the Adequacy of Probable Maximum Precipitation Estimation Methods. Journal of Hydrologic Engineering, 24(4): 05019005. DOI:doi:10.1061/(ASCE)HE.1943-5584.0001768

Karl, T., Koss, W.J., 1984. Regional and national monthly, seasonal, and annual temperature weighted by area, 1895-1983.

Karl, T.R., Knight, R.W., Plummer, N., 1995. Trends in high-frequency climate variability in the twentieth century. Nature, 377(6546): 217-220.

Kaspi, Y., Schneider, T., 2011. Winter cold of eastern continental boundaries induced by warm ocean waters. Nature, 471(7340): 621-624.

Katz, R.W., Parlange, M.B., Naveau, P., 2002. Statistics of extremes in hydrology. Advances in water resources, 25(8-12): 1287-1304.

Kerr, R.A., 2000. A North Atlantic climate pacemaker for the centuries. Science, 288(5473): 1984-1985.

Klemes, V., 1993. Probability of extreme hydrometeorological events-a different approach.

Klemes, V., Nikleva, S., Chin, W., 1992. Probability of a PMP—A feasibility study. Dam Safety, 1992: 1-16.

Kotz, S., Nadarajah, S., 2000. Extreme value distributions: theory and applications. World Scientific.

Kripalani, R., Kulkarni, A., 2001. Monsoon rainfall variations and teleconnections over South and East Asia. International Journal of Climatology, 21(5): 603-616.

Kunkel, K.E. et al., 2013. Probable maximum precipitation and climate change. Geophysical Research Letters, 40(7): 1402-1408.

Larkin, T.J., Bomar, G.W., 1983. Climatic atlas of Texas. 3.

Leathers, D.J., Yarnal, B., Palecki, M.A., 1991. The Pacific/North American teleconnection pattern and United States climate. Part I: Regional temperature and precipitation associations. Journal of Climate, 4(5): 517-528.

Lee, K., Gao, H., Huang, M., Sheffield, J., Shi, X., 2017. Development and Application of Improved Long-Term Datasets of Surface Hydrology for Texas. Advances in Meteorology, 2017: 13. DOI:10.1155/2017/8485130

Lee, O., Park, Y., Kim, E.S., Kim, S., 2016. Projection of Korean probable maximum precipitation under future climate change scenarios. Advances in Meteorology, 2016.

Li, C. et al., 2019. Larger increases in more extreme local precipitation events as climate warms. Geophysical Research Letters.

Li, W., Li, L., Fu, R., Deng, Y., Wang, H., 2011. Changes to the North Atlantic Subtropical High and Its Role in the Intensification of Summer Rainfall Variability in the Southeastern United States. Journal of Climate, 24(5): 1499-1506. DOI:10.1175/2010jcli3829.1

Life on the Brazos River, 2013. Floods of the Brazos River in Texas, Brazos Flood of 1899.

López-Moreno, J.I. et al., 2011. Effects of the North Atlantic Oscillation (NAO) on combined temperature and precipitation winter modes in the Mediterranean mountains: Observed relationships and projections for the 21st century. Global and Planetary Change, 77(1): 62-76. DOI:https://doi.org/10.1016/j.gloplacha.2011.03.003

Lott, G.A., 1953. THE UNPARALLELED THRALL, TEXAS. Monthly Weather Review.

Lyons, S.W., 1990. Spatial and temporal variability of monthly precipitation in Texas. Monthly weather review, 118(12): 2634-2648.

Mailhot, A., Beauregard, I., Talbot, G., Caya, D., Biner, S., 2012. Future changes in intense precipitation over Canada assessed from multi-model NARCCAP ensemble simulations. International journal of climatology, 32(8): 1151-1163.

Marani, M., Zanetti, S., 2015. Long-term oscillations in rainfall extremes in a 268 year daily time series. Water Resources Research, 51(1): 639-647. DOI:10.1002/2014wr015885

Maurer, E.P., 2007. Uncertainty in hydrologic impacts of climate change in the Sierra Nevada, California, under two emissions scenarios. Climatic change, 82(3-4): 309-325. DOI:10.1007/s10584-006-9180-9

McIntyre, M.E., Palmer, T., 1983. Breaking planetary waves in the stratosphere. Nature, 305(5935): 593-600.

Mejia, G., Villegas, F., 1979. Maximum precipitation deviations in Colombia, Third Conference on Hydrometeorology, American Meteorological Society, pp. 74-76.

Micovic, Z., Schaefer, M.G., Taylor, G.H., 2015. Uncertainty analysis for probable maximum precipitation estimates. Journal of Hydrology, 521: 360-373.

Mishra, A.K., Singh, V.P., 2010. Changes in extreme precipitation in Texas. Journal of Geophysical Research: Atmospheres, 115(D14).

Mo, K.C., 2010. Interdecadal Modulation of the Impact of ENSO on Precipitation and Temperature over the United States. Journal of Climate, 23(13): 3639-3656. DOI:10.1175/2010jcli3553.1

Monette, A., Sushama, L., Khaliq, M., Laprise, R., Roy, R., 2012. Projected changes to precipitation extremes for northeast Canadian watersheds using a multi-RCM ensemble. Journal of Geophysical Research: Atmospheres, 117(D13).

Moore, B.J., Keyser, D., Bosart, L.F., 2019. Linkages between Extreme Precipitation Events in the Central and Eastern United States and Rossby Wave Breaking. Monthly Weather Review, 147(9): 3327-3349.

Narasimhan, B., Srinivasan, R., Quiring, S., Nielsen-Gammon, J., 2008. Digital Climatic Atlas of Texas: Texas A&M University, Texas Water Development Board Contract, Report 2005-483-5591.

NASS, U., 2007. Census of agriculture. US Department of Agriculture, National Agricultural Statistics Service, Washington, DC.

NCEI, N.C.f.E.I., 2019. Billion-Dollar Weather and Climate Disasters: Table of Events. In: Administration, N.O.a.A. (Ed.).

Nguyen, V., Nguyen, T.-D., Ashkar, F., 2002. Regional frequency analysis of extreme rainfalls. Water science and technology, 45(2): 75-81.

NOAA, 2020. What is a Rossby wave?

NOAA, N.C.f.E.i., 2017. Is Houston America's Flood Capital? weather.com.

NOAA, N.C.f.E.i., 2018. Climate at a Glance: Statewide Time Series.

Nogueira, R.C., Keim, B.D., 2010. Annual volume and area variations in tropical cyclone rainfall over the eastern United States. Journal of climate, 23(16): 4363-4374.

Norris, J., Chen, G., Neelin, J.D., 2019. Thermodynamic versus dynamic controls on extreme precipitation in a warming climate from the Community Earth System Model Large Ensemble. Journal of Climate, 32(4): 1025-1045.

North, G.R., Schmandt, J., 1995. The impact of global warming on Texas: A report of the task force on climate change in Texas. University of Texas Press.

NRC, N.R.C., 1994. Estimating Bounds on Extreme Precipitation Events.

NWS, N.W.S., 2017. Tropical Cyclone Climatology for the Upper Texas Coast, Tropical Cyclone Climatology for South East Texas.

NWS, N.W.S., 2018. South Texas Heavy Rain and Flooding Event: June 18-21, 2018. In: Office, W.F. (Ed.). National Oceanic and Atmospheric Administration, Corpus Christi, TX.

NWSI, N.W.S.I., 2017. Observational Quality Control - General (National Weather Service Instruction 10-1305). In: Department of Commerce, N.O.A.A. (Ed.).

Ottersen, G. et al., 2001. Ecological effects of the North Atlantic oscillation. Oecologia, 128(1): 1-14.

Pangaluru, K. et al., 2018. Estimating changes of temperatures and precipitation extremes in India using the Generalized Extreme Value (GEV) distribution, AGU Fall Meeting Abstracts.

Papalexiou, S., Koutsoyiannis, D., 2006. A probabilistic approach to the concept of Probable Maximum Precipitation. Advances in Geosciences, 7: 51-54.

Papalexiou, S.M., Dialynas, Y.G., Grimaldi, S., 2016. Hershfield factor revisited: Correcting annual maximum precipitation. Journal of hydrology, 542: 884-895.

Papalexiou, S.M., Montanari, A., 2019. Global and Regional Increase of Precipitation Extremes Under Global Warming. Water Resources Research, 55(6): 4901-4914. DOI:10.1029/2018wr024067

Papin, P.P., Bosart, L.F., Torn, R.D., 2017. A climatology of central American gyres. Monthly Weather Review, 145(5): 1983-2000.

Parazoo, N.C. et al., 2015. Influence of ENSO and the NAO on terrestrial carbon uptake in the Texas-northern Mexico region. Global Biogeochemical Cycles, 29(8): 1247-1265.

Parker, J., McIntyre, D., Noble, R., 2010. Characterizing fecal contamination in stormwater runoff in coastal North Carolina, USA. Water research, 44(14): 4186-4194.

Paulhus, J.L., Gilman, C.S., 1953. Evaluation of probable maximum precipitation. Eos, Transactions American Geophysical Union, 34(5): 701-708.

Pendergrass, A.G., 2018. What precipitation is extreme? Science, 360(6393): 1072-1073.

Pfahl, S., Madonna, E., Boettcher, M., Joos, H., Wernli, H., 2014. Warm conveyor belts in the ERA-Interim dataset (1979–2010). Part II: Moisture origin and relevance for precipitation. Journal of Climate, 27(1): 27-40.

Philip, G., Watson, D.F., 1982. A precise method for determining contoured surfaces. The APPEA Journal, 22(1): 205-212.

PRISM Climate Group, 2011. PRISM climate data. In: University, O.S. (Ed.), Annual high-resolution climate data sets for the conterminous United States.

Quadrelli, R., Wallace, J.M., 2004. A simplified linear framework for interpreting patterns of Northern Hemisphere wintertime climate variability. Journal of Climate, 17(19): 3728-3744.

Rajah, K. et al., 2014. Changes to the temporal distribution of daily precipitation. Geophysical Research Letters, 41(24): 8887-8894.

Rajsekhar, D., Mishra, A.K., Singh, V.P., 2013. Regionalization of Drought Characteristics Using an Entropy Approach. Journal of Hydrologic Engineering, 18(7): 870-887. DOI:10.1061/(asce)he.1943-5584.0000683

Rakhecha, P., Deshpande, N., Soman, M., 1992. Probable maximum precipitation for a 2-day duration over the Indian Peninsula. Theoretical and applied climatology, 45(4): 277-283.

Rakhecha, P., Soman, M., 1994. Estimation of probable maximum precipitation for a 2-day duration: Part 2—North Indian region. Theoretical and applied climatology, 49(2): 77-84.

Ramon, A., 2019. El Niño is back - What that means for Central Texas.

Reclamation, Brekke, L., Thrasher, B., Maurer, E., Pruitt, T., 2013. Downscaled CMIP3 and CMIP5 climate and hydrology projections: Release of downscaled CMIP5 climate projections, comparison with preceding information, and summary of user needs. US Dept. of the Interior, Bureau of Reclamation, Technical Services Center, Denver.

Renard, B., Lall, U., 2014. Regional frequency analysis conditioned on large-scale atmospheric or oceanic fields. Water Resources Research, 50(12): 9536-9554.

Richman, M., Lamb, P., Angel, J., 1991. Relationships between monthly precipitation over central and eastern North America and the Southern Oscillation, Preprints 5th Conf. Climate Variations. American Meteorological Society Boston, MA, pp. 151-158.

Risser, M.D., Wehner, M.F., 2017. Attributable human-induced changes in the likelihood and magnitude of the observed extreme precipitation during hurricane Harvey. Geophysical Research Letters, 44(24): 12,457-12,464.

Ropelewski, C., Halpert, M., 1989. Precipitation patterns associated with the high index phase of the Southern Oscillation. Journal of climate, 2(3): 268-284.

Roque-Malo, S., Kumar, P., 2017. Patterns of change in high frequency precipitation variability over North America. Scientific reports, 7(1): 10853.

Rosenzweig, C., Tubiello, F.N., Goldberg, R., Mills, E., Bloomfield, J., 2002. Increased crop damage in the US from excess precipitation under climate change. Global Environmental Change, 12(3): 197-202.

Roth, D., 2010. Texas hurricane history. National Weather Service, Camp Springs, MD.

Rousseau, A.N. et al., 2014. Development of a methodology to evaluate probable maximum precipitation (PMP) under changing climate conditions: Application to southern Quebec, Canada. Journal of hydrology, 519: 3094-3109.

Ryoo, J.-M. et al., 2013. Impact of Rossby wave breaking on US West Coast winter precipitation during ENSO events. Journal of climate, 26(17): 6360-6382.

Salas, J.D., Gavilán, G., Salas, F.R., Julien, P.Y., Abdullah, J., 2014. Uncertainty of the PMP and PMF. Handbook of engineering hydrology: modeling, climate change, and variability, Book II, CRC Press, Taylor & Francis Group: 575-603.

Schlef, K.E., Moradkhani, H., Lall, U., 2019. Atmospheric Circulation Patterns Associated with Extreme United States Floods Identified via Machine Learning. Scientific reports, 9(1): 7171. DOI:10.1038/s41598-019-43496-w

Schmaltz, J., 2003. MODIS Rapid Response Team (Chapter 10. Extratropical Cyclones and Anticyclones). NASA/GSFC.

Schneider, N., Cornuelle, B.D., 2005. The forcing of the Pacific decadal oscillation. Journal of Climate, 18(21): 4355-4373.

Schreiner, L.C., Riedel, J.T., 1978. Probable maximum precipitation estimates, United States east of the 105th meridian. Department of Commerce, National Oceanic and Atmospheric Administration.

Schroeder, E., 1987. Floods in central Texas. United States Geological Survey.

Schroeder, E., Massey, B., Waddell, K.M., 1979. Floods in Central Texas, August 1978. 2331-1258, US Geological Survey.

Schwierz, C., Dirren, S., Davies, H.C., 2004. Forced waves on a zonally aligned jet stream. Journal of the atmospheric sciences, 61(1): 73-87.

Seneviratne, S.I. et al., 2012. Changes in climate extremes and their impacts on the natural physical environment.

Service, N.W., 2015. NWS Lubbock, TX, Rain and Severe storms in early May 2015.

Sharif, H.O., Jackson, T., Hossain, M., Bin-Shafique, S., Zane, D., 2010. Motor vehicle-related flood fatalities in Texas, 1959–2008. Journal of Transportation Safety & Security, 2(4): 325-335.

Sharif, H.O., Jackson, T.L., Hossain, M.M., Zane, D., 2014. Analysis of flood fatalities in Texas. Natural Hazards Review, 16(1): 04014016.

Sicular, G.M., 1969. Comments on "Misconceptions in hydrology and their consequences" by Vujica Yevjevich. Water Resources Research, 5(2): 537-538.

Silva, G.A.M., Ambrizzi, T., 2006. Inter-El Niño variability and its impact on the South American low-level jet east of the Andes during austral summer − two case studies. Adv. Geosci., 6: 283-287. DOI:10.5194/adgeo-6-283-2006

Simonović, S.P., 2012. Floods in a changing climate: risk management. Cambridge University Press.

Singh, A., 2016. Computation of Probable Maximum Precipitation (PMP) and Its Uncertainty.

Snedecor, G.W., Cochran, W.G., 1989. Statistical Methods, eight edition. Iowa state University press, Ames, Iowa.

Špitalar, M. et al., 2014. Analysis of flash flood parameters and human impacts in the US from 2006 to 2012. Journal of Hydrology, 519: 863-870.

Sprenger, M., Martius, O., Arnold, J., 2013. Cold surge episodes over southeastern Brazil–a potential vorticity perspective. International journal of climatology, 33(12): 2758-2767.

Stanglin, D., 2019. 5 deaths now linked to flooding in Texas after Tropical Storm Imelda. In: Today, U. (Ed.).

Stedinger, J.R., 1993. Frequency analysis of extreme events. in Handbook of Hydrology.

Stratz, S.A., Hossain, F., 2014. Probable maximum precipitation in a changing climate: Implications for dam design. Journal of Hydrologic Engineering, 19(12): 06014006.

Tatli, H., Menteş, Ş.S., 2019. Detrended cross-correlation patterns between North Atlantic oscillation and precipitation. Theoretical and Applied Climatology. DOI:10.1007/s00704-019-02827-7

TBRA, T.B.R.A., 2018. What is the Brazos River?

TCEQ, T.C.o.E.Q., 2016. Probable maximum precipitation study for texas.

Tian, L., Leasor, Z., Quiring, S.M., 2017. Potential to improve precipitation forecasts in Texas through the incorporation of multiple teleconnections. International Journal of Climatology, 37(10): 3863-3872.

Tomlinson, E., 1993. Probable Maximum Precipitation Study for Michigan and Wisconsin. Electric Power Research Institute, Palo Alto, Ca, TR-101554, 1.

Tomlinson, E., Kappel, B., Diederich, P., Parzybok, T., Hultstrand, D., 2008. Nebraska Statewide Probable Maximum Precipitation (PMP) Study. Applied Weather Associates.

Tomlinson, E.M., Henz, J.F., Williams, R.A., 2003. Technical Review for the Probable Maximum Precipitation (PMP) Site-Specific Study for Cherry Creek Reservoir. RFP PDA-0133W-Cherry Crk Denver, Colorado.

Tomlinson, E.M., Kappel, W.D., 2009. Dam safety: Revisiting PMPs. Hydroworld. com.[Available online at http://www. hydroworld. com/articles/hr/print/volume-28/issue-7/cover-story/dam-safety-revisiting. html.].

Trenberth, K.E., Fasullo, J.T., Shepherd, T.G., 2015. Attribution of climate extreme events. Nature Climate Change.

Trenberth, K.E., Hurrell, J.W., Stepaniak, D.P., 2006. The Asian monsoon: global perspectives, The Asian Monsoon. Springer, pp. 67-87.

TWDB, T.W.D.B., 2012. Chapter 4 : climate of Texas, Texas.

U.S. Geological Survey, U., 2008. EDNA Derived Watersheds for Major Named Rivers, Elevation Derivatives for National Applications (EDNA).

van Montfort, M.A., 1990. Sliding maxima. Journal of Hydrology, 118(1-4): 77-85.

van Montfort, M.A., 1997. Concomitants of the Hershfield factor. Journal of hydrology.

van Oldenborgh, G.J. et al., 2017. Attribution of extreme rainfall from Hurricane Harvey, August 2017. Environmental Research Letters, 12(12): 124009.

Wallace, J.M., Gutzler, D.S., 1981. Teleconnections in the geopotential height field during the Northern Hemisphere winter. Monthly Weather Review, 109(4): 784-812.

Wang, S.S., Zhao, L., Yoon, J.-H., Klotzbach, P., Gillies, R.R., 2018. Quantitative attribution of climate effects on Hurricane Harvey's extreme rainfall in Texas. Environmental Research Letters, 13(5): 054014.

Watson, D.F., 1985. A refinement of inverse distance weighted interpolation. Geoprocessing, 2: 315-327.

Wehner, M.F., 2013. Very extreme seasonal precipitation in the NARCCAP ensemble: model performance and projections. Climate Dynamics, 40(1-2): 59-80.

Wells, F.C., Schertz, T.L., Flugrath, M.W., 1984. Effects of October 1981 flood on the quantity and quality of water in selected streams and reservoirs in the Brazos River Basin, Texas. US Geological Survey.

Wernli, H., Sprenger, M., 2007. Identification and ERA-15 climatology of potential vorticity streamers and cutoffs near the extratropical tropopause. Journal of the atmospheric sciences, 64(5): 1569-1586.

White, A.B., Moore, B.J., Gottas, D.J., Neiman, P.J., 2019. Winter storm conditions leading to excessive runoff above California's Oroville Dam during January and February 2017. Bulletin of the American Meteorological Society, 100(1): 55-70.

WMO, W., 2009. Manual for Estimation of Probable Maximum Precipitation. Geneva: World Meteorological Organization.

WMO, W.M.O., 1986. Manual for estimation of probable maximum precipitation. Secretariat of the World Meteorological Organization.

Wood, A.W., Leung, L.R., Sridhar, V., Lettenmaier, D., 2004. Hydrologic implications of dynamical and statistical approaches to downscaling climate model outputs. Climatic change, 62(1-3): 189-216.

Yan, H. et al., 2011. A record of the Southern Oscillation Index for the past 2,000 years from precipitation proxies. Nature Geoscience, 4(9): 611.

Yevjevich, V., 1968. Misconceptions in hydrology and their consequences. Water Resources Research, 4(2): 225-232.

Zelinsky, D.B., Daniel, 2019. Tropical Storm Imelda Tropical Cyclone Update. National Hurricane Center, Miami, Florida.

Zhang, Y., Singh, V.P., Byrd, A.R., 2019. Basin-Scale Statistical Method for Probable Maximum Precipitation with Uncertainty Analysis. Journal of Hydrologic Engineering, 24(2): 04018067. DOI:doi:10.1061/(ASCE)HE.1943-5584.0001759